Report

A review of the model comparison of transportation and deposition of radioactive materials released to the environment as a result of the Tokyo Electric Power Company's Fukushima Daiichi Nuclear Power Plant accident

September 2, 2014

Sectional Committee on Nuclear Accident

Committee on Comprehensive Synthetic Engineering, Science Council of Japan

This report is the results of deliberations of the Sectional Committee on Nuclear Accident, Committee on Comprehensive Synthetic Engineering, Science Council of Japan、 reflecting the results of deliberations of the Subcommittee to Review the Investigation on Environmental Contamination Caused by the Nuclear Accident and the results of the Working Group for Model Intercomparison in the Subcommittee.

The members of the Sectional Committee on Nuclear Accident

Chairperson	Yagawa, Genki(associate member)	The president of Board of Directors, Nuclear safety Research Association
Vice-chairperson	Yamaji, Kenji(member of 3rd section)	The Director-General, Research Institute of Innovative Technology for the Earth
Secretary General	Matsuoka, Takeshi(member of 3rd section)	Part-time Lecturer, Utusnomiya University
Secretary General	Shibata, Tokushi(associate member)	Executive Director, Japan Radioisotope Association
	Iawta, Shuichi(associate member)	Professor, The Graduate School of Project Design
	Nariai, Hideki(special associate member)	Professor Emeritus, University of Tsukuba
	Ninokata, Hisashi(associate member)	Professor Emeritus, Tokyo Institute of Technology
	Sasao, Mamiko(associate member)	Professor Emeritus, Tohoku University
	Sawada, Takashi(special associate member)	Secretary General, Atomic Energy Society of Japan
	Sekimura, Naoto(associate member)	Professor, the University of Tokyo
	Shiratori, Masaki(associate member)	Professor Emeritus, Yokohama National University
	Takeda, Toshiichi(associate member)	Professor, Research University of Fukui
	Yamamoto, Ichiro	Professor, Nagoya University

The members of the Subcommittee to Review the Investigation on Environmental Contamination Caused by the Nuclear Accident

Chairperson	Shibata, Tokushi(associate member)	Executive Director, Japan Radioisotope Association
Vice-chairperson	Nakajima, Teruyuki(member of 3rd section)	Professor, The university of Tokyo
Secretary General	Igarashi, Yasuhito	Chief of Laboratory, Meteorological Research Institute
Secretary-General	Tsuruta, Haruo	Special Researcher, The University of Tokyo
	Ebihara, Mitsuru	Professor, Tokyo Metropolitan University
	Hattori, Takatoshi	Research Scientist, Central Research Institute 0f Electric Power Industry
	Hoshi, Masaharu	Professor Emeritus, Hiroshima University
	Ishimaru, Takashi	Professor, Tokyo University of Marin Science and

		Tecnology
	Masumoto, Kazuyoshi	Professor, High-Energy Accelerator Research
Organization		
	Onda, Uichi	Professor, University of Tsukuba
	Otsuka, Takaharu(associate member)	Professor, the University of Tokyo
	Saito, Kimiaki	Principal Researcher, Japan Atomic Energy Agency
	Shinohara, Atsushi	Professor, Osaka University
	Takahashi, Tomoyuki	Associate Professor, Kyoto University
	Tanihata, Isao	Professor, Osaka University
	Uematsu, Mitsuo	Professor, The University of Tokyo
	Uchida, Shigeo	Chief of Laboratory, National Institute of Radiological Science
	Urabe, Itsumasa	Professor, Fukuyama University
	Yoshida, Naohiro	Professor, Tokyo Institute of Technology

The members of the Working Group for Model Intercomparison in the Subcommittee to Review the Investigation on Environmental Contamination Caused by the Nuclear Accident

Cairperson	Nakajima, Teruyuki(member of 3rd section)	Professor, The university of Tokyo
	Hayami, Hiroshi	Research Scientist, Central Research Institute 0f Electric Power Industry
	Igarashi, Yasuhito	Meteorological Research Institute
	Kajino, Mizuo	Japan Meteorological Agency
	Kurihara, Osamu	National Institute of Radiological Science
	Kobayashi, Takuya	Japan Atomic Energy Agency
	Maki, Takashi	Meteorological Research Institute
	Masumoto, Yukio	Japan Agency for Marine-Earth Science and Technology The university of Tokyo
	Morino, Yu	National Institute for Environmental Studies
	Nagai, Haruyasu	Japan Atomic Energy Agency
	Sekiyama, Tsuyoshi	Meteorological Research Institute
	Shibata, Tokushi	Japan Radioisotope Association
	Takemura, Toshihiko	Kyushu University
	Takigawa, Masayuki	Japan Agency for Marine-Earth Science and Technology

Tanaka, Taichu	Meteorological Research Institute
Tsumune, Daisuke	Research Scientist, Central Research Institute 0f Electric Power Industry

Contributors to the report:

Bailly du Bois, Pascal (IRSN, France)

Bocquet, Marc (CEREA, France)

Boust, Dominique (IRSN, France)

Brovchenko, Igor (IMMSP, Ukraine)

Choe, Anna (SNU, Korea)

Christoudias, Theo (Cyprus Institute, Cyprus)

Didier, Damien (IRSN, France)

Dietze, Heiner (GEOMAR, German)

Garreau, Pierre (IFREMER, France)

Higashi, Hironori (NIES, Japan)

Jung, Kyung Tae (KIOST, Korea)

Kida, Shinnichiro (JAMSTEC, Japan)

Le Sager, Philippe (KNMI, Netherland)

Lelieveld, Jos (Max-Planck-Institute for Chemistry)

Maderich, Vladimir S. (IMMSP, Ukraine)

Miyazawa, Yasumasa (JAMSTEC, Japan)

Park, Soon-Ung (SNU, Korea)

Quelo, Denis (IRSN, France)

Saito, Kazuo (MRI, Japan Meteorological Agency, Japan)

Shimbori, Toshiki (MRI, Japan Meteorological Agency, Japan)

Uchiyama, Yusuke (Kobe University, Japan)

van Velthoven, Peter (KNMI, Netherland)

Winiarek, Victor (CEREA, France)

Yoshida, Sachiko (WHOI, USA)

Preface

This report evaluates and compares the models used to analyze the transportation and deposition of radioactive materials that were released into the environment after the Tokyo Electric Power Compan's Fukushima Daiichi Nuclear Power Plant (FDNPP) accident on March 11, 2011. A Working Group for Model Intercomparison was formed in July 2012 under the Subcommittee of Investigation on the Environmental Contamination Caused by the Nuclear Accident in the Sectional Committee on Nuclear Accident, the Committee Comprehensive Synthetic Engineering, Science Council of Japan (SCJ). The purpose of this working group (SCJ WG) is to compare existing model results and to assess the uncertainties in the simulation results. The emerging knowledge will be invaluable for various applications designed to mitigate environmental contamination in wide areas. The working group solicited international colleagues and groups to provide their model simulation results for the intercomparison.

This report evaluates the simulation results of nine regional atmospheric models, six global models and eleven oceanic models for the transportation of radioactive materials; the results were provided by the contributing groups that responded to the solicitation. We greatly appreciate the national and international support and assistance in this initiative. We hope that this reports will provide assistance in societal efforts to recover from disasters by providing scientific knowledge of the modeling capability of existing models.

Teruyuki Nakajima, Chair, Working Group for Model Intercomparison

Tokushi Shibata, Chair, Subcommittee to Review the Investigation on Environmental Contamination Caused by the Nuclear Accident, in the Sectional Committee on Nuclear Accident, Committee on Comprehensive Synthetic Engineering, SCJ

Contents

1. Introduction

The Tohoku Region Pacific Coast Earthquake occurred at 14:46 JST on March 11, 2011; 13-m high tsunami waves arrived at the Tokyo Electric Power Company's Fukushima Daiichi Nuclear Power Plant (FDNPP) at 15:27, and the diesel engine of the plant stopped at 15:41 (TEPCO, 2011). A large amount of radioactive materials were released by the explosion of the 1st reactor housing at 15:36 on March 12 and of the 3rd reactor housing at 11:01 on March 14. Monitoring data suggested that there were other emission sources to the atmosphere from depressurized ventilation of the reactors and to the ocean from leakages of contaminated cooling water.

The atmospheric pressure regime in the spring of 2011 was of a prevailing winter pattern with strong northwesterly winds; therefore, a large amount of the released materials, at least more than 60% of the amount released to the atmosphere, were transported to the Pacific Ocean (Takemura et al., 2011; JAEA workshop, 2012). Field and airborne measurements showed that a complex distribution of deposited radioactive materials was formed by various migrating pressure systems and precipitation prevailing at the time. The data showed hot spots exceeding 1,000 kBq m^{-2} ^{137}Cs occurring beyond the 30-km area around the power plant (Morino et al., 2011). The 3rd (May-July 2011) and 4th (October-November, 2011) MEXT (Ministry of Education, Culture, Sports, Science and Technology, Japan) airborne monitoring of the air dose rate indicated that the air dose rate decreased in the Abukuma Mountains and increased in the coastal region, which suggested a significant transportation of the radioactive materials via rivers. A portion of the radioactive materials were discharged directly to the ocean. Ship observation after April 2011 detected a wide areal distribution of radioactive cesium across the North Pacific Ocean. There were hot spots of a high ^{137}Cs concentration of 196 Bq m^{-3}, which were two orders higher than what was found in the surrounding region (Aoyama et al., 2012; JAEA workshop, 2012). The total deposition of ^{137}Cs on the land surface of Japan is estimated as about 2.7 PBq from the airborne monitoring.

As previously stated, a wide area was contaminated by the radioactive materials emitted from the power plant accident, and the characteristic distributions of the radioactive materials were simulated by various models, including the SPEEDI (System for Predictions of Environmental Emergency Dose Information) operational model. The amount of radioactive

1

[137]Cs released to the atmosphere was estimated to be in a range from 9 to 37 PBq (Aoyama et al., 2012; Stohl et al., 2012; Terada et al., 2012; Kobayashi et al., 2013; Winiarek et al., 2014). The amount of direct discharge to the ocean was estimated to be in a range from 2.3 to 26.9 PBq (Kawamura et al., 2011; Tsumune et al., 2012; Estournel et al., 2012; Miyazawa et al., 2012; Bailly du Bois et al., 2012; JAEA workshop,2012). Large uncertainties were caused by insufficient monitoring data and meteorological data that resulted from a loss of monitoring posts after the tsunami, electricity outages, and errors in the model and inversion scheme. The distribution of radioactive xenon gas and iodine, which have short decay times, are important for estimating the early phase exposure; however, these distributions are difficult to retrieve other than by model simulation.

Based on this situation, a thorough review of the existing modeling capability in the simulation of radioactive materials dispersal is important for improving models and observation systems, which are required to evaluate the contamination effects and mitigation actions to reduce the amount of radioactive material in the environment.

In this report we compared the simulation results from nine regional atmospheric models, six global atmospheric models and eleven oceanic models that were provided by global groups and based on the events of the Fukushima Daiichi Nuclear Power Plant accident.

2. Notes for comparison

The contributing groups were asked to provide their best simulation results for the 2013 spring accident at the FDNPP. Unified conditions were not imposed for the comparison; therefore, there were large differences in the model setup (grid resolution, integration time interval, etc.) and data (meteorological data, emission scenario, etc.) used to constrain the simulation, which simplified the evaluation of the accuracy of the compared models. However, it was difficult to investigate the causes of differences in the simulation results, so we produced sensitivity tests using several models to study how the model parameters controlled the key processes in the models.

The following three chapters present the intercomparison results from the regional atmospheric models, global atmospheric models, and oceanic models. Each chapter begins with a description of the model specifications and setup procedure for the simulation, which is followed by the results of the model comparisons. Chapter 6 illustrates an emission source estimation using the JMA inverse model to discuss the emission scenario uncertainties.

3. Regional atmospheric model intercomparison

3.1. Introduction

Several researchers have reported that the transport and deposition of radionuclides released from the accident at the FDNPP were strongly affected by the regional-scale meteorological field and geography (e.g., Chino et al., 2011; Morino et al., 2011). The SCJ WG for radionuclide dispersion modeling, therefore, organized a subgroup to assess the regional-scale dispersion and deposition of radionuclides caused by the accident. The 9 members of the SCJ WG for regional models have provided a total of 9 simulations. Table 3.1 summarizes the resolution, target area, and treatment of radionuclides in each model. Certain members have conducted additional simulations with different release rates or different wet deposition schemes to evaluate such impacts on the dispersion and deposition of radionuclides.

3.2. Regional models participating in the SCJ WG

Table 3.1 summarizes the horizontal resolution, horizontal gird sizes, and vertical layers of the attending models. Almost all of the models cover the east side of Japan, including the Fukushima and Kanto area, with cloud-resolving (3-5 km) grids. The objective of most of the model simulations is to understand the processes of local transport and deposition that occurred in March and April 2011. Figure 3.1 shows the computation domain for each model. In contrast, the model domain from the Seoul National University (SNU) model covers East Asia, and the objective of the SNU model simulation is to assess the continental transport of radionuclides in Asia. The horizontal resolution of the SNU model is relatively larger than the resolution of the other models that target the local transport over east Japan; however, it is still higher than most of the global models, and the result of the SNU model simulation is included in the intercomparison of regional models. The details for each model are found in Appendix A.

For an intercomparison of the total amount of deposited radionuclides over the land and sea, an overlapped domain between 138.0E and 142.5E longitude and 34.5N and 40.5N latitude was selected. The outputs from all of the participating models were interpolated into 0.1 degree × 0.1 degree grids within the domain. The calculation period was also different in each model, and we selected the common calculation period from 00Z March 12, 2011 to 00Z April 1, 2011. The total amount of deposited radionuclides over the land and sea was

estimated using these grid cells, and the accumulated deposition was calculated during this period. The Ministry of Education, Culture, Sports, Science and Technology of Japan (MEXT) conducted observations from aircraft after the accident (cf. http://radb.jaea.go.jp/mapdb/download.html), and the observational data were also interpolated into the common domain for the intercomparison. The observational flights in the spring of 2012 were used for the intercomparison, but the observed values might be affected by deposition after April 2011, resuspension from the land surface, and transition into the deep soil or river water.

3.3. Meteorological overview

A summary of the meteorological conditions during the critical phases of the atmospheric emissions was included in the first report of the WMO (WMO, 2011) and in reports by several other researchers (Morino et al., 2011; Kinoshita et al., 2011; Korsakissok et al., 2011; Stohl et al., 2012; Sugiyama et al., 2012).

The key results are summarized as follows:

March 9 – 11: A weak low pressure trough over eastern Japan from March 9 to 11 caused light rain from the 9th until the morning of the 12th.

March 12 – 13: A high pressure system moved eastward along the south coast of the main island of Japan from the 12th through the 13th. The wind direction was from the south below 1 km and from the west above 1 km on the afternoon of March 12, the time of the hydrogen explosion at reactor number one.

March 14 – 17: Another weak low pressure trough moved eastward off of the southern coast of the main island from the 14th until the 15th and then moved towards the northeast and developed rapidly after the 15th. Light rain was observed from the 15th until the morning of the 17th because of a weak low pressure system, which moved northeastward off of the east coast of Japan. In particular, rain was observed in the Fukushima Prefecture from 1700 JST March 15 until 0400 JST March 16 (Kinoshita et al., 2011), which corresponded with significant emissions. The low-level winds were from the southwest during the morning of the 14th, which corresponded with the hydrogen explosion at reactor number three. The 950 hPa winds were from the west until the morning of the 15th; however, they changed to a north-northeast direction during the day of the 15th, which corresponded with the container burst of reactor number two. Chino et al. (2011) estimated that the maximum ^{131}I emissions occurred between 0900 and 1500 JST (0000-0600 UTC). After 1500 JST, the winds turned to a direction from the east-southeast and then changed to north after 0000 JST on the 16th

(1500 UTC 15th).

March 18 – 19: High pressure dominated during this period, and the winds were generally from the west.

March 20 – 22: A low pressure system passed over the main island from March 20 to 22 and caused moderate rain in the Kanto area (Ibaraki, Chiba, Tochigi, Saitama Prefectures and Tokyo) from the 20th until the 23rd.

3.4. Accumulated deposition of ^{137}Cs

Figure 3.2 shows the horizontal distributions of the accumulated deposition of ^{137}Cs until 00Z 1 April 2011. A high-deposit area from the FDNPP is clearly observed to the north up to Fukushima city, and the maximum value exceeds 8×10^5 Bq m^{-2} in this area. Several related papers mentioned that this high-deposit area was related to the passage of low pressure from March 14 to 15 (cf. Chino et al., 2011; Katata et al., 2012; Morino et al., 2011; Takemura et al., 2011). Therefore, this structure can be reproduced by most of the models except SNU, which applied a lower horizontal resolution (27 km) than the others (3-5 km).

There is also a high-deposit area in the central area of the Fukushima Prefecture (Naka-dori region) and Tochigi Prefecture. It is estimated the deposition in this area corresponded to the weak precipitation occurring in these areas on the afternoon of March 15. Some models (e.g., MRI, NIES, and JMA) succeeded in reproducing the accumulated deposition over this area. The JAMSTEC model showed a weak deposition despite being driven by the same meteorological data (JMA MSM) as used by the NIES and JMA groups. However, the meteorological field was recalculated by the meteorological models (MM5, WRF, etc.) to drive the chemical transport model; so although they are based on the same meteorological data (JMA-MSM), there might be a small difference in the meteorological fields in the models caused by differences of the meteorological models, model domains, and model configurations.

There are additional high-deposit areas to the south of the FDNPP in Ibaraki Prefecture and north in Iwate Prefecture. The transport to southward areas might have occurred on the 14, 16, 20, and 21 of March. Certain models (e.g., CRIEPI, CEREA, IRSN, and JAEA) show a high deposition over the southern areas. Deposits over the northern Tohoku areas, such as the Iwate Prefecture, are clearly observed in some models (e.g., JAEA and JAMSTEC). In contrast, the CRIEPI, CEREA, and SNU models do not show a large amount of accumulated deposits over the northern Tohoku area.

Figure 3.3 illustrates the scatter plot of the accumulated deposits of ^{137}Cs until 00Z 1

April 2011. Each dot shows the model and observed values in the same cells over the interpolated domain, which is mentioned in section 1.1. Most of the models were able to estimate the accumulated deposition of ^{137}Cs in March 2011 in the range of a factor of 10 and 0.1. The ensemble mean of the models (black squares) reproduced the observed values, although certain models (IRSN and MRI) tended to overestimate the observed values, whereas other models (JAMSTEC, etc.) tended to underestimate the observed values.

The total amount of the accumulated deposits of ^{137}Cs over the land and sea in the models and from the MEXT aircraft observations are shown in Table 3.2. The simulated and observed values were interpolated into the same domain and grid cells, which was mentioned in section 1.1 and shown in Fig. 3.3. The difference in the estimated values was caused by the difference of meteorological fields, source terms, and deposition processes. In the observation, there were no data over the ocean, and the estimated amount was 2.65 PBq. Most of the models showed 1.3-3.8 PBq over the land, and these values were close enough to the observed values. However, the contributions of the wet and dry deposits are dissimilar. The MRI and NIES models estimated that the wet deposition process caused most of the deposits, and the IRSN and SNU models estimated that dry deposition played an important role. An estimated deposit of approximately 0.9-5.5 PBq of ^{137}Cs occurred in March 2011 over the coastal ocean; this estimate is common to all of the model domains.

3.5. Ratio of accumulated deposition of radionuclides (^{137}Cs to ^{131}I)

Figure 3.4 shows the horizontal distributions of the ratio of accumulated deposition of ^{137}Cs to that of ^{131}I until 00Z 1 April 2011. The difference in the area ratio is caused by the different levels of emissions at the FDNPP and different removal processes among the radionuclides. The models in Fig. 3.4 commonly used the source term estimated by the JAEA and driven by the output of the JMA MSM meteorological model; therefore, the main cause of the difference of ratios among the models might have been differences in the removal process from the atmosphere and differences in the interpolated or re-calculated meteorological fields for each time step of the chemical transport models. Some models (CRIEPI, JAEA, JAMSTEC, and JMA) show values between 0.05 and 0.5 over land. The JAEA, JAMSTEC, and JMA models apply a wet removal process based on the precipitation intensity, and the MRI model shows a relatively large value, indicating that ^{131}I is relatively smaller relative to the other models, especially over land. In contrast, the NIES model shows a relatively smaller value (0.01 to 0.1). All of the models show relatively smaller values over the Sea of Japan, with the two Lagrangian models (JAEA and JMA) showing clear land-sea

6

contrasts around the Sea of Japan.

3.6. The impact of different release rates on the concentration and deposition of radionuclides

A modeling group from the NIES conducted simulations with three sets of emission data, which were from JAEA (Terada et al., 2012), the Norwegian Institute for Air Research (NILU) (Stohl et al., 2012), and Tokyo Electric Power Company (TEPCO) (TEPCO, 2012). All three emission estimates are based on inversion methods using simulation models and observational data. The JAEA analysis combined local- and regional-scale models, the NILU used a global-scale model, and TEPCO used a local-scale model. The model from the JAEA uses a grid size of 1 km for the regional scale and 3 km for the eastern area of Japan, and the model from TEPCO uses a grid size of 1 km.

The model performance is evaluated by a comparison between the CTM results and the airborne monitoring data. The simulation results with the JAEA emissions (standard simulation) are the most consistent with observations. In high-deposition areas ($\geq$10 kBq m^{-2}), the standard simulation reproduces the observations within one order of magnitude in most cases (96%), the simulation with the NILU emissions overestimates the observations by more than one order of magnitude for 12% of the observational area, and the simulation with the TEPCO emissions underestimates the observations by more than one order of magnitude for 11% of the observational area (Figure 2 and Table 2 of Morino et al., 2013). Overall, the simulations using the JAEA emission estimates best reproduce the observed deposition patterns over eastern Japan. This result suggests that to simulate the deposition patterns of fine particles on a regional scale, emission estimates should also be conducted with a regional-scale model rather than a local- or global-scale model.

3.7. Sensitivity tests of parameters on the deposition

A modeling group from the NIES compared three wet deposition settings. In the CMAQ model, wet deposition rates of accumulation-mode aerosols are calculated by considering the washout time, which is calculated from the ratio of the water content of precipitation to that of clouds (Byun and Schere, 2006). The wet deposition module is process based, and the wet deposition amounts of aerosols calculated with the CMAQ have been validated in several previous studies (Appel et al., 2011). The NIES group also conducted a simulation with the wet deposition module of the JAEA model (WD2 case) (Terada et al., 2012). In the model,

the wet deposition rates are calculated using a scavenging coefficient (Λ), which is a function of the precipitation rate (cf. Appendix A4). This wet deposition module is an empirical module with fitting parameters included.

In the WD2 simulation, the high-deposition areas extended farther from the FDNPP compared to the observations and the standard simulation. Simply multiplying the scavenging coefficient of the JAEA model by a factor of 10 improved the model's reproduction of the observed deposition pattern. The wet deposition modules of Terada et al. (2012) appear to underestimate Λ, and a simulation with Λ multiplied by a factor of 10 produced more accurate observations. As Λ varies greatly among studies (Morino et al., 2013), the choice of Λ is a source of much uncertainty. In an atmospheric simulation of radionuclides after the Chernobyl accident, a wet deposition scheme based on relative humidity was able to more accurately reproduce the observed radiocesium deposition than a parameterization based on the precipitation rates (Brandt et al., 2002). These results indicate that wet deposition modules based only on precipitation rates include large uncertainties; therefore, the process-based wet deposition module is recommended.

3.8. Statistical analysis on accumulated deposition of ^{137}Cs

A series of statistical analyses were conducted until 0Z 1 April 2011 for the modeled and observed accumulated deposition of ^{137}Cs. As in section 1.4, the modeled and observed values were interpolated into the same domain and grid cells. Observational data over the ocean was not available from the MEXT aircraft observation; therefore, the comparison between modeled and observed values was only conducted for cells with observed values that exceeded 10,000 Bq m^{-2}. The statistical results of the attended models are summarized in Table 3.3. Each column denotes a correlation (r), fractional bias (FB), figure of merit in space (FMS), factor of exceedance (FOEX), percentage of cells within a factor of 2 (%FA2), Kolmogorov-Smirnov parameter (KSP), which was defined as the maximum absolute difference among the cumulative distributions of observed and calculated deposition, and overall metrics, which were defined as the function of the particular metrics, respectively. A detailed explanation of the overall metrics can be found in Appendix A of the WMO report (WMO, 2013). Most of the models showed good correlations with the observed distribution, and the IRSN showed a relatively lower ($r<0.5$) correlation because of the overestimation of deposition in Niigata Prefecture. FB is a metric for overestimation or underestimation; the CEREA, IRSN, JAEA, and JMA estimates had an FB>20%, and the CRIEPI, JAMSTEC, and SNU estimates had an FB<20%. The FMS is a metric for the similarity of the distributed

pattern, and the CEREA, IRSN, CRIEPI, JAEA, and NIES estimates had an FMS>60. The JAMSTEC estimate did not show a deposition in Naka-dori of Fukushima Prefecture and Kanto area, and it had an FMS that was relatively lower than other models. The FOEX and %FA2 are metrics for the area fraction of reproducibility in each cell, and the JAEA and CEREA estimates showed a good performance. The %FA2 of the NIES estimate was 57%, which indicated that the NIES model can estimate the observed values within a factor of 2 for 57% of the cells. For more complex evaluations, metrics 1 to 4 were calculated using four different functions using other metrics (r, FB, FMS, FOEX, %FA2, and KSP). The CEREA, CRIEPI, JAEA, MRI, and NIES estimates showed good performances with these metrics.

These statistical analyses were applied to the ensemble mean of all of the attended models. The ensemble mean showed a better performance than did the best single model, such as the NIES, in some metrics.

3.9. Summary

This review summarized the current activity of the regional atmospheric model groups. The 9 members of the SCJ WG for regional models provided 9 simulations. The model domain, horizontal and vertical resolution, meteorological fields, and source terms were different in each model, and a portion of the differences in the models might have been caused by differences in the model configurations. For more detailed analyses, a series of sensitivity tests with the same configuration (source term, meteorological fields, etc.) should be performed.

The results are summarized as follows:

1) meteorological fields play an important role in radionuclide deposition, and the differences in the model treatments of deposition and in the configuration of meteorological models, such as in their microphysics and convection parameters, might cause a large difference in the horizontal distribution of accumulated deposition;

2) the wet deposition process has a strong impact on the reproducibility of deposition, especially on March 15;

3) ensemble means might be useful for the estimation of accumulated deposition.

Table 3.1. List of attending models.

Organizations	Model	Horizontal Resolution	Number of grids	Layers	Tracer models
CEREA	Polyphemus	Approximately 4 km	270×260	15	Eulerian
CRIEPI	CAMx	5 km	190×180	30	Eulerian
IRSN	ldX	Approximately 10 km	301×201	11	Eulerian
JAEA	GEARN	3 km	227×317	28	Lagrangian
JAMSTEC	WRF-Chem	3 km	249×249	34	Eulerian
JMA-MRI	NHM-LETKF-Chem	3 km	213×257	19	Eulerian
JMA	JMA-RATM	5 km	601×401	50	Lagrangian
NIES	CMAQ	3 km	237×237	34	Eulerian
SNU	ETM	27 km	164×119	25	Eulerian

Table 3.2. Total amount of accumulated deposition of ^{137}Cs over the land and sea until 0Z 1 April, 2011. Units are PBq. The MEXT aircraft observation was based on the value on 31 May, 2012. Percentages of each removal process to the total emissions are also shown for the model calculations.

	over the land		over the sea		Total depo. over the target region	Total emission
	total dep.	percentage of wet dep.	total dep.	percentage of wet dep.		
MEXT aircraft	2.65		-		-	-
CEREA	3.35(17%)	68%	2.62(14%)	85%	5.97 (31%)	19.3
CRIEPI	2.37 (27%)	79%	0.90 (10%)	54%	3.27 (37%)	8.8
IRSN	3.14 (15%)	46%	5.52 (27%)	71%	8.66 (42%)	20.6
JAEA	3.79 (43%)	67%	1.22(14%)	65%	5.01 (57%)	8.8
JAMSTEC	1.95 (22%)	67%	1.45 (16%)	67%	3.40 (39%)	8.8
JMA	2.65(30%)	50%	1.18 (13%)	36%	3.83(44%)	8.8
MRI	3.31 (38%)	92%	1.72 (20%)	97%	5.03 (57%)	8.8
NIES	2.90(33%)	98%	1.06(12%)	96%	3.96 (45%)	8.8
SNU	1.29 (15%)	32%	1.76 (20%)	36%	3.05(35%)	8.8
ensemble mean	2.75(27%)	67%	1.94(16%)	67%	4.69(43%)	11.3
standard deviation	0.73(10%)	20%	1.36(5 %)	22%	1.68(9 %)	4.6

Table 3.3. Statistical analysis of the accumulated deposition of ^{137}Cs. *r*, FB, FMS, FOEX, %FA2, and KSP denote the correlation, fractional bias, figure of merit in space, factor of exceedance, percentage of a factor of two, and Kolmogorov-Smirnov parameter, respectively. Metrics 1-4 are functions of these statistical values for the evaluation of forecast precision, with higher values showing a better performance.

|	*r*	FB	FMS	FOEX	%FA2	KSP	Metric1	Metric2	Metric3	Metric4
CEREA	0.79	0.09	74.32	-8.74	49.45	12.84	3.28	3.03	4.10	4.60
CRIEPI	0.60	-0.25	63.39	-19.95	40.44	22.40	2.85	2.62	3.45	3.85
IRSN	0.39	0.30	63.39	-17.49	38.52	28.69	2.28	2.05	2.99	3.32
JAEA	0.76	0.22	68.85	-8.74	40.16	22.68	3.10	2.81	3.92	4.33
JAMSTEC	0.62	-0.38	26.50	-37.43	13.93	54.37	2.44	2.32	2.70	2.84
MRI	0.49	0.17	45.90	-18.58	18.03	36.34	2.53	2.25	3.16	3.34
JMA	0.68	0.44	49.45	-17.76	27.87	35.79	2.64	2.43	3.29	3.57
NIES	0.85	0.03	68.31	-18.58	57.10	19.13	3.37	3.25	3.99	4.57
SNU	0.27	-0.81	42.08	-26.50	19.40	39.34	2.05	1.83	2.52	2.72
ensemble	0.77	0.04	70.41	-13.56	49.86	22.19	3.22	3.04	3.98	4.49
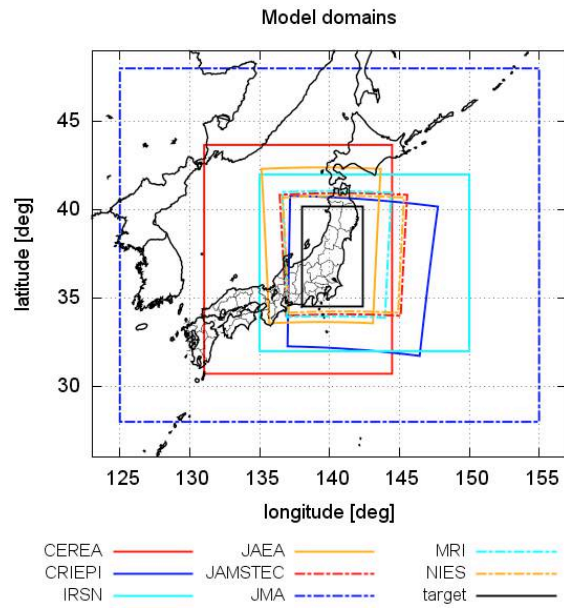
Figure 3.1. Model domains of the regional models evaluated by the SCJ WG. The domain for SNU is excluded because it covers the East Asia region.
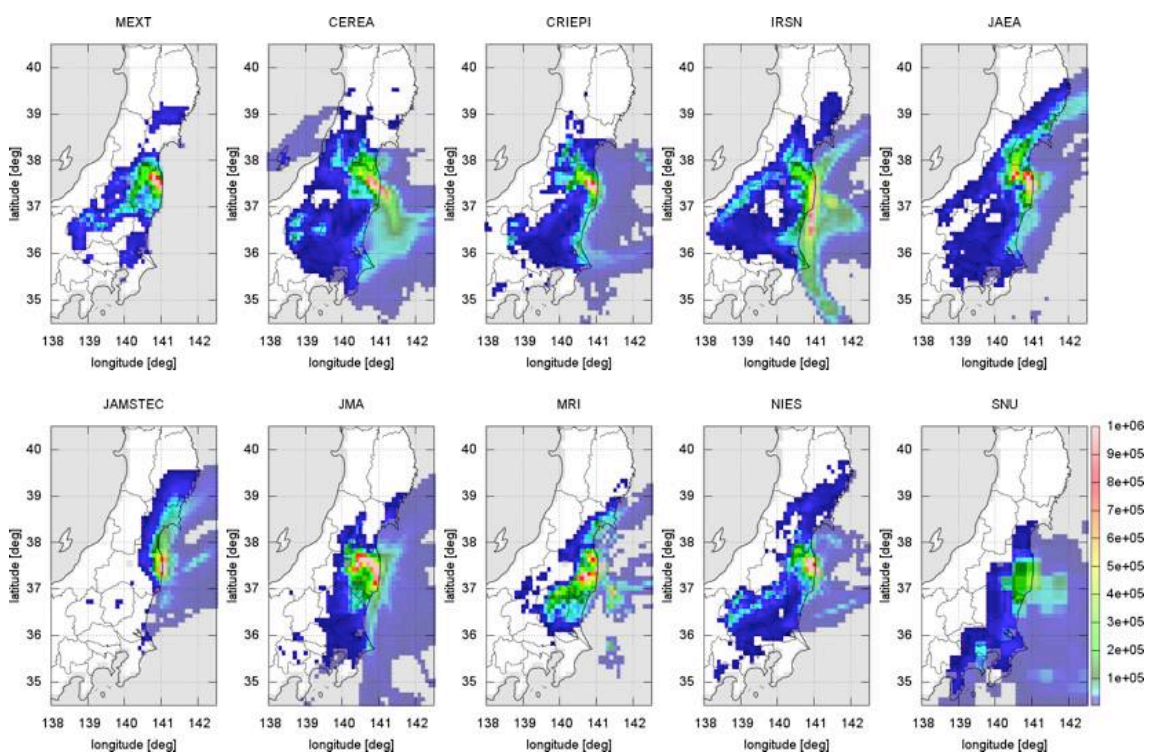

Figure 3.2. Latitude-longitude distributions of the accumulated deposition of ^{137}Cs until 00Z 1 April 2011. Units are Bq m^{-2}. The shaded region denotes the fraction of ocean in the WRF model that exceeds 50% of each of the grids.
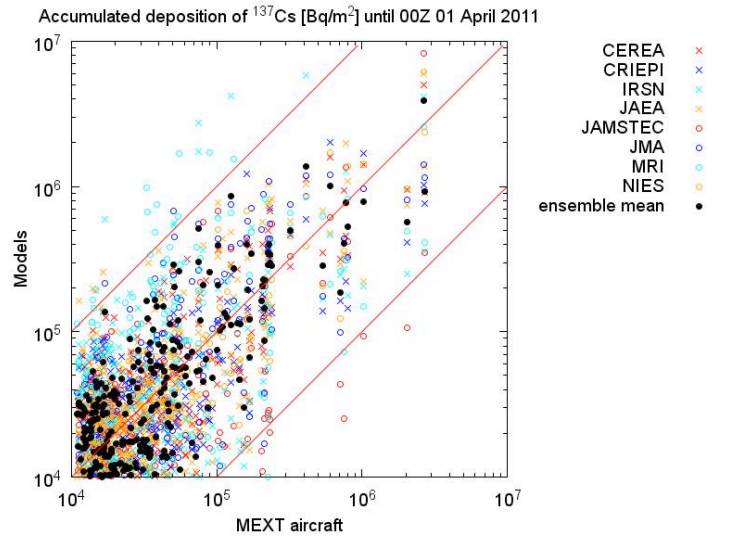
13

Figure 3.3. Scatter plot of the accumulated deposition of ^{137}Cs over the land within the common domains of the evaluated models. The X-axis shows the MEXT aircraft observations, and the Y-axis shows the regional models in the same cell. Black circles denote the ensemble of all of the attended models, and red lines denote factors of 10, 1, and 0.1.
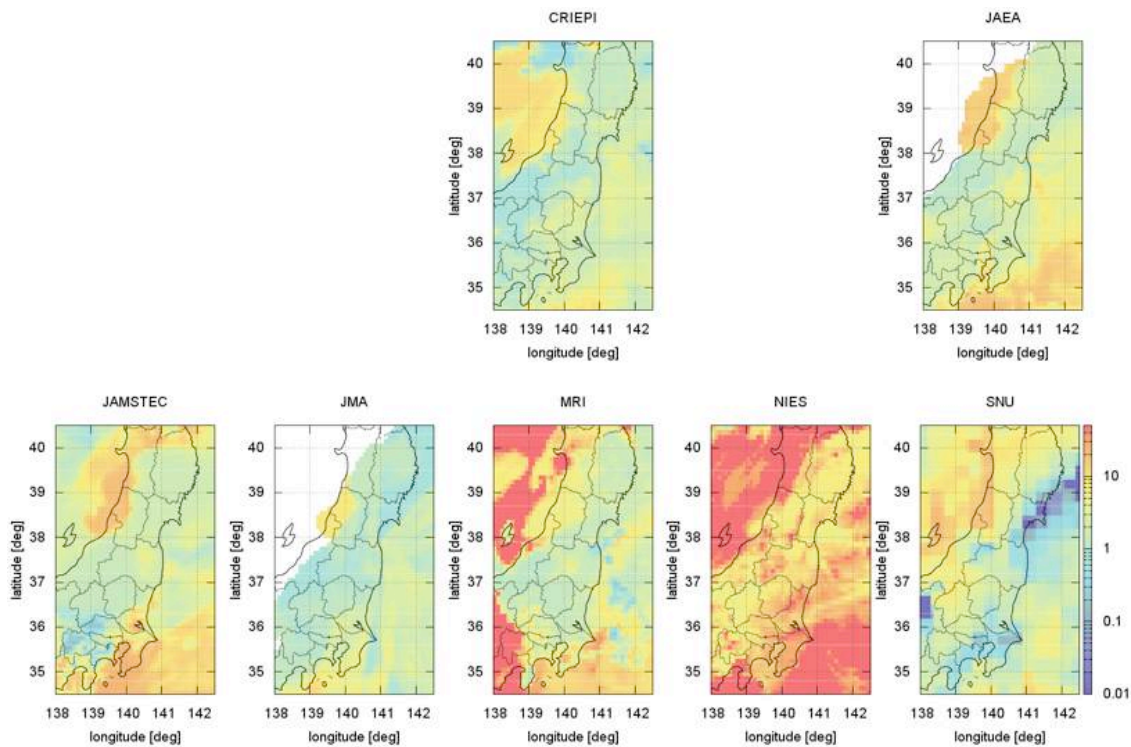

Figure 3.4. Latitude-longitude distributions of the ratio of the accumulated deposition of ^{137}Cs to the accumulated deposition of ^{131}I until 00Z 1 April 2011. Only models that evaluate ^{131}I and ^{137}Cs are shown. The color scale is same as in Fig. 4 of Torii et al. (2013).

14

4. Global atmospheric model intercomparison

4.1. Models

The intercomparison of long-range transport models used to estimate the radionuclides released from the FDNPP included five global transport models, one regional transport model, and 12 simulated results. Four of the five global models, SPRINTARS, EMAC, MASINGAR-1, and MASINGAR mk-2, are global aerosol models that are on-line coupled with general circulation models. The remaining models include the global transport model TM5 and the regional transport model MRI-PM/r, which are off-line models that use the assimilated meteorological fields or previously calculated meteorological fields by another model. The details of the participating models are described in Appendix A, and the specifications of the models are listed in Table 4.1.

In this intercomparison experiment, all of the participating models are grid point Eulerian or semi-Lagrangian advection models; no Lagrangian particle dispersion models are included. However, the global transport studies with numerical simulations include Lagrangian atmospheric dispersion models, such as those be Stohl et al. (2012).

4.2. Estimated time series of the radionuclides emission

In this intercomparison experiment, the source terms of the radionuclides are not specified; therefore, the participating research organizations selected or assumed the source terms. The simulations include source terms that were determined from inversion analyses by the Japan Atomic Energy Agency (JAEA) (Chino et al., 2011; Terada et al., 2012) and Stohl et al. (2012) (Fig. 4.1).

The JAEA estimated the time series of the radionuclides (^{131}I and ^{137}Cs) released from the FDNPP accident by inverse analysis. The total release of ^{137}Cs until the end of April 2011 was 12.6 PBq, which was estimated by Chino et al. (2011) and updated to 8.8 PBq by Terada et al. (2012). In the inverse analysis from the JAEA, only the observations within Japan were used. Stohl et al. (2012) estimated the time series of the releases of ^{133}Xe and ^{137}Cs using an inversion analysis method and included global observations using the atmospheric dispersion model FLEXPART. The estimated total release of ^{137}Cs until 20 April was 36.6 PBq (range of uncertainty of 20.1 – 53.1 PBq), which was approximately 4-fold greater than the estimate

15

by the JAEA. Stohl et al. (2012) estimated the total release of ^{133}Xe as 15.3 EBq (range of uncertainty of 12.2 – 18.3 EBq).

4.3. Global mass budget

Table 4.2 shows the simulated global total, dry and wet depositions of ^{137}Cs on March 31, 2011. In all of the simulations, most of the released ^{137}Cs was removed by the wet deposition processes of precipitation. The ratio of dry deposition varied by models, and the percentage of the dry deposition to total deposition ranged from 0 to 12%. The range of the variation of dry/wet deposition ratio was small compared with the intercomparison of the regional model simulations.

4.4 Temporal variation of the total atmospheric loading of [137]Cs

Figure 4.2 shows the temporal variation of the daily averaged global total atmospheric loading of [137]Cs. The simulations using the JAEA release rate show complex temporal variations. All of the simulated total atmospheric loadings show a maxima from March 15 to 20 and reach 0.7 – 2.7 PBq. The maximum atmospheric loadings of ^{137}Cs differ by a factor of 3 – 4. The plausible cause of the difference can be attributed to the differences in the deposition processes among the models. The simulations with the JAEA release rate show a maxima of atmospheric loading at the end of March, and the loading reaches 1 – 3 PBq.

However, simulations using the Stohl et al. (2012) release rate show a much larger atmospheric loading than the simulations using the JAEA emissions, which was expected. The maximum total loadings appear on March 15, 2011, and the total atmospheric loading reaches 10 – 16 PBq. Five days after the peak, the atmospheric loadings of ^{137}Cs increase again and reach 6 – 10 PBq from March 19 to 20. After the second peak, the total atmospheric loadings gradually decrease with time. The maxima of the simulated loading of ^{137}Cs at the end of March shows a distinct difference between the JAEA and Stohl et al. (2012) release rate of [137]Cs.

4.5 Temporal variation of daily deposition of [137]Cs

The time series of the global total daily deposition of ^{137}Cs are depicted in Fig. 4.3a and Fig. 4.3b. Most of the simulations with the release rate by JAEA show a maxima of the daily global total deposition of ^{137}Cs on March 15, 20 and 30, 2011 (Fig. 4.3a). However, some

differences exist in the temporal variation of the daily total deposition, and there are simulations that show a maxima of daily total deposition on March 25 and April 2. Most of the simulations show the maximum total deposition of approximately $1 - 3$ PBq day^{-1} on March 15.

The simulations with the estimated release rate by Stohl et al. (2012) show a maximum total deposition on March 15, 2011, and the daily total deposition reaches $8 - 11$ PBq day^{-1} (Fig. 4.3b). A second maximum of the daily deposition appears from March $20 - 21$.

4.6. Horizontal distribution of the total ^{137}Cs deposition

Figure 4.4 illustrates the horizontal distribution of the total deposition of ^{137}Cs at the end of March 2011. All of the simulated results show that the ^{137}Cs deposited in a wide area of the Northern Hemisphere, concentrated in the Pacific Northwest region. Common characteristics of the deposition are found from the FDNPP to the Aleutian Islands and the eastern region of the Kamchatka Peninsula, which stretches to the northwestern region of North America. However, differences in the simulations are found among the models and the employed source term of ^{137}Cs. The simulated ^{137}Cs distributions indicate greater differences with longer distances toward the eastern side of the FDNPP, namely in Europe and Russia, which suggests that the differences are caused by the different lifetimes of ^{137}Cs in the atmosphere caused by the wet deposition process.

The simulated distributions suggest that a portion of the ^{137}Cs that leaked into the North Pacific Ocean reached the Pacific Southwest region by a northeasterly wind from the Asian winter monsoon. The observatories in Taiwan (Huh et al., 2011) and Vietnam (Long et al., 2012) and the CTBTO observatory in the Philippines detected radionuclides that were possibly from the FDNPP. However, the magnitude of the deposition of simulated ^{137}Cs over Southeast Asia showed large differences between the models.

4.7. Comparison with observed atmospheric concentrations

The simulated results were compared with the atmospheric concentrations measured by the observatories of the Comprehensive Nuclear-Test-Ban Treaty Organization (CTBTO) and by the European network of radionuclide measurements (Masson et al., 2011). Appendix B includes a brief description of the observed data. Figure 4.5 shows the scatterplots of the observed and simulated daily average atmospheric concentrations of ^{137}Cs. In the range of relatively high ^{137}Cs concentrations (> 0.01 μBq m^{-3}), the simulated concentrations are

broadly within the range of a factor of 10 from the observed concentration. However, some of the simulated results, especially those using the JAEA source terms, show underestimations in the low concentration range ($< \sim 0.01 \ \mu\text{Bq m}^{-3}$), which is likely resulted from the JAEA source term being derived from an inversion analysis that only includes observations from within Japan and tends to underestimate the release rate of ^{137}Cs that flows to the Pacific side. From the comparison of scatterplots, the models with higher horizontal resolution do not necessarily produce better results.

The models that use both the JAEA and Stohl et al. (2012) source terms, the MASINGAR 1/mk-2 and EMAC T106/T255 show different tendencies. The MASINGAR 1 and mk-2 tend to overestimate the ^{137}Cs with the Stohl et al. (2012) source term, whereas it tends to underestimate the ^{137}Cs concentration with the JAEA source term. However, the EMAC T106 and T255 are reasonably consistent with the Stohl et al. (2012) source term and tend to underestimate the ^{137}Cs concentration with the JAEA source term. From these results, we cannot conclude which of these source terms more realistically represents the release rate of ^{137}Cs.

4.8. Ensemble average

To derive the statistical average and magnitude of variance of the global simulations evaluated in the intercomparison, an ensemble analysis was performed. Because the horizontal resolutions of the simulated results were different between the models, the data were resampled into a $1° \times 1°$ grid. The simulated results that did not use the JAEA source terms from Terada et al. (2012) were scaled to the magnitude of Terada et al. (2012) so that the relative importance of the spatial variations were equally evaluated among the simulations. Figure 4.6 shows the ensemble average and the coefficient of variation (the ratio of the standard deviation to the average) of the total ^{137}Cs deposition until the end of March 2011. Relatively small coefficients of variation can be found in the highly contaminated area of the Pacific Northwest region, which indicates that the uncertainties of the ^{137}Cs deposition amount were relatively small. Areas that were further apart from the FDNPP showed larger coefficients of variation, which means that considerable variation existed among the simulations and that the simulated results were highly uncertain.

4.9. Summary

For the intercomparison of the global transport of radionuclides from the FDNPP

accident, five global transport models and one regional transport model contributed to the long-range transport comparison, and 12 simulated results were submitted. The simulated results included source terms that were inversely analyzed by the Japan Atomic Energy Agency (Chino et al., 2011; Terada et al., 2012) or Stohl et al. (2012). The simulated results were compared with each other and with available observations. Most of the models removed ^{137}Cs from the atmosphere mainly by wet deposition, which accounted for 88 to 100% of the total deposition. The results showed a large dependence on the differences in the treatment and magnitude of wet depositions and, therefore, the lifetime of the ^{137}Cs.

Generally, the contributed results were relatively consistent in the pattern of ^{137}Cs deposition over the Northwestern Pacific, which stretched to the Aleutian Islands and reached the western side of North America. Differences were found in the long-range transportation to areas of Europe and Russia. The models also exhibited differences in the transport to Southeast Asia by the Asian winter monsoon.

The comparison of the simulated results with the observed data of the atmospheric concentration of ^{137}Cs were relatively consistent, although the simulated results tended to underestimate the low concentration range (< ~0.01 µBq m^{-3}). From the intercomparison, we cannot conclude which of these source terms of ^{137}Cs (JAEA or Stohl et al. (2012)) was more realistically representative of the release rate of ^{137}Cs.

Table 4.1. Specifications of the participating numerical models.

Model name	SPRINTARS	MASINGAR mk-2	MASINGAR-1	MPIC/ EMAC v1.92	TM5	MRI-PM/r
Institute	Kyushu University	MRI, JMA	MRI, JMA	Cyprus Institute	KNMI	MRI, JMA
Region	Global	Global	Global	Global	Global	Regional
Source term	JAEA (Terada et al. 2012)	JAEA (Terada et al. 2012), Stohl et al.(2012)	JAEA (Terada et al. 2012), Stohl et al.(2012)	JAEA (Chino et al. 2011), Stohl et al.(2012)	JAEA (Terada et al. 2012)	JAEA (Terada et al. 2012)
Resolution (grids)	T213 (640×320)	TL319 (640×320)	T106 (320×160)	T106 (320×160), T255 (768×384)	3° × 2° (120×90)	60 km (234×120)
Layers	20 (~8 hPa)	40 (~0.4 hPa)	30 (~0.4 hPa)	31 (~10 hPa)	60	20 (~10 km)
Eulerian or Lagrangian	Euler	Euler	Euler	Euler	Euler	Euler
Dynamics	Online (MIROC)	Online (MRI-AGCM 3)	Online (MRI/JMA 98)	Online (ECHAM5)	Offline (ECMWF)	Offline (WRFv3)
Meteorological Analysis	NCEP reanalysis, nudging technique	JCDAS (extended, near real time JRA-25), Newtonian nudging technique	JCDAS (extended, near real time JRA-25), Newtonian nudging technique	ECMWF ERA-Interim (for nudging dynamics only, precipitation is model generated)	ECMWF Operational Data	NCEP FNL analysis, grid nudging technique

Table 4.2. Simulated total, wet and dry deposition of ^{137}Cs until March 31, 2011.

|	Total Deposition [PBq]	Total wet Deposition [PBq]	Total dry Deposition [PBq]	Wet/Total ratio[%]
SPRINTARS	8.33	7.30	1.03	87.6
SPRINTARS1	8.42	7.43	0.99	88.2 [†]
MASINGAR mk-2 (JAEA)	7.05	6.93	0.13	98.2
MASINGAR mk-2 (Stohl)	34.61	34.08	0.53	98.5 [†]
MASINGAR-1 (JAEA)	6.63	6.45	0.18	97.3
MASINGAR-1 (Stohl)	32.86	31.97	0.9	97.3 [†]
EMAC T255 (JAEA)	5.46	5.10	0.36	93.4
EMAC T255 (Stohl)	34.59	33.13	1.45	95.8 [†]
EMAC T106 (JAEA)	5.50	5.24	0.25	95.4
EMAC T106 (Stohl)	34.27	32.74	1.53	95.5 [†]
KNMI TM5 (JAEA)	8.28	8.28	0.0	100.0 [†]
MRI-PM/r	4.45	3.85	0.6	86.5
ensemble mean	15.87	15.21	0.72	93.4
standard deviation	13.51	13.19	0.49	4.6

† : excluded from the ensemble calculation
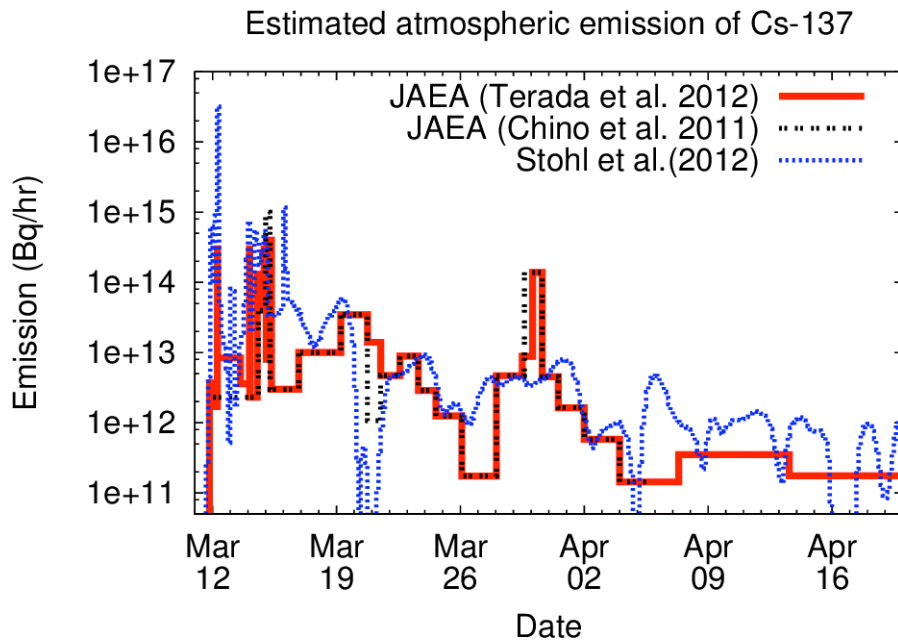
Figure 4.1. Comparison of the time series of the estimated source terms of ^{137}Cs used in the intercomparison of the global transport simulations.
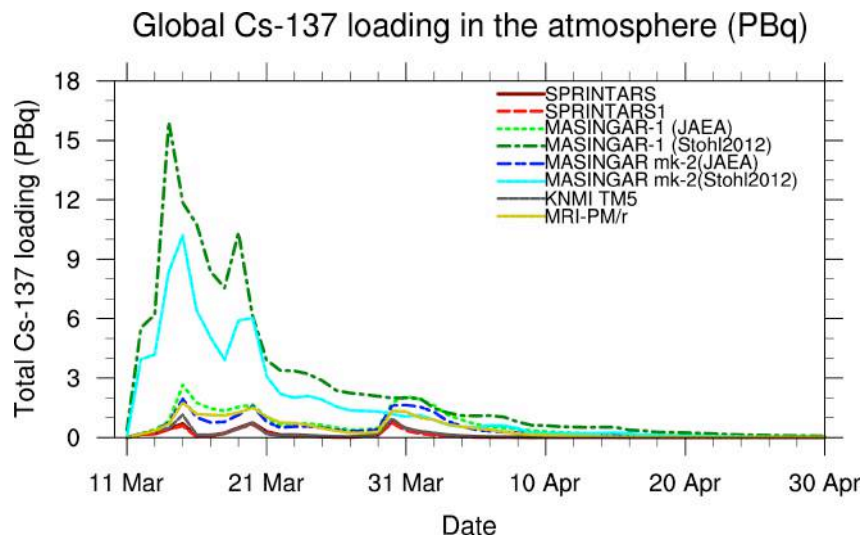

Figure 4.2a. Comparison of the time series of the simulated global total atmospheric loading of ^{137}Cs.
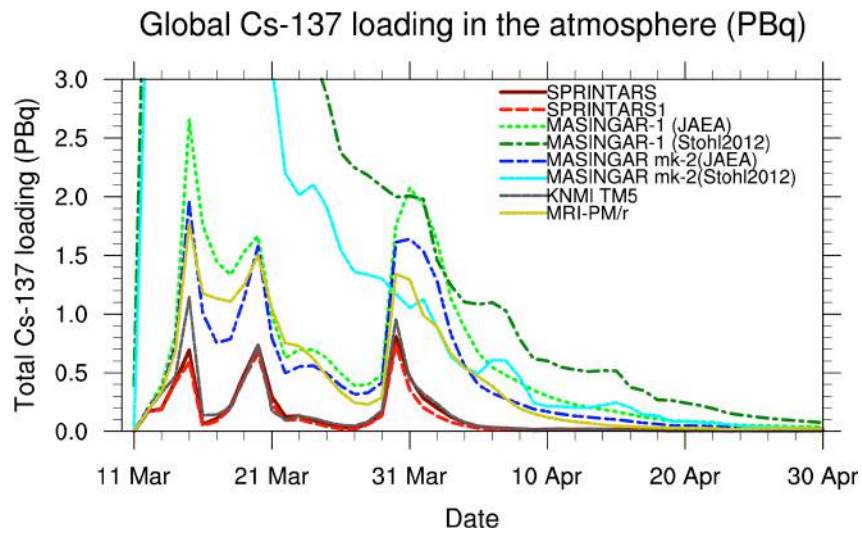
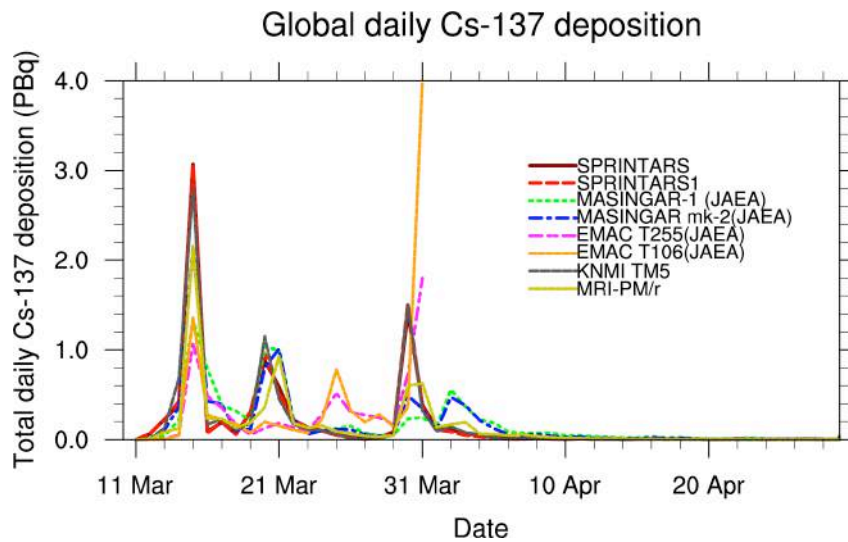Figure 4.2b. Same as Fig. 4.2a but with a different ordinate scale.

Figure 4.3a. Comparison of the time series of the simulated global total daily deposition of ^{137}Cs with estimated source terms by the JAEA (Chino et al., 2011; Terada et al., 2012).
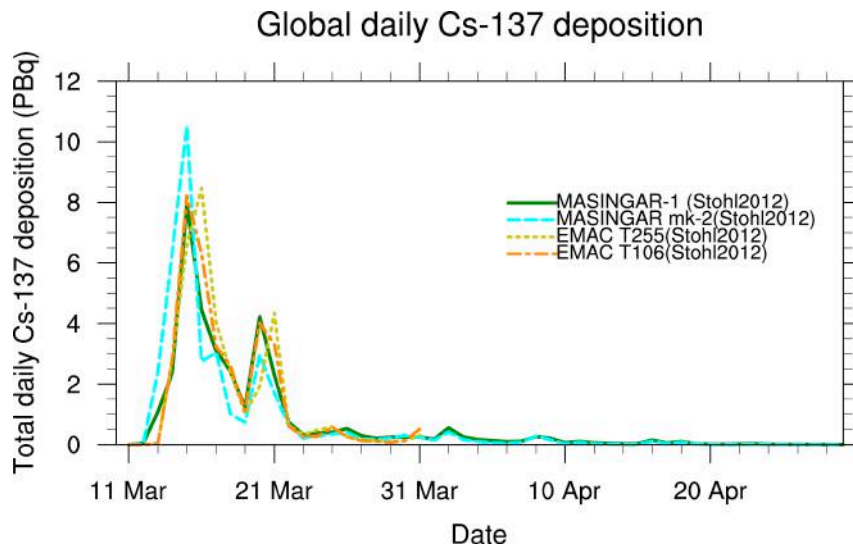
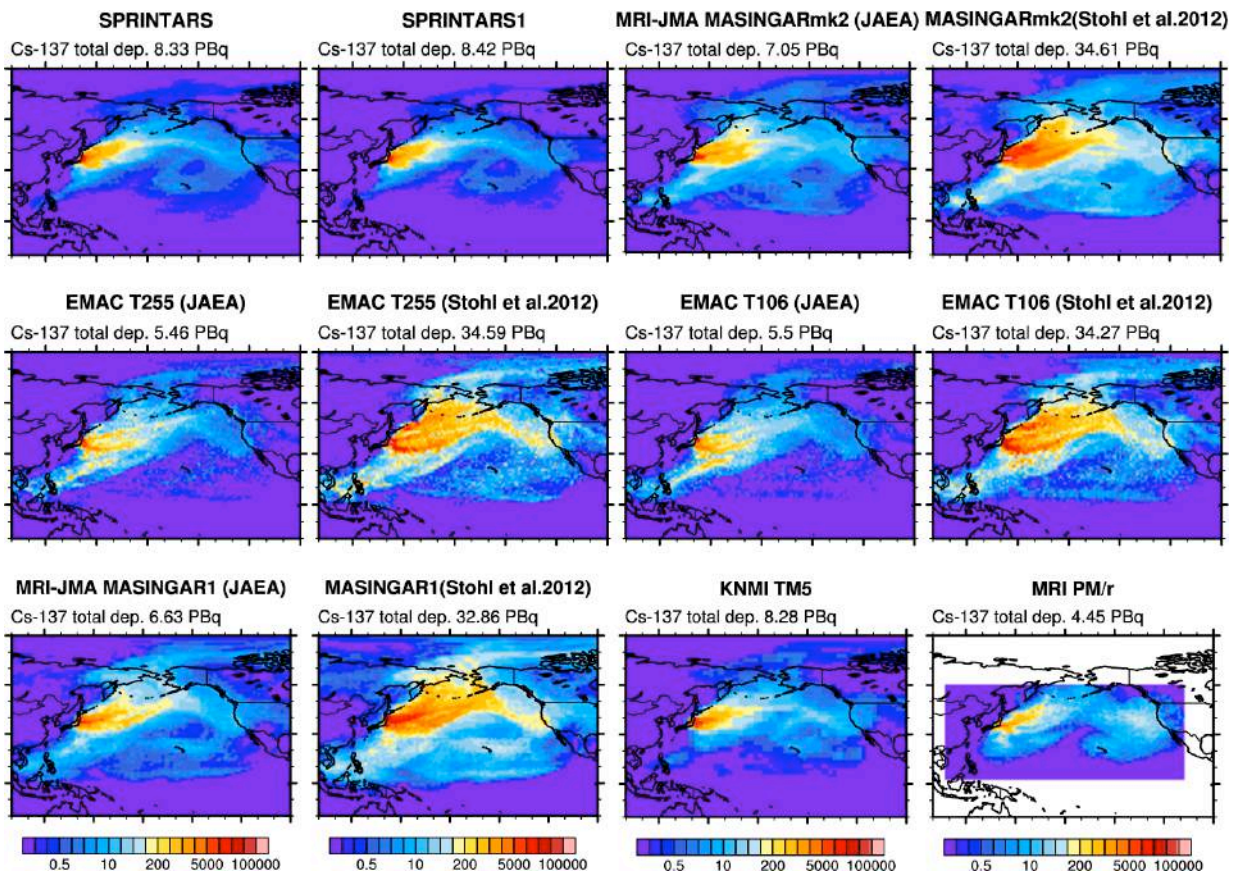Figure 4.3b. Same as Fig. 4.3a but with estimated source terms by Stohl et al. (2012).

Figure 4.4. Horizontal distributions of the accumulated ^{137}Cs deposition from March 11 to 31, 2011. Units are Bq m^{-3}.
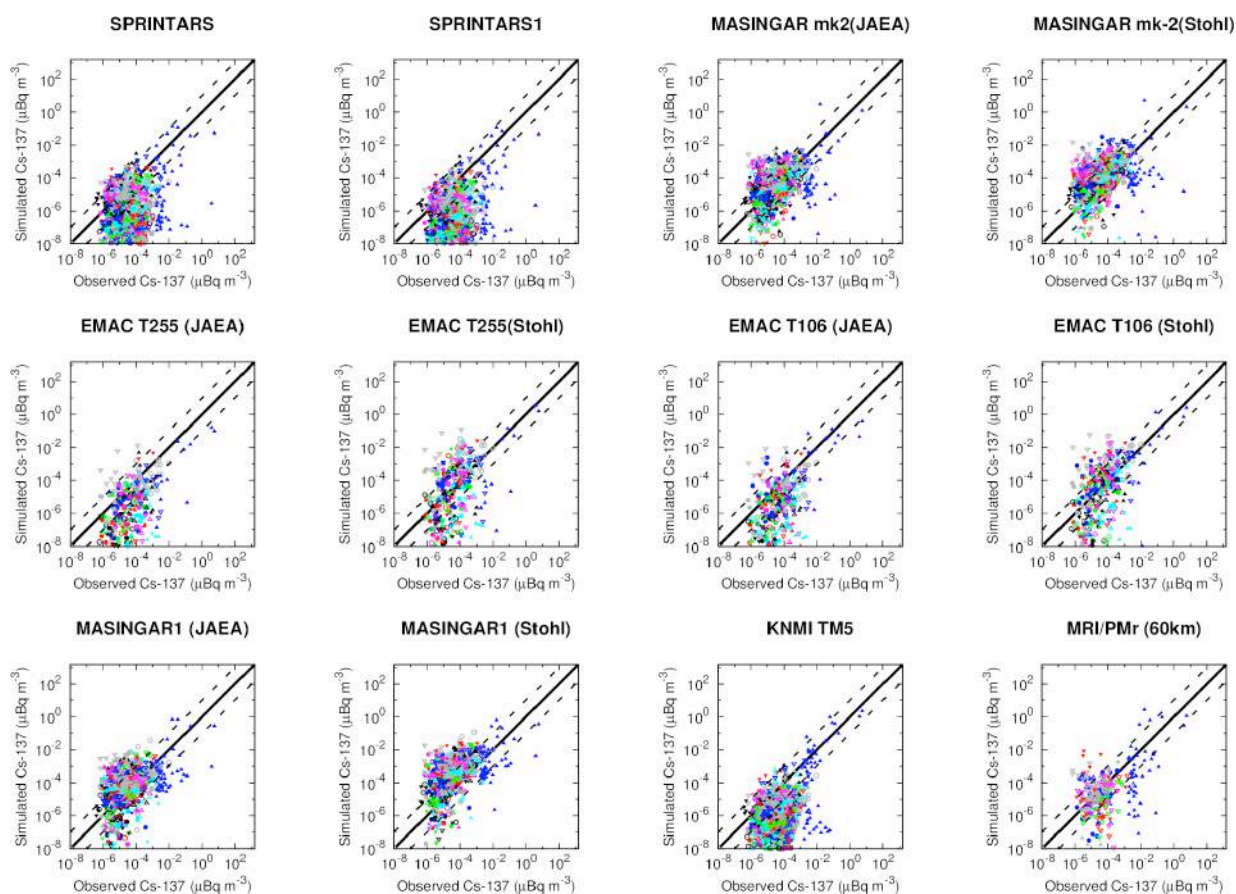
Figure 4.5. Scatter plots of the observed and simulated atmospheric ^{137}Cs concentrations. The thick solid line in the middle is the one-to-one line, and the upper and lower dashed lines are overestimates and underestimates by a factor of 10.

(a) Ensemble averaged ^{137}Cs total deposition (11 Mar. - 31 Mar.)
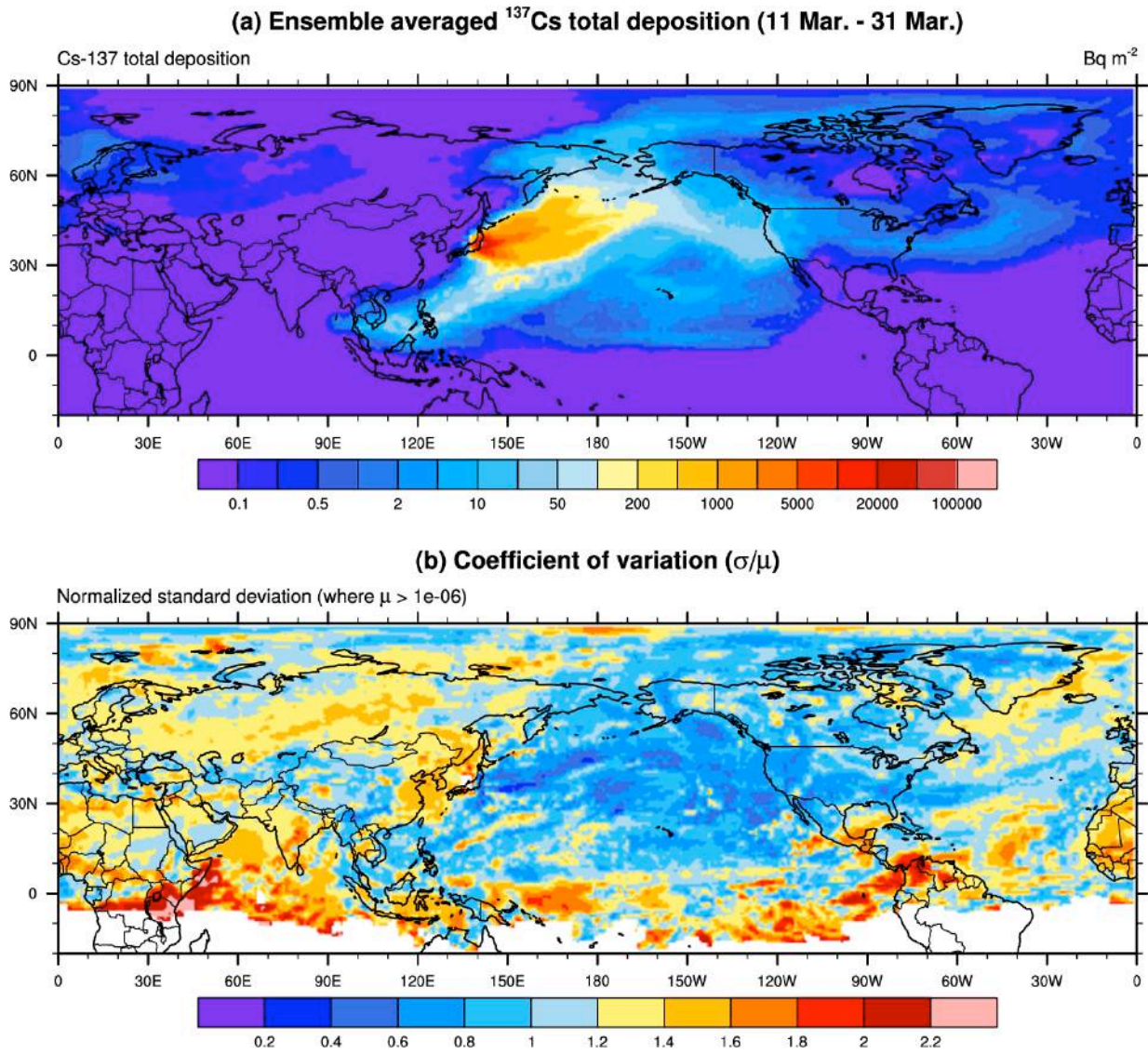
(b) Coefficient of variation (σ/μ)

Figure 4.6. (a) Ensemble average and (b) coefficient of variation of the accumulated deposition of ^{137}Cs until March 31, 2011 with the evaluated simulations.

26

5. Oceanic dispersion model intercomparison

5.1. Models

The oceanic dispersion model intercomparison is based on eleven models from ten groups. The numerical models for the dispersion of radionuclides in the ocean generally consist of two parts. The first part is an oceanic circulation model that calculates evolving circulation patterns in which the observed physical parameters can be directly assimilated or the assimilated fields can be used as the boundary conditions. The second part is a dispersion model that calculates the movement and spread of radionuclides in the ocean based on the circulation patterns produced by the oceanic circulation models. The specification of basic model settings and characteristics for the participating models are listed in Table 5.1, and the model domains are summarized in Fig. 5.1. Detailed descriptions for each model can be found in Appendix A.

The domain, grid system, and grid spacing differ significantly among the models and reflect the different main foci of their studies. In addition, there are two conceptually different formulations of the radionuclide dispersion calculation. Seven models use the Eulerian framework, and the remaining four models utilize Lagrangian particle tracking methods.

All of the models have a source term of the radionuclide directly discharged from the FDNPP. For the temporal evolution of the direct discharge, some models adopt a scenario similar to the one proposed by the JAEA (JAEA type; see Kawamura et al., 2011), which incorporates shorter time-scale variations, whereas the other models utilize a simplified scenario proposed by the CRIEPI (CRIEPI type; see Tsumune et al., 2012). The total amount of directly discharged ^{137}Cs differs significantly among the models, and the values range from 3.5 PBq to 26.9 PBq (Fig. 5.2).

The seven models also include ^{137}Cs deposited to the ocean surface from the atmosphere, and the deposition is calculated by the atmospheric dispersion models. Figure 5.3 shows the horizontal distribution of accumulated ^{137}Cs depositions until April 1st, 2011 from the seven models, and significant differences in the spatial distribution and the amount of deposition are found among the models. The uncertainty in the source terms and models themselves is inevitably mirrored in the subsequent results of oceanic dispersion.

27

5.2. Dispersion of surface ^{137}Cs activity

The ten-day averaged ^{137}Cs concentrations and circulation fields at the upper-most level of each model in a region off of the Tohoku area are compared in Fig. 5.4 to Fig. 5.7. The monitoring observation results are also shown in Fig. 5.4 and Fig. 5.6 as a reference for the model results. Here, we only show the results for the March 22-31 and April 21-30 periods. Appendix B summarizes all of the ten-day averaged data until the end of June 2011.

March 22-31

The monitoring data indicate high concentrations of ^{137}Cs larger than 20,000 Bq m^{-3} along the coast near the FDNPP (Fig. 5.4(l)). The data from the observation stations 30 km offshore from the coast also show ^{137}Cs contamination with a magnitude of approximately 10,000 to 15,000 Bq m^{-3}. The lack of observations, unfortunately, makes it difficult to assess the details of the simulated ^{137}Cs distributions at the end of March.

Most of the models capture the high ^{137}Cs concentration along the coast of Fukushima that tends to expand southward at the end of March (Fig. 5.4). The surface current fields in these models demonstrate a weak southward flow at a magnitude of 10 cm s^{-1} or less along the coast in front of the FDNPP (Fig. 5.5). The local flow patterns along the coast are susceptible to wind forcing over this region, show a higher temporal variability associated with synoptic weather disturbances, and subsequently generate coastal trapped waves in the ocean.

A large difference among the model results in terms of the ^{137}Cs distribution pattern is generated from the assumptions of atmospheric deposition. The ^{137}Cs distributions in the KIOST/IMMSP, Kobe U, MSSG, and WHOI-3D models with no atmospheric deposition are confined along the Fukushima coast, whereas those in the CRIEPI, JAEA, JCOPE, NIES, and WHOI-2D models with atmospheric deposition indicate relatively large ^{137}Cs concentrations in a wide region, even in the offshore area. Relatively large concentrations in a region near the Sendai Bay in the latter five models are a distinct example of the difference. Note that the IRSN model includes an atmospheric deposition at the sea surface; however, the deposited area is limited to the coastal region near the FDNPP (see Fig. 5.3).

Another important factor that determines the distribution of ^{137}Cs in offshore regions is a broad southward flow off of the Tohoku area in a region east of 141.5°E and north of approximately 36.5°N with the magnitude of 20 to 50 cm s^{-1} (e.g., Fig. 5.5(a), (i), (k), and others). The ^{137}Cs contamination in the offshore region tends to spread southward between the coast and the region of the southward flow. Concurrently, the southward flow brings

water with a low-contamination from the north and creates complex spatial distributions of ^{137}Cs concentrations. The contaminated water is then captured by the northern flank of the eastward flowing Kuroshio Current (see Fig. 5.4(i) and Fig. 5.4(j) for clear examples).

Although the general tendencies of the current fields and ^{137}Cs distributions are similar, the small-scale distributions are different among many models. Such an example can be observed in the eddy-like structures of the surface current and associated ^{137}Cs distributions off of the coast of Ibaraki in the region between 36.7°N and the Kuroshio Current. Clear examples of the anticyclonic eddy can are centered at 36.4°N, 141°E in the KIOST/IMMSP (Fig. 5.5(f)) and MSSG (Fig. 5.5(h)) cases. A similar eddy structure with weaker magnitude can also be observed in other model results (see the figures for April 1-10 in Appendix B); however, the structure appears as part of a strong dipole eddy structure in the JAEA (Fig. 5.5(d)) and WHOI-3D (Fig. 5.5(k)) results. The horizontal distribution of the sea-surface temperature and chlorophyll-a concentrations from satellite observations indicate a warm-core eddy-like feature off the coast of Ibaraki from the end of March to May (see Appendix C), which indicates anti-cyclonic circulation. The ^{137}Cs concentrations of the CRIEPI, JAEA, JCOPET, and NIES results are affected by the eddy structure, whereas those in the other models did not reach the region of these eddies by the end of March.

April 21-30

In the observations for April 21-30, the high ^{137}Cs concentration spreads toward the offshore area by the end of April, whereas the radioactivity along the line 30 km offshore reduces slightly to an approximate value of 10,000 Bq m^{-3} or less, except for three locations where a value of more than 20,000 Bq m^{-3} are observed (Fig. 5.6(l)). New observation stations are set in the region off of Ibaraki; however, the observed values are all under the detection level, which is set to 10,000 Bq m^{-3} for this time period.

Most of the models show a northeasterly dispersion of the ^{137}Cs at the end of April (Fig. 5.6); this dispersion appears to be associated with the northeastward surface flow distributed near the FDNPP that is linked to the anticyclonic circulation off of the Ibaraki coast (Fig. 5.7). This northeastward dispersion is broadly consistent with the radioactivity distribution near the coast of the FDNPP that was observed by aerial measurements on April 18, 2011 (Appendix D), although the observation shows only a limited area near the FDNPP. The anticyclonic circulation off the Ibaraki coast tends to prevent the high ^{137}Cs from coming down to the south along the coast. The IRSN and WHOI-2D cases, however, show high ^{137}Cs concentration off of the Ibaraki coast, most likely as a result of weak or no anticyclonic eddy

in the circulation fields.

However, the southern or southeasterly movements of the ^{137}Cs in the offshore region can also be observed in many of the model results except for the IRSN and MSSG cases. This relatively high ^{137}Cs transported to the south or southeast is captured by the northern flank of the Kuroshio Current, which spreads the ^{137}Cs quickly to the east into the interior of the Pacific Ocean. The above suggests that the surface circulations in the region between 37°N and the Kuroshio Current are sensitive to the small-scale current fields that are mainly associated with the meso-scale eddies and variability of the Kuroshio Current, which in turn are strongly affected by the data assimilation processes in the larger domain models.

Note that the observed monitoring stations can cover only a small portion of the region with relatively high concentrations, which suggests the necessity of a wider monitoring network to estimate the radionuclide distribution and to evaluate the model results.

5.3. Comparison with observed time series

To verify the model performance in reproducing a time series of the surface ^{137}Cs concentration near the FDNPP, we have compared the time series of the simulated ^{137}Cs concentrations at the Fukushima Dai-ni (2F) NPP, Iwasawa coast (Fig. 5.8), and 30 km offshore monitoring stations (Fig. 5.9) with the observed values. The 2F NPP and Iwasawa coast are located approximately 10 km and 16 km south of the FDNPP, respectively. Until mid-April, many of the models produced relatively accurate reproductions of the time variations at the 2F NPP, including the short period of variability from late March and early April, which is associated with the local wind variations. Although a gradual decrease of the ^{137}Cs concentrations is well-simulated by all of the models, half of the models underestimate the ^{137}Cs concentrations after mid-April. One reason for this underestimation could have resulted from influences of the atmospheric deposition in March and early April still existing over a large area near the coast as well as the offshore regions. As will be discussed later, however, the atmospheric deposition into the ocean appears small in all of the models and causes an underestimation of the ^{137}Cs concentrations near the 2F NPP. Another possible reason for the underestimation is the northward flow along the Fukushima coast during late April that is mentioned in section 2; in this flow, water with low ^{137}Cs concentrations is transported from the south to the Fukushima coast. However, as a result of a lack of any observed current data for this time period off the coast of Fukushima, it is difficult to evaluate the simulated current field, especially near the coastal region.

The discrepancy between the observed and simulated time series becomes larger in

general for the 30-km offshore stations. Because the direct discharge of ^{137}Cs from the FDNPP starts in late March and because the four models (GEOMAR, KIOST/IMMSP, Kobe U, and MSSG) without atmospheric deposition significantly underestimate the ^{137}Cs concentration during March, it is reasonable to assume that this offshore contamination during March and early April is a result of atmospheric deposition. This is consistent with the conclusion of Tsumune et al. (2012), who analyzed the ratio of the ^{131}I/^{137}Cs activities. Even the models that include atmospheric deposition underestimate the ^{137}Cs concentrations before mid-April. This suggests that all of the atmospheric deposition data may be too small to provide adequate boundary conditions for the oceanic dispersion simulations.

Again, most of the models produced a significant underestimation of the ^{137}Cs concentrations in late April and May. Therefore, more thorough analyses and comparisons of the current fields and associated dispersion of ^{137}Cs are necessary to determine the possible reasons for the discrepancy, which may be different from those for the coastal region.

5.4. Comparison with R/V Ka'imikai-o-Kanaloa observations

Additional important observed reference data for the evaluation of the model performance in reproducing the ^{137}Cs dispersion was collected during the R/V Ka'imikai-o-Kanaloa (KOK) cruise in June 2011 in the Kuroshio extension region and a region off of the Fukushima and Ibaraki coasts (Buesseler et al., 2012). Fig. 5.10 and Fig. 5.11 compare the horizontal distribution of ^{137}Cs at the sea surface and at a depth of 100 m, respectively, between each model result and the observed values. Most of the model results indicate that the ^{137}Cs spreads across a much wider area, particularly to the north and northeast of the observation array, compared to the observed region. All of the models capture the region of high ^{137}Cs concentrations off the coast of Fukushima and Ibaraki at the surface, whereas several models do not show the high concentration off the coast at a 100 m depth. The R/V KOK observations demonstrate that the maximum concentration of ^{137}Cs at the surface does not appear at the observation station closest to the FDNPP but at the stations at approximately 36.3°N, 141.7°E. As suggested by Buesseler et al. (2012), the meso-scale eddies and associated streamer-like structures can be observed in several model results, which supports the rapid spread of ^{137}Cs as a result of relatively strong ocean currents. However because the simulated current fields in each model differ significantly as a result of the different model settings and nonlinear nature of the current variations, each model shows a different horizontal distribution of ^{137}Cs concentrations in the study area.

The total inventory of ^{137}Cs within the observed area is reported as 1.9 to 2.1 PBq

(Buesseler et al., 2012). Fig. 5.11 also indicates the inventory values within the observed area in the middle of June for each model result, in which the value spans from 1.33 PBq to 4.52 PBq. These wide-spread inventories in the simulated results reflect different vertical profiles of ^{137}Cs averaged within the observed area (Fig. 5.12). Three models (IRSN, JCOPET, and NIES) that produce high inventory values tend to overestimate the subsurface ^{137}Cs concentrations in the off-shore region (35.0°N-38.0°N, 143.5°E-147.0°E), whereas the other models appear to underestimate the concentrations in the layer below a depth of 25 m. However, in the near-shore region (36.0°N-38.0°N, 141.4°E-143.5°E), all of the models tend to underestimate the concentrations compared to the observed values. Such differences in vertical profiles among the model results could have been caused by the different vertical mixing parameterizations and mixing coefficients used in each model. In addition, the surface momentum, heat and freshwater fluxes may also affect the vertical mixing process near the sea surface. Another factor controlling the vertical profiles, particularly near the bottom, might be a scavenging process and the transport of radionuclides between the sea-water and bottom sediments. Observations at this stage do not show the importance of the latter processes on the ^{137}Cs concentrations in the whole water column. However, they may be important in the near-shore region when water that is highly contaminated by ^{137}Cs is discharged directly from the FDNPP and generates "hot spots" of highly contaminated areas on the sea floor. Most of the models except for the JAEA, KIOST/IMMSP, and MSSG do not incorporate the scavenging and transport processes near the bottom in their model formulations.

5.5. Concluding remarks

Although there are notable similarities among the model results, significant discrepancies are identified in both the spatial distributions and temporal variations of the ^{137}Cs concentration as shown in Sections 5.2 and 5.3. Considering the quantitative differences among the models due to mixing and scavenging/transport effects, a simple comparison is not straightforward. Detailed systematic comparison studies, such as ones that use the same radionuclide forcing with different models and/or the same model with different forcing scenarios, are required. Considering the significant uncertainty in the surface flux forcing, ocean circulation fields, and mixing and scavenging/transport parameterizations, we cannot conclude at this stage which model produces the most accurate simulations of the ^{137}Cs distribution discharged by the FDNPP accident. Further efforts under international coordination are required.

Table 5.1. Model specifications

| Model	Resolution (degrees)	Grids	Dispersion model type	Atmospheric Fallout	Direct discharge	Note
CRIEPI	1/120 ×1/120	855 × 615	Euler	CRIEPI	CRIEPI type (3.5 PBq)	
GEOMAR	1/8 × 1/10	480 × 284	Euler	N/A	Instant release (2.3 PBq)	Using 1993 ECMWF forcing, which yields similar oceanic conditions as 2011 (Dietze and Kriest, 2012)
IRSN	1/48 × 1/60	623 × 743	Euler	IRSN pX	IRSN (26.9 PBq)	Wind-tuned Case
JAEA	1/54 × 1/72	191 × 218	Lagrangian	JAEA	JAEA type (3.5 PBq)	
JCOPET	1/36 × 1/36	830 × 578	Euler	JAMSTEC	CRIEPI type (6.0 PBq)	
KIOST	1/60 × 1/60	601 × 661	Euler	N/A	JAEA type (3.8 PBq)	Original grid is an unstructured system
Kobe U	1km × 1km	512 × 512	Euler	N/A	CRIEPI type (6.9 PBq)	Model domain is rotated horizontally to align with the Fukushima coastline
MSSG	1/55.6×1/55.6	168 × 239	Lagrangian	N/A	CRIEPI type (5.7 PBq)	
NIES	1/20 × 1/20	91 × 97	Euler	NIES	CRIEPI type (3.6 PBq)	
WHOI-2D	1/10 × 1/10	351 × 111	Lagrangian	Stohl et al. (2012)	JAEA type (16.2 PBq)	Geostrophic flow with satellite sea-surface height data
WHOI-3D	1/10 × 1/10	170×101	Lagrangian	N/A	JAEA type (16.2 PBq)	NCOM output
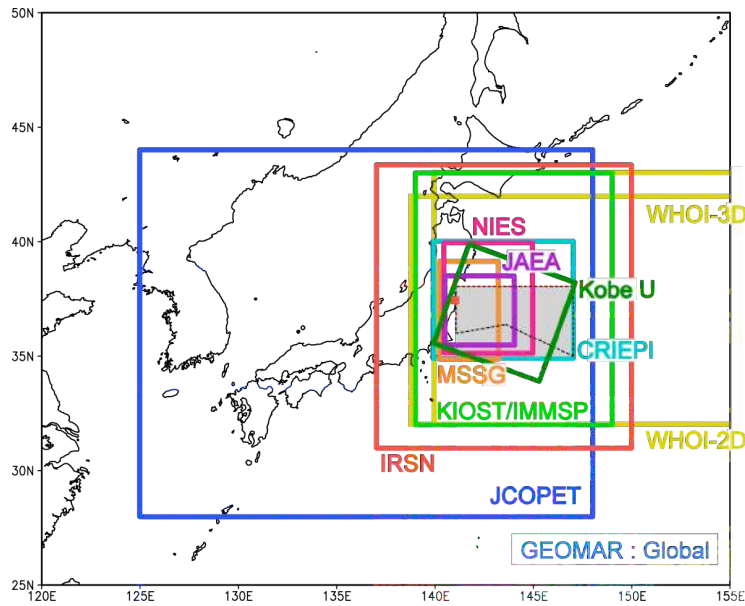
Figure 5.1. Domain of each model evaluated in the model intercomparison. A red square indicates the location of the FDNPP. The region surrounded by dotted lines shows the area of observations conducted by the KOK cruise (Buesseler et al., 2012), and the gray square is the region in the models compared with the KOK observations.
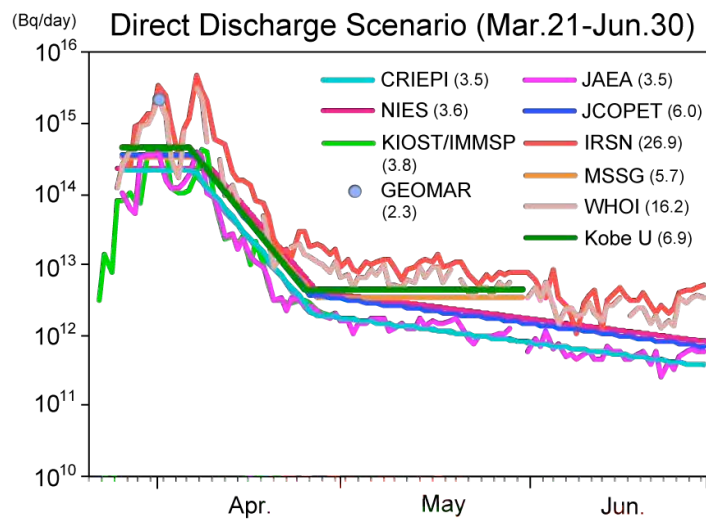

Figure 5.2. Time series from March 21 to June 30, 2011 of the ^{137}Cs direct discharge from the FDNPP into the ocean in each model. Numbers in parentheses in the legend indicate the total discharged amount of ^{137}Cs for each model.
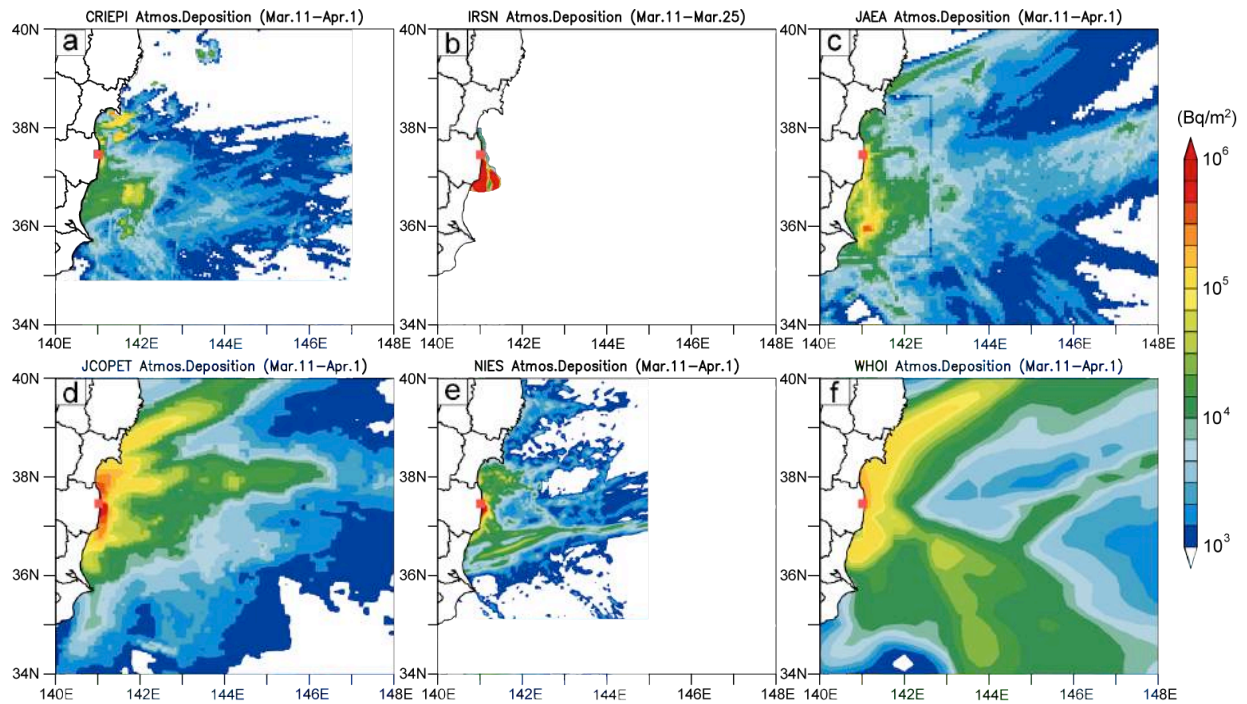
Figure 5.3. Cumulated atmospheric deposition of ^{137}Cs from March 11 to April 1, 2011 for the (a) CRIEPI, (b) IRSN, (c) JAEA, (d) JCOPET, (e) NIES, and (f) WHOI models. Only the deposition over the ocean is shown. Note that the period of accumulation is from March 11 to 25 for the IRSN case. The WHOI-2D and WHOI-3D models use the same atmospheric deposition as shown in (f).
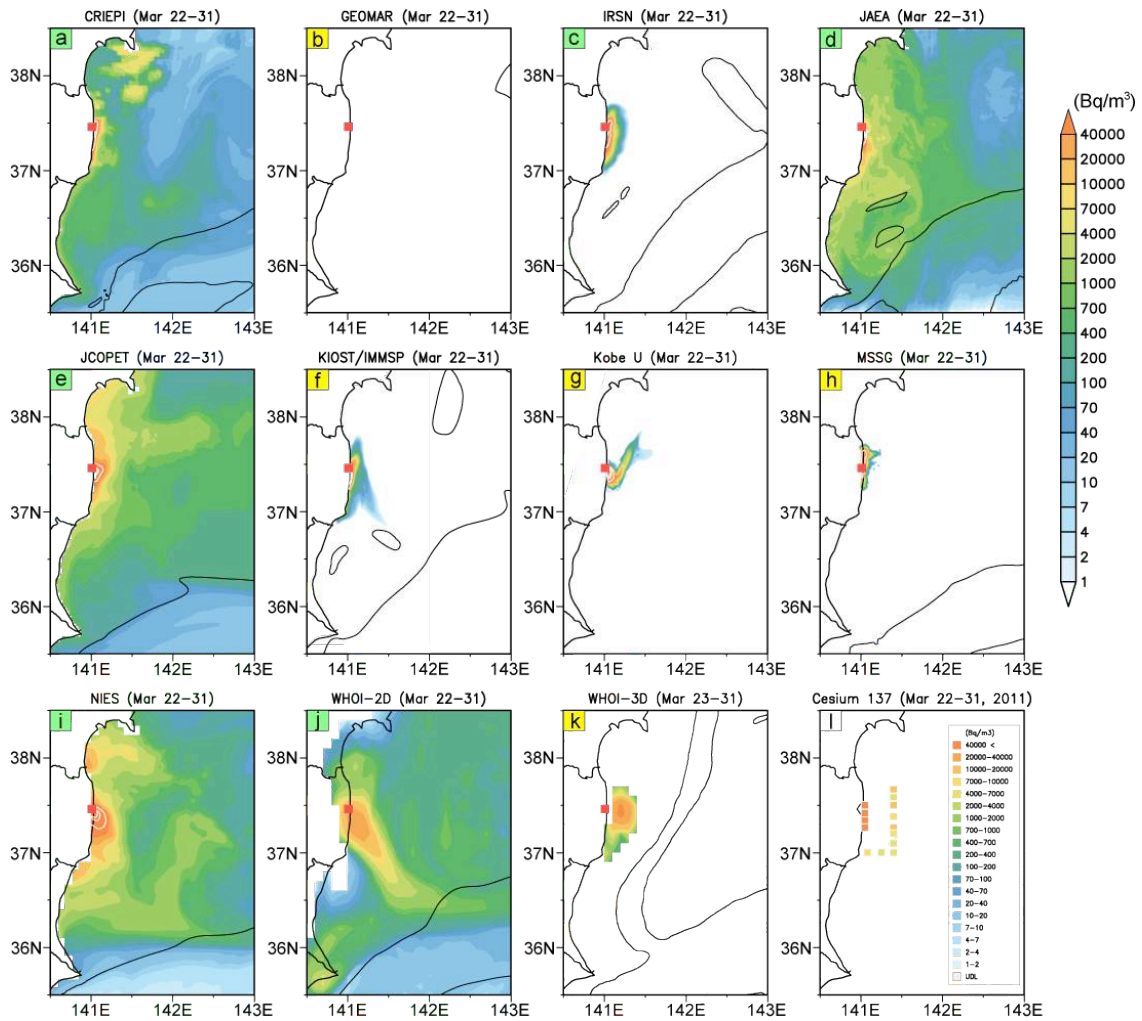
35

Figure 5.4. (a)-(k) Horizontal distributions of the ^{137}Cs concentrations averaged over a 10-day period from March 22 to 31, 2011, with the name of the models indicated above each panel. Red squares indicate the location of the FDNPP. Black thin lines superimposed onto the ^{137}Cs concentration indicate contours of 0.5 m/s of surface current magnitude and show the general locations of the Kuroshio Current and other dominant features in this region. Panels with green (yellow) labels show results from models with (without) atmospheric deposition. Panel (l) shows the distribution of the observed ^{137}Cs concentrations during the same 10-day period.
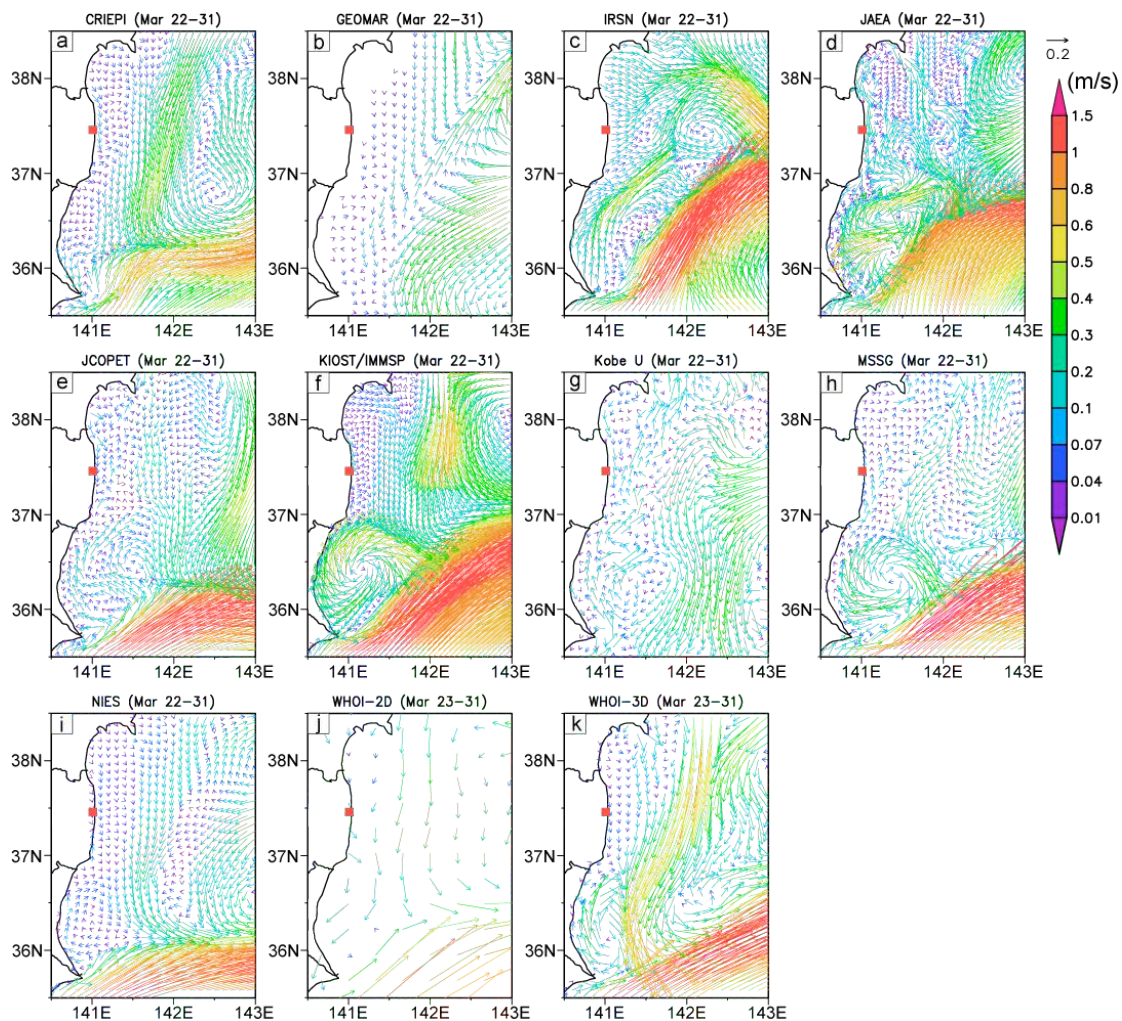
Figure 5.5. Horizontal distribution of surface velocity fields averaged over a 10-day period from March 22 to 31, 2011 that was simulated in each model. The model name appears above each panel. The WHOI-2D has a course resolution based on the observed sea-surface height data with the geostrophic calculation. Other results are based on high-resolution ocean models. Note that the GEOMAR is forced by the ECMWF fluxes from 1993, which yields oceanic conditions similar to those actually encountered in 2011 (see Dietze and Kriest, 2012).
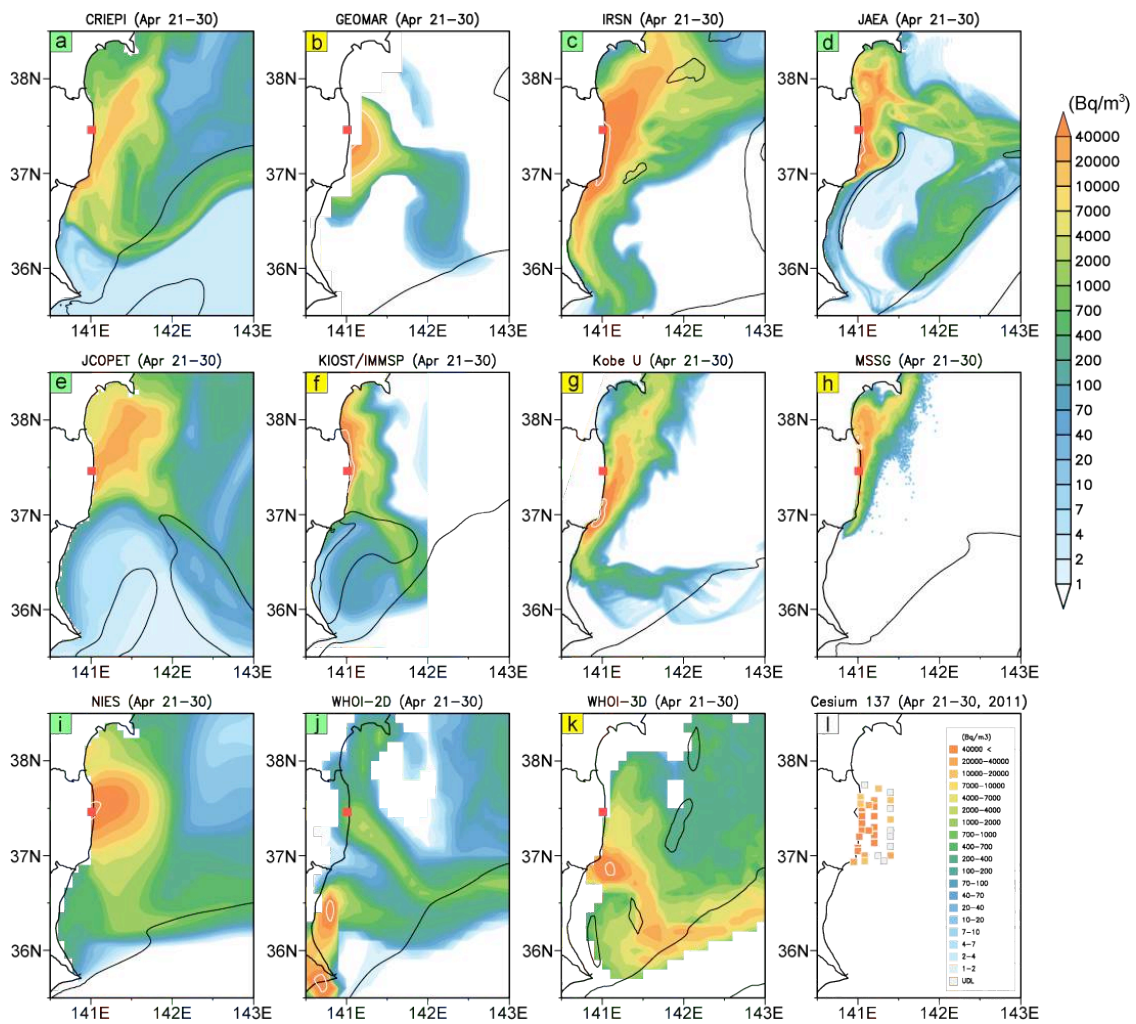
Figure 5.6. Same as in Fig. 5.4 except for the 10-day average during the period from April 21 to April 30, 2011.
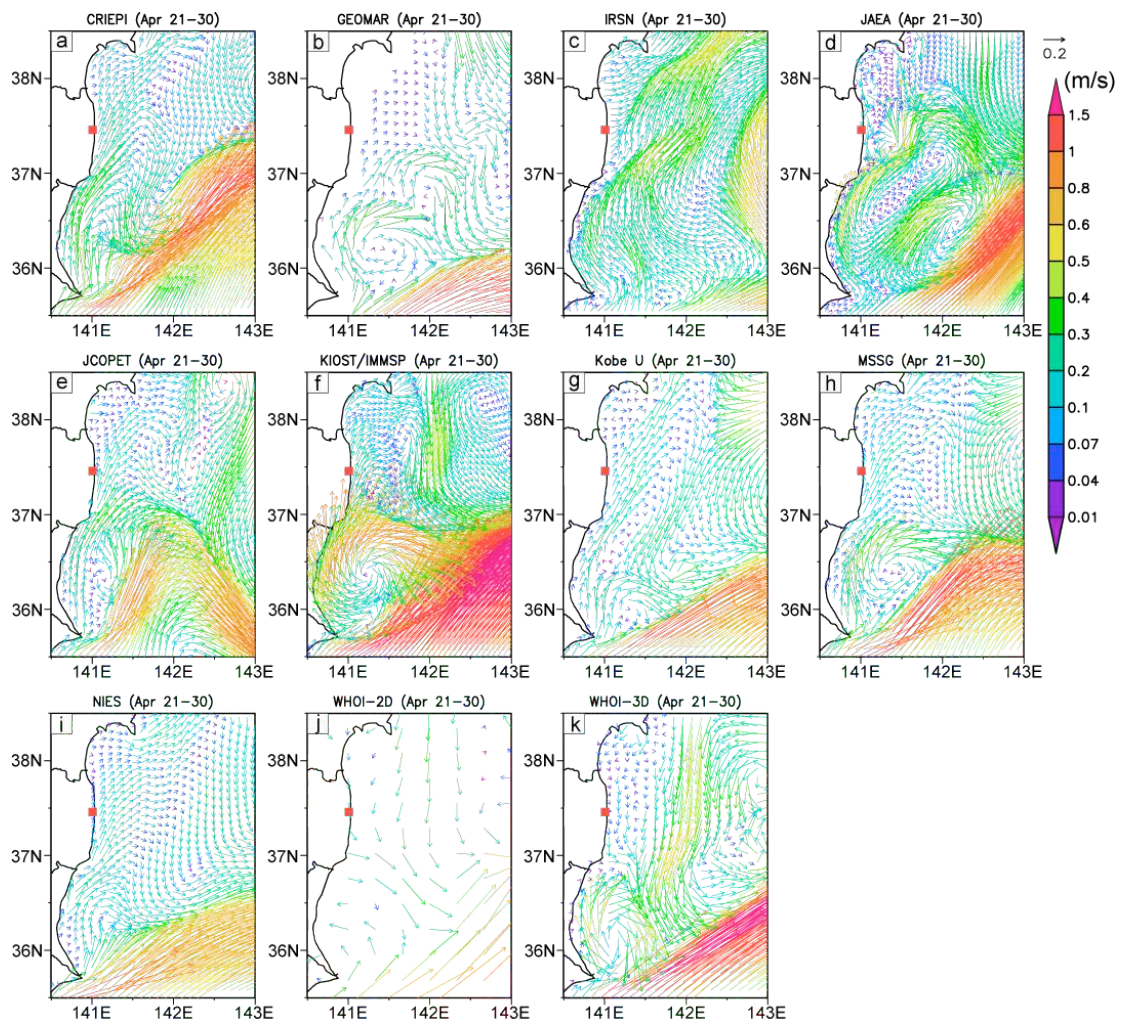
Figure 5.7. Same as in Fig. 5.5 except for the 10-day average during the period from April 21 to April 30, 2011.
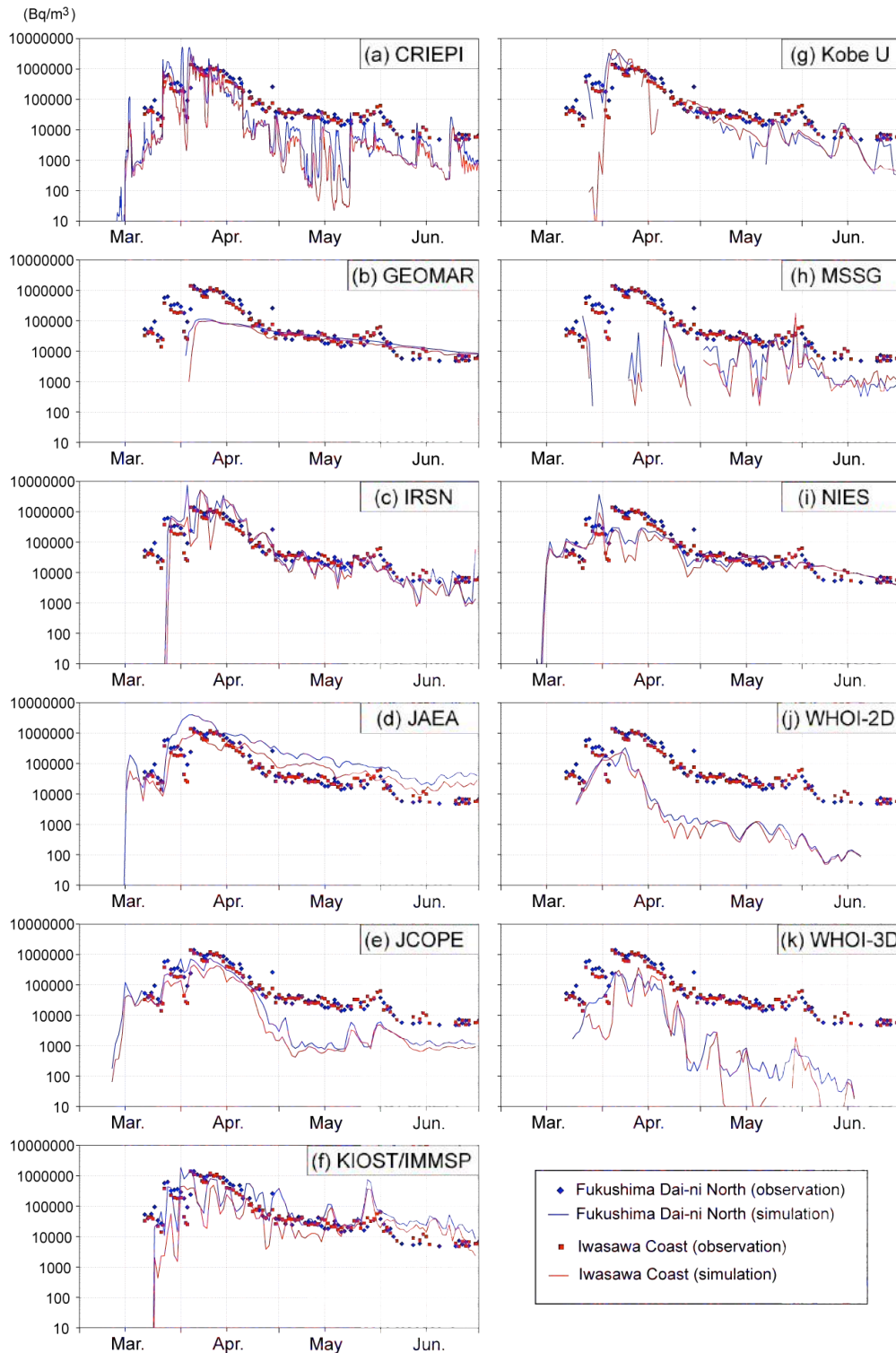
Figure 5.8. Time series of ^{137}Cs concentrations during March through June 2011 at the Fukushima Dai-ni (2F) Nuclear Power Plant and the Iwasawa coast. The observed values are indicated by solid diamonds, whereas the simulated time series are shown with solid lines (blue: Fukushima Dai-ni Nuclear Power Plant, red: Iwasawa coast).

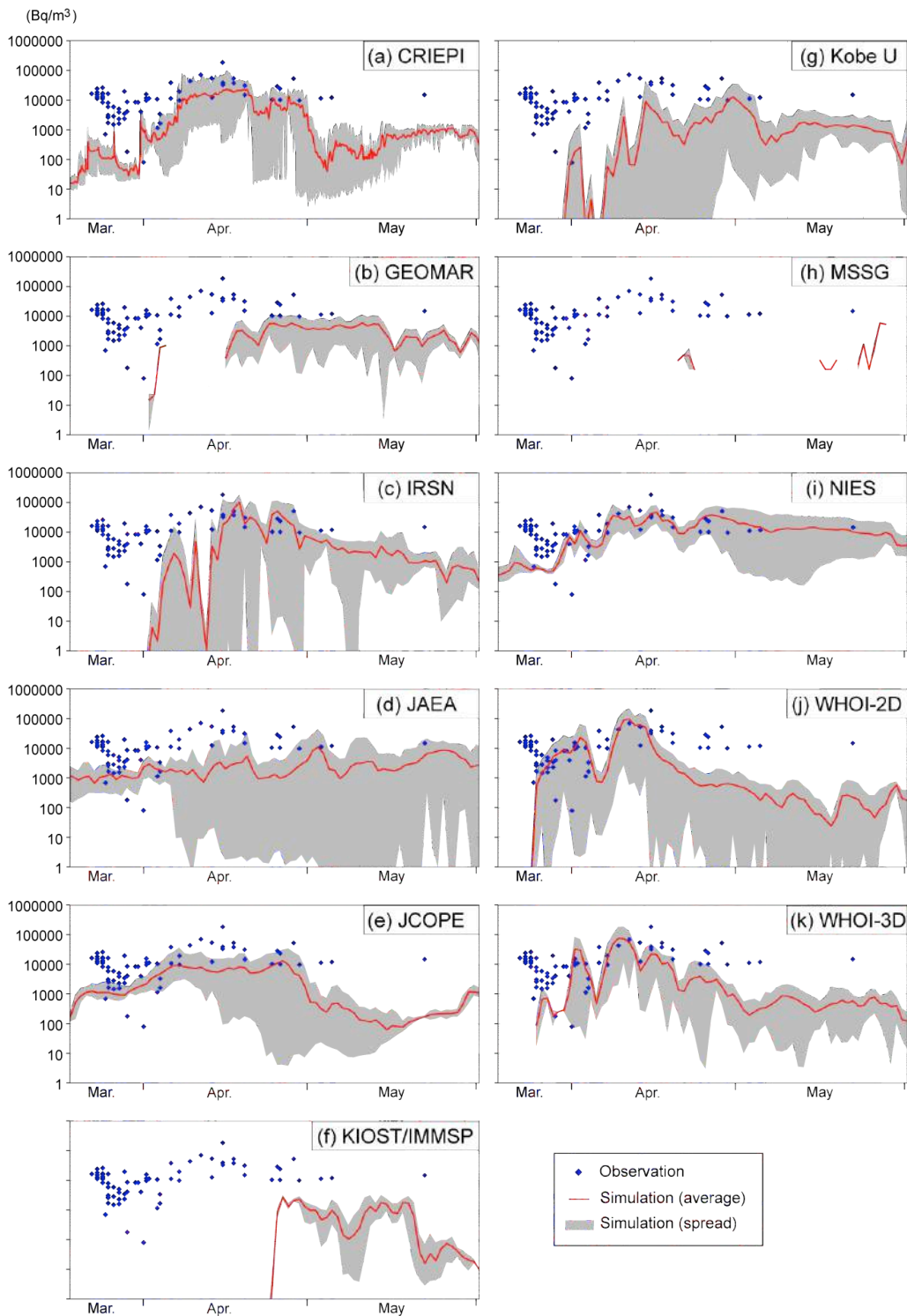Figure 5.9. Time series of ^{137}Cs concentrations at the monitoring stations 30 km offshore of the FDNPP from March 18th to June 1st, 2011. The observed values from ten stations are indicated by blue solid diamonds. The simulated time series that was averaged over the locations of ten observation stations is shown by the red line. Gray shading indicates the spread of the time series at ten locations for each model.
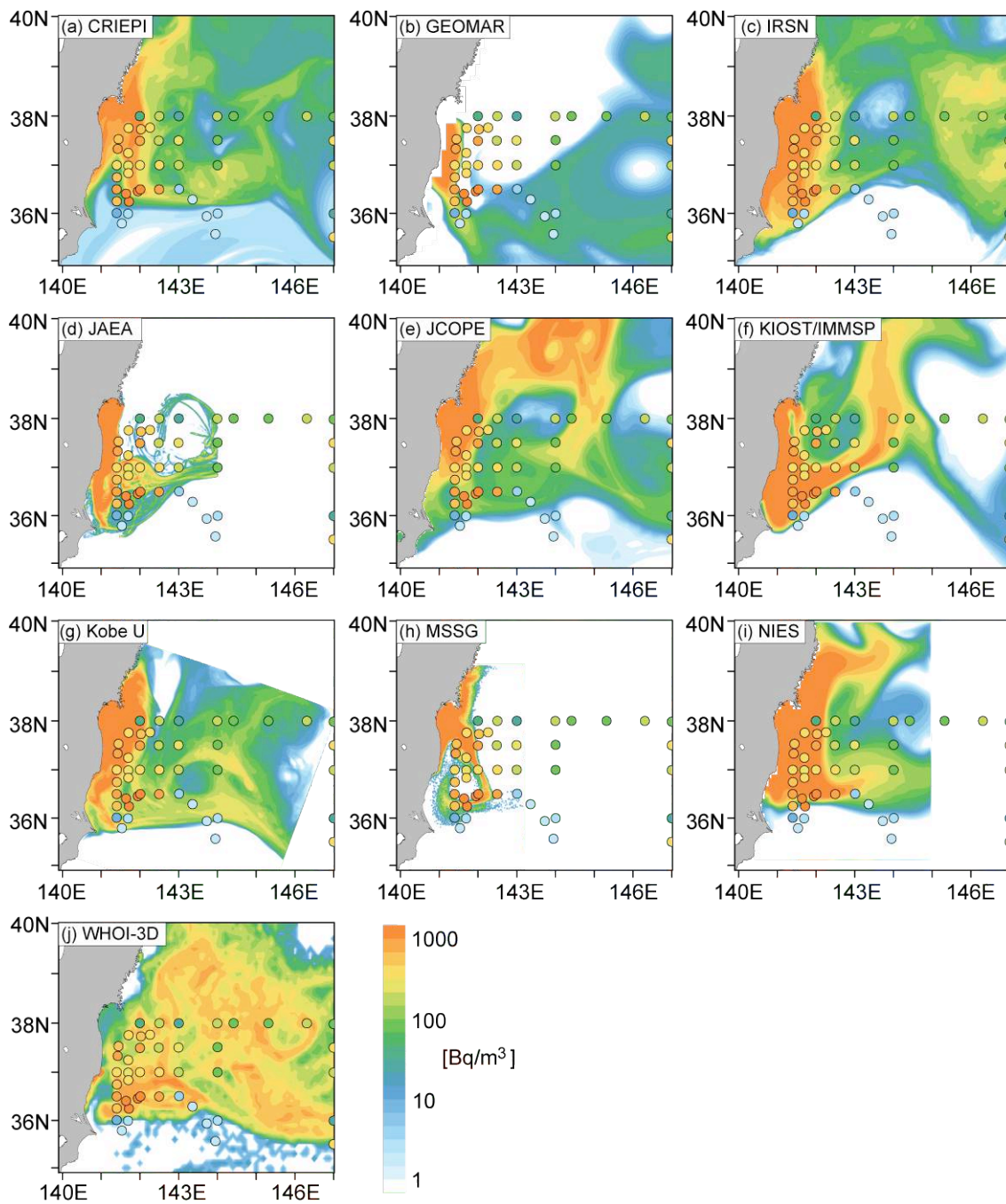
Figure 5.10. Horizontal distribution of surface ^{137}Cs concentrations averaged from June 8-18, 2011. The simulated distributions are shaded in color, and the observed values are indicated by circles with the same color-scale.

Figure 5.11. Same as in Fig. 5.10 except for at a depth of 100 m. Numbers in parentheses shown in the upper-right corner of each panel indicate the ^{137}Cs inventory within the R/V KOK observation area from the surface to a depth of 200 m. Unit for the inventory is in Peta Bq.
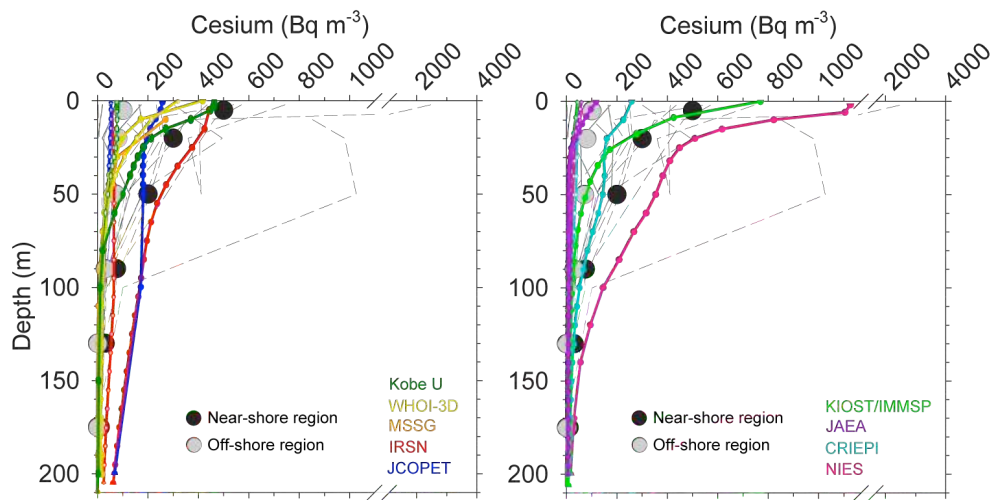
Figure 5.12. Vertical profiles of ^{137}Cs averaged over the area of the R/V KOK observations. Black and gray dots indicate the observed values of 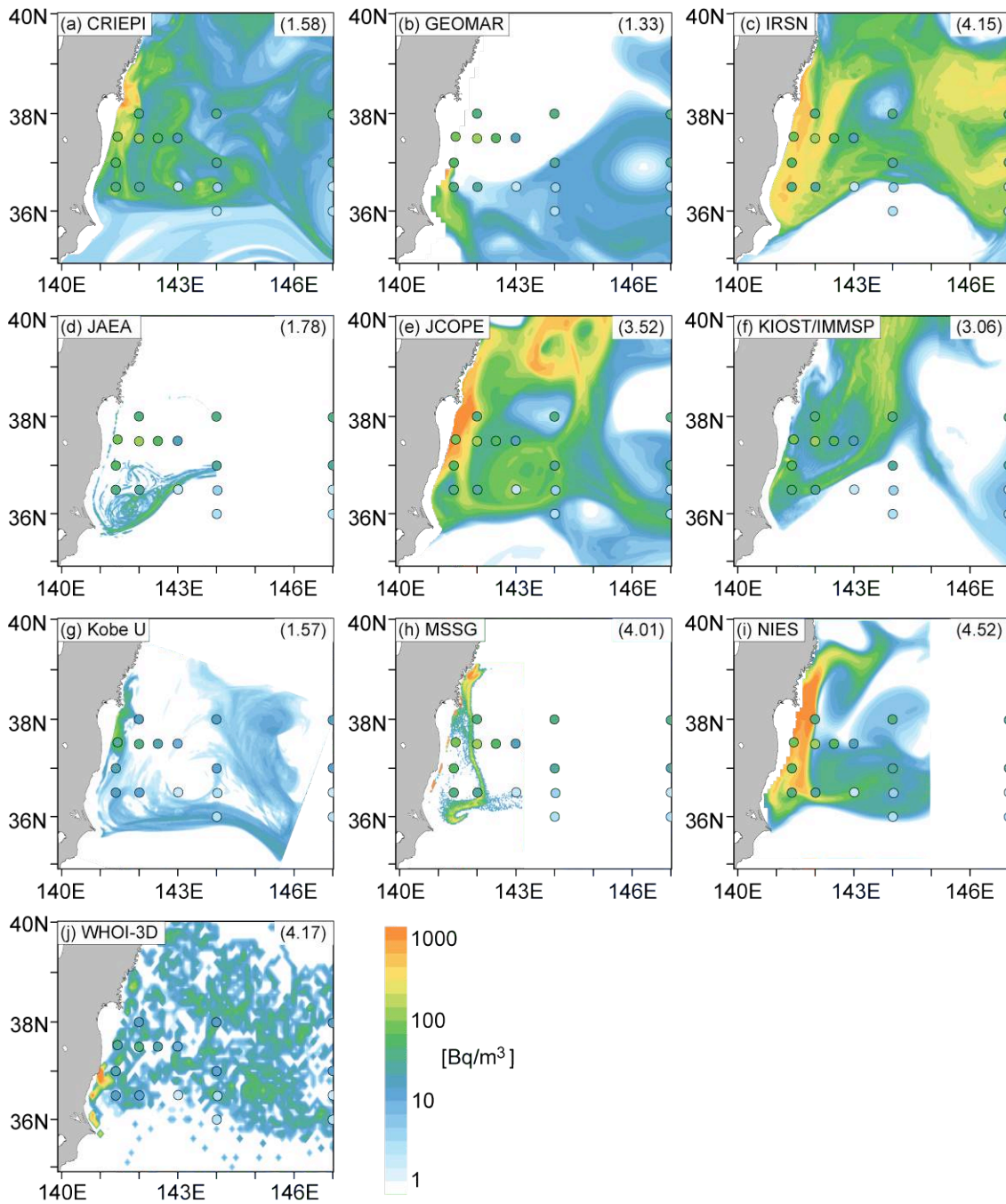^{134}Cs for the near-shore region and off-shore region, respectively (after Buesseler et al., 2012). The simulated vertical profiles for the near-shore region (lines with open circles) and off-shore region (lines with solid circles) are shown. The observed values for the left panel and right panel are the same except that the simulated profiles are from different models. Note that we compare the simulated profiles of ^{137}Cs to the observed values of ^{134}Cs because the only available profile in Buesseler et al., 2012 is for ^{134}Cs and because the ratios of concentrations between ^{134}Cs and ^{137}Cs in the study area are almost one in June.

6. Emission source estimation

6.1. Introduction

As described in the previous model inter-comparison sections, the results of the tracer transport simulations of the radionuclides varies significantly depending on the prior source term conditions. More than three years have passed since the accident at the Fukushima FDNPP; however, a robust source term estimation still has not been obtained. Chino et al. (Chino et al., 2011) from the Japan Atomic Energy Agency (JAEA) used a reverse method in which they compared radionuclide observational data and their regional tracer transport model (SPEEDI) simulation results to obtain the emission time series of ^{137}Cs and ^{131}I. Their results suggested that the ^{137}Cs total emission amount from the FDNPP for the period of March 11 - April 19 is 9.1 PBq and that the maximum emissions occurred from March 14 and 15 (Chino et al., 2011). They also found that there were large emission events at March 21-22 and March 30-31. Terada et al. (2012) modified this result and obtained a ^{137}Cs total emission of 8.8 PBq. An important condition of their analyses was that only Japanese land observation sites were used; therefore, they could not constrain the radionuclide plumes that were transported to the Pacific Ocean. However, Stohl et al. (2012) combined a tagged tracer global tracer transport model (FLEXPART) results and observation data from the global radionuclide monitoring network operated by a preparatory commission for the Comprehensive Nuclear-Test-Ban Treaty Organization (CTBTO) through a Bayesian synthesis inversion (Maki et al., 2011). Stohl et al.'s results suggested that the total ^{137}Cs estimation in the period was 36.6 PBq. The result was a factor of 4 larger than the result by Chino et al. (2011) and Terada et al. (2012). Their analysis assessed the radionuclide plumes that were transported to the Pacific Ocean because they used widely covered observation data in the Northern Hemisphere and global transport model. However, Stohl et al.'s transport model is a Lagrangian transport model, and they released a large amount of tracer particles to simulate their transport, diffusion and deposition processes. The Lagrangian models have features that can precisely calculate transport processes; however, they cannot estimate diffusion (turbulent, cumulus and planetary boundary layers) and deposition (wet and dry) processes in detail. Such features might affect their diffusion and deposition processes, which are the most important processes in the long-range aerosol tracer transport. In this section, a new estimation of the ^{137}Cs source term is shown by combining the global observation network data, global Eulerian aerosol transport model and Bayesian synthesis inversion

(Maki et al., 2011).

6.2. Analysis Method

The present method used tagged simulation results by the global Eulerian aerosol model MASINGAR (Tanaka et al., 2005) in which the horizontal resolution was TL319 (approximately 60 km). Tagged tracers (^{137}Cs) from the lowest model layer (surface to 50 m) were released every three hours with 1Tg/hr to accumulate the daily mean. It was assumed that the released ^{137}Cs was attached to hydrophilic aerosols that had radii of 0.7 μm and occurred by dry and wet deposition. One of the merits in using tagged tracer simulations was that after the^{137}Cs source term emission time-series were obtained, we could also obtain the atmospheric concentrations and depositions of ^{137}Cs by simply calculating the linear combination of the source term estimations and tagged tracer simulation results. Using this feature, we could construct a near-real-time prediction system by combining the properly distributed observation network and operational system of the tagged tracer transport model (an emission prediction scenario is required when using such a system operationally). The daily mean observation data of 51 global sites (CTBTO(Hoffmann et al., 2000), RING OF FIVE(Masson et al., 2011)、University of California(Smith et al., 2014, Taiwan Academia Sinica(Hsu et al., 2012) and Meteorlogical Research Institute (Igarashi et al., 2009)) were collected (Fig. 6.1), and the analysis period was the 40 days from March 11 to April 19. We tested two prior emission estimates. The first estimate was the JAEA posterior emissions (Terada et al., 2012) and the second was the NILU prior emission (not posterior) (Stohl et al., 2012) because our observational data were similar to the data from their study. To consider the observational error and space representational error, the observational error was set to 20%. The prior flux uncertainty shows the ratio between the observation and prior flux uncertainty, and several sensitivity tests were examined by changing the prior emission flux uncertainties from 10% to 5000%.

6.3. Results and discussion

We selected the Stohl's source term estimation (Stohl et al., 2012) as our prior emission to compare the mismatch between observation data and estimated concentration. We also set the prior flux uncertainty to 100% after several sensitivity tests. The total ^{137}Cs emission amount from the FDNPP for the period of March 11 to April 19 was 19.4 PBq, and its

uncertainty was estimated as 3.6 PBq. In the present inverse analysis, the emission height level did not have as much of an affect in the estimated time-series of the source term. The maximum ^{137}Cs occurred on March 15 and the emission amount was larger than that of the prior estimates. The results suggest that there were emission events from March 18-22 and from March 28-30 (Fig. 6.2); however, the 28-30 March emission amount was smaller than that of the Chino et al. and Terada et al. estimation.

In our analysis, we obtained an intermediate result between that of Stohl et al. (2012) and Terada et al. (2012) using tagged tracer simulation results, global observation data and an inverse model, and the results were consistent with other analysis results (Table 6.1). By combining this result and the tagged simulation results, the atmospheric concentrations and deposition estimates of ^{137}Cs were evaluated. However, there are several issues to be discussed in the analysis. One of the most important issues is that we used only one model, and the bias of the model transport could directly affect the estimated source term. To obtain a robust source term estimation, we should collect many tagged model simulation results with common experimental settings and compare their estimated source terms. Another issue is the horizontal resolution of the model. To obtain a fine horizontal and temporal resolution, we should use a regional chemical transport model and collect hourly observation data. Currently, we do not have enough observation data for the Pacific Ocean; therefore, we should make use of marine deposition observation data to improve the analysis.

Table 6.1. Recent ^{137}Cs source term estimations from the FDNPP.

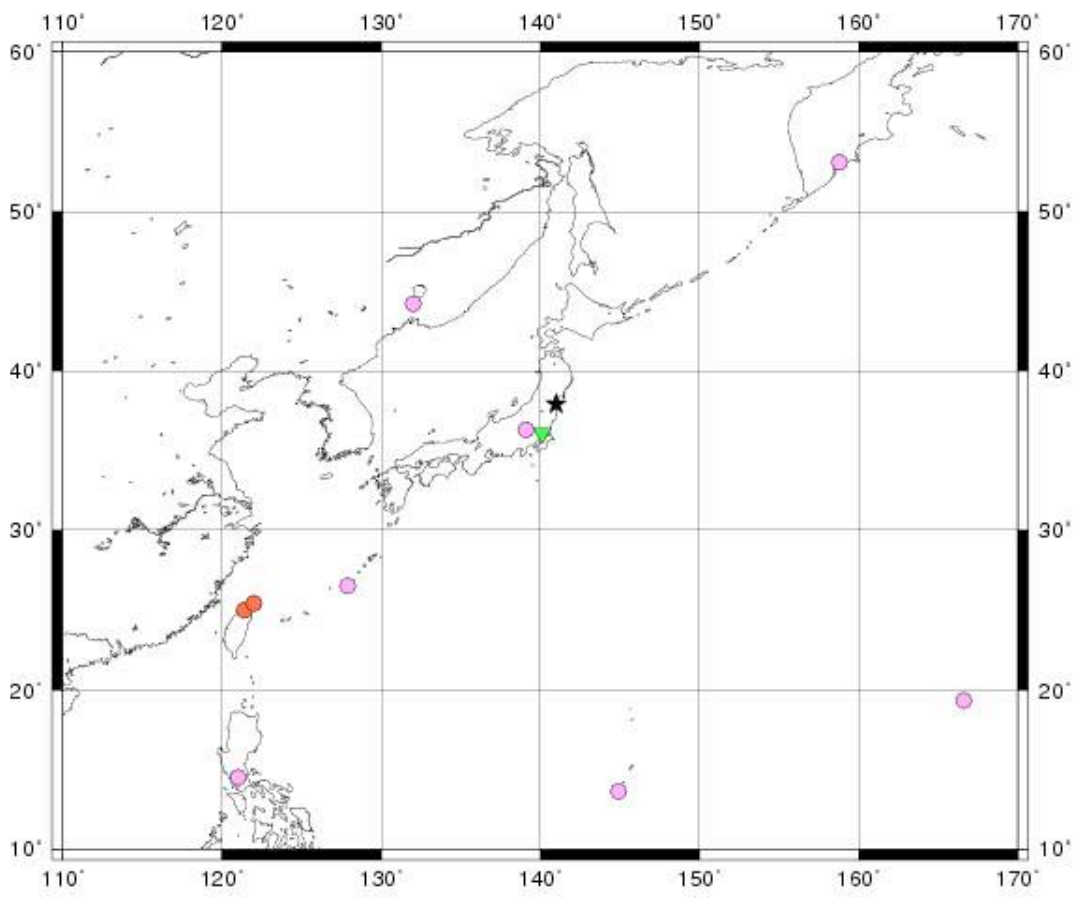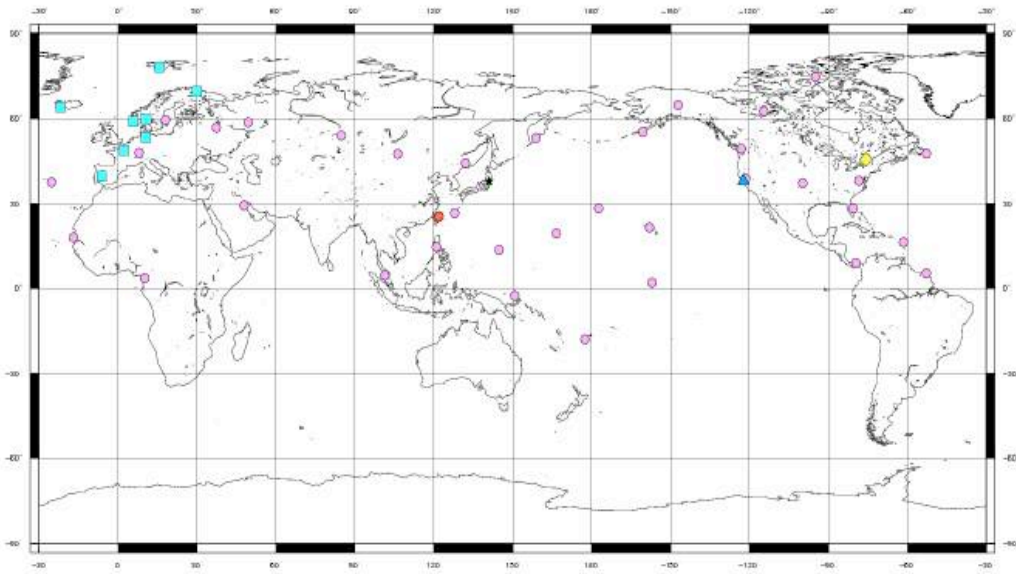| References	Total flux F_A	Range	To–F_A ratio of land deposition of 2.65PBq (%)	Period	Remarks
This study	19.4	16.4–22.4	13.7	3/11–4/19	Cs137 conc.; Global Eulerian model + Inversion
MEXT (2011) and Chino et al. (2011)	15.5	14–17	17.1		From obs. and numerical model analysis
Kobayashi et al. (2013)	13.0	–	20.4	3/12–3/20	Cs137 conc and sea surface conc.; Regional Lagrangian model, oceanic dispersion simulation + Reverse method
Saunier et al. (2013)	15.5	–	17.1	3/11–3/27	Gamma dose ratio obs.; Regional Eulerian model + Inversion.
Stohl et al. (2012)	36.6	20.1–53.1	7.2	3/10–4/20	Cs137 conc.; Global Lagrangian model + Inversion
Terada et al. (2012)	8.8	–	30.1	3/10–3/31	Cs137 conc.; Regional Lagrangian model + Reverse method
Winiarek et al. (2014)	15.5	11.6–19.3	17.1	3/11–3/26	Cs137 conc and sea surface deposition; Regional Eulerian model + Inversion.
mean±standard deviation(σ)	17.8 ±8.2		17.5±6.4		
data within 2σ from the mean	14.6±3.2		19.2±5.2		

Figure 6.1. Observation data used in this study. Red, green and blue circles show the CTBTO, Ro5 and other observation data, respectively.
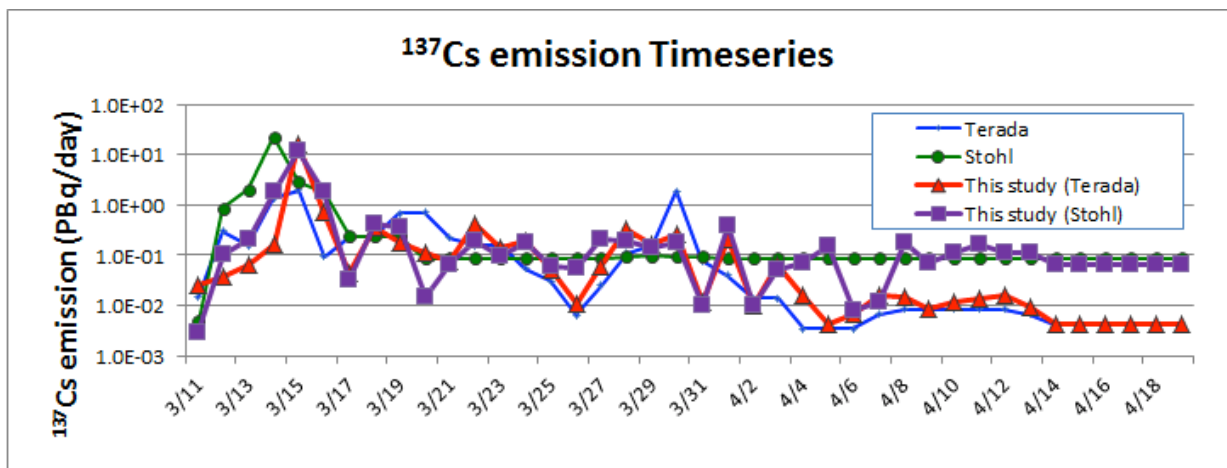
Figur 6.2. ^{137}Cs emission time series from the FDNPP Blue, orange, red (thick) and purple (thick) lines show the Terada prior, Syohl prior, inversed posterior (Terada prior) and inversed posterior (Stohl prior) ^{137}Cs emission time series, respectively.

7. Summary and concluding remarks

A summary of findings from past studies and the current study are presented below:

- JMA model estimate of the amount of ^{137}Cs released to the atmosphere until the end of March 2011 is 19.4±3.0 PBq. The estimate including results of the past studies is 17.8±8.2 PB (Table 6.1). The estimate only with values within twice the standard deviation around the mean value is 14.6±3.2 PBq.

- The amount of direct discharge to the ocean is estimated in the range of 2.3 to 26.9 PBq.

- Regional atmospheric model results show that the land area deposition ratio to the total emission is 27±10% (Table 3.2). On the other hand, the MEXT aircraft observation on May 31, 2012 shows a deposition of 2.7 PBq over the land. This observed value and the estimated total emission in each model lead to a land area deposition ratio of 18±6% in average. The value becomes 19±5% if the total emission within twice the standard deviation is use for evaluation. The differences are caused by errors in model simulation, estimation of the total emission, and estimation of the land-dopositted amount from the aircraft observation. We need future investiation to reduce the erros.

50

● The global atmospheric model comparison indicates that the wet doposition over the globe is 93±5% of the total ^{137}Cs emissions assumed in the models. The regional atmospheric model comparison, on the other hand, shows that the ratio over the simulation regions is 68±19%. The ratio over the Japanese land area is similar to this value. The difference between ratios of global and regional simulations is mainly caused by difference in the model regions, but model differences are also not negligible.

● Models are capable of depicting the main features of observed radioactive material distributions. There are, however, large uncertainties in the quantitative comparisons of the simulation results, especially in the amount of wet deposition, which is largely dissimilar in the different models. In addition, the eddy simulations in the coastal oceans have large differences between models.

● Migrating atmospheric pressure systems frequently change the wind direction and vertical shear; therefore, the simulated distributions of the deposition patterns over the land and ocean are sensitive to the assumed meteorological data and emission scenarios. Accurate and high temporal resolution scenarios must be reconstructed through future efforts of extensive assimilation and inversion.

● Estimates of depositions to the ocean through atmospheric fallout and direct discharge are required to reproduce the observed ^{137}C concentrations in the ocean. The atmospheric deposition of ^{137}Cs to the ocean is underestimated before mid-April. It is, therefore, needed to improve the deposition of radioactive materials from atmosphere to ocean for improved simulation of ocean transport of the materials.

● The skill of the models depends on the performance of the dynamic frameworks, chemical transportation processes, dry and wet deposition processes and other elements. Therefore, significant improvements can be made to the models through collaborative works among different communities.

● The estimated emission scenarios by local and global analyses are different; therefore, a combined inversion analysis with both local and global data is required. Therefore, the work shown in Chapter 6 must be extended to include high spatial resolution inversions using regional models.

Acknowledgments

Appendix

Appendix 3A. Model description for regional atmospheric model intercomparison

3A.1. Centre d'Enseignement et de Recherche en Environnement Atmosphérique (CEREA)

The simulations of the radionuclides from the FDNPP were performed with the chemistry transport model Polar3D, which is the Eulerian model of the Polyphemus platform; this model has been validated by the European Tracer Experiment, Algeciras incident and Chernobyl accident (Quélo et al., 2007).

^{137}Cs and ^{131}I are modeled as passive gaseous tracers with radioactive decay, and their half-lives are 11,000 and 8.04 days, respectively. Dry deposition is modeled using a simple scheme with a constant deposition velocity: $v^{dep} = 0.2$ cm s^{-1} for ^{137}Cs and $v^{dep} = 0.5$ cm s^{-1} for ^{131}I. The wet scavenging rate Λ^s used in this study is based on Brandt et al.(2002). The advection is implemented by a third-order direct space-time scheme with a Koren-Sweby flux limiter function. Because of the sharp gradients, such a limiter should be used. The diffusion scheme is integrated through an implicit second-order Rosenbrock scheme that has a three-point spatial scheme and directional splitting. The model is configured with a spatial resolution of 0.05° (270×260 grids) and 15 vertical levels ranging from 0 to 8000 m.

The initial source terms for ^{137}Cs and ^{131}I were obtained by inverse modeling of active concentrations in the air at the mesoscale using a rigorous estimation of the error level (Winiarek et al., 2012). A finer source term for ^{137}Cs was obtained by inverse modeling of several datasets that included the active concentrations in the air and the deposition measurements; a rigorous estimation of the errors was attached to each dataset (Winiarek et al., 2014). For the first estimation, the ECMWF meteorological fields were used; they were available every 3 h at a spatial resolution of 0.25°×0.25° using the mesoscale meteorological model WRF. Using the parameterizations described in Winiarek et al. (2014), fields were generated every hour with a spatial resolution of approximately 0.05°× 0.05°.

3A.2. Central Research Institute of Electric Power Industry (CRIEPI)

A modeling group from the CRIEPI simulated radionuclides using the Comprehensive Air Quality Model with Extensions (CAMx) version 5.40.1 (ENVIRON, 2011) that was driven by WRF version 3.2.1 (Grell et al., 2005). The chemical module of the CAMx was modified to analyze the advection, diffusion, radioactive decay, and dry and wet deposition of gaseous and particulate ^{131}I and particulate ^{132}I, ^{132}Te, ^{134}Cs and ^{137}Cs. The particulate radionuclides were assumed to be equivalent to $PM_{2.5}$ (particulate matter < 2.5 μm). The model domain covered the east side of Japan with 5-km grids, and the model had 34 layers up to 100 hPa. The wet deposition process, which was originally based on Seinfeld and Pandis (1998), was modified to analyze the vertical re-distribution of radionuclides by precipitation. The dry deposition process was based on Zhang et al. (2001) and Zhang et al. (2003) for particulate and gaseous radionuclides, respectively. The objectively analyzed dataset (MANAL) constructed by the JMA was used as the lateral boundary and initial condition for the WRF. Analysis nudging using MANAL was applied for the meteorological field during the simulation. The release rates of ^{131}I and ^{137}Cs were from Terada et al. (2012).

3A.3. Institut de Radioprotection et Sûreté Nucléaire (IRSN)

The atmospheric transfer modeling group from the IRSN simulated radionuclide dispersion using the Eulerian model ldX that was derived from PLAIR 3D. The simulation submitted to the working group was driven by the meteorological fields from the JMA forecast (0.05°×0.05°). The source term used here was described in Mathieu et al. (2012). Built in 2011, this source term was mostly based on the analysis of the dose rate measurement to determine doses that may have been taken during the catastrophe. The dry deposition model was based on a deposition velocity value of 2×10^{-3} m s^{-1} for aerosols. The wet deposition was modeled by a scavenging coefficient $L=L_0P$, where P is the precipitation (mm h^{-1}) read from the ECMWF fields, and L_0 is a constant defined per radionuclides (aerosols: 5×10^{-4} h s^{-1} mm^{-1}). The details for this model are described in Korsakissok et al. (2013), and the revised release rate using this model can be found in Saunier et al. (2013).

3A.4. Japan Atomic Energy Agency (JAEA)

The WSPEEDI model (Terada et al., 2008) was constructed by expanding the function of SPEEDI with a combination of the non-hydrostatic mesoscale atmospheric model MM5

(Grell et al., 1994) and Lagrangian particle dispersion model GEARN (Terada and Chino, 2008). The MM5 is a community model that has users all over the world, and it is used as the official weather forecast by some countries. It has many useful functions, such as nesting calculations and 4-D data assimilation, and numerous options for parameterizations for cloud microphysics, cumulus clouds, the planetary boundary layer (PBL), radiation, and land surface schemes. The Lagrangian particle dispersion model GEARN calculates the atmospheric dispersion of radionuclides by tracing the trajectories of a large number (typically a million) of marker particles discharged from a release point. The horizontal model coordinates are the map coordinates, and the vertical coordinates are the terrain-following coordinates (z*-coordinates). By using the meteorological field predicted by the MM5, the GEARN model calculates the movement of each particle affected by the advection from the mean wind and subgrid-scale turbulent eddy diffusion. The GEARN model also has a function of nesting calculations for two domains corresponding to the MM5 nested domains. Two nested domains of the GEARN model are calculated concurrently by different executables on parallel computers, and the marker particles that flow out and in across the boundary of the inner domain are exchanged between domains. Part of the radioactivity in the air is deposited on the ground surface by turbulence (dry deposition) and precipitation (wet deposition). The decrease in radioactivity that results from dry deposition is calculated for each particle using the dry deposition velocity (0 m s^{-1} for noble gases, 3×10^{-3} m s^{-1} for iodine, and 10^{-3} m s^{-1} for other nuclides, which does not consider the chemical form and particle size) based on the typical value for short vegetation (Sehmel, 1980). The decrease in radioactivity of each particle by wet deposition is calculated by the scavenging coefficient that is calculated at each grid cell for any nuclides except for the noble gases and is based on the precipitation intensity for convective and non-convective rains predicted by the MM5. The scavenging coefficient (Λ) based on the study by (Brenk and Vogt, 1981) is calculated at each grid cell for any nuclides except for noble gases in the GEARN model as

$$\Lambda = \alpha\left(F_c I_c + F_n I_n\right)^{\beta}$$

where α ($=5\times10^{-5}$) and β ($=0.8$) are the empirical constants, and I_c and I_n are the precipitation intensities (*mm h^{-1}*) for convective and non-convective rains, respectively, that are predicted by the MM5. F_c and F_n are the unity at grid cells below the convective and non-convective

cloud heights, respectively; the value is zero at other grid cells. The air concentration in each Eulerian cell averaged over an output time interval and total surface deposition accumulated during the time interval are calculated by summing the contributions of each particle to the cell. The radioactive decay is calculated at each time step and integrated into both the air concentration and surface deposition calculations, although the decay chains are not considered. The radiological doses are calculated by multiplying the air concentration and deposition by conversion factors (ICRP, 1995). The performance of this model system was evaluated by its application in the field tracer experiment over Europe, ETEX (Furuno et al., 2004) and the Chernobyl nuclear accident (Terada et al., 2004; Terada and Chino, 2005; 2008).

3A.5. Japan Agency for Marine-Earth Science and Technology (JAMSTEC)

A modeling group from the JAMSTEC simulated the radionuclides using the Weather Forecast and Research (WRF) model with an online chemical module (WRF/Chem) version 3.4.1 (Grell et al., 2005). The chemical module of WRF/Chem was modified to analyze the advection, diffusion, and dry and wet deposition of ^{131}I and ^{137}Cs. The model domain covered the east side of Japan with 3-km grids, and the model had 35 layers up to 100 hPa. The wet deposition process was based on Maryon et al. (1996), and the dry deposition process was based on Maryon et al. (1992) and Klug (1992) for ^{131}I and ^{137}Cs, respectively. The mesoscale model (MSM) dataset constructed by the Japan Meteorological Agency (JMA) was used as the lateral boundary and the initial condition. Analysis nudging using the JMA-MSM and observational nudging with ground-based observations by the JMA was applied for the meteorological field during the simulation. The release rates of ^{131}I and ^{137}Cs were taken from Terada et al. (2012).

3A.6. Japan Meteorological Agency (JMA)

The Japan Meteorological Agency (JMA) provided its operational mesoscale (MESO) analysis, radar/rain gauge-analyzed precipitation (RAP) data, and simulated results from the JMA Regional Atmospheric Transport Model (JMA-RATM) in a collaboration with the WMO task team that was convened by the request of the United Nations Scientific Committee on the Effects of Atomic Radiation (UNSCEAR). The JMA-RATM is a tracer

transport model that can be driven by the MESO analysis. The model applies a Lagrangian scheme (Iwasaki et al., 1998; Seino et al., 2004) with many tracer particles that follow advection, horizontal and vertical diffusion, gravitational settling, dry deposition and wet scavenging processes. The JMA-RATM was originally developed at the JMA for photochemical oxidant predictions (Takano et al., 2007) and volcanic ash fall forecasts (Shimbori et al., 2009) in Japan. The details of the original RATM were described by Shimbori et al. (2010).

For the prediction of radionuclides, the implementation of dry and wet deposition schemes were improved. Regarding the wet deposition for light particles, only washout processes (below-cloud scavenging) were considered. The below-cloud scavenging rate was from Kitada (1994). The grain size distribution assumed a lognormal with a mean diameter of 1 μm, standard deviation of 1 (upper cutoff of 20 μm), and a uniform particle density of 1 g cm^{-3}. Calculations of the JMA-RATM were conducted according to the WMO task team's agreed upon protocol with a horizontal concentration and deposition grid resolution of 5 km using a unit source emission rate (Draxler et al., 2013). For the SCJ model intercomparisons, the revised JAEA release rate by Kobayashi et al. (2013) was used, and the time step of Lagrangian trace calculations was changed to 5 minutes from the original of 10 minutes. In addition, the precipitation rate of solid water (snow and graupel) in the JMA-MESO analysis was used for wet scavenging in addition to that of rain. The details of the revised JMA-RATM are described in Saito et al. (2014).

3A.7. Meteorological Research Institute, Japan Meteorological Agency (JMA-MRI)

We used the Regional Air Quality Model 2 (RAQM2; Kajino et al. (2012), Adachi et al. (2013), which implements a triple-moment modal aerosol dynamics module assuming a log-normal size distribution of the aerosol populations. This model describes the nature of the aerosol dynamic processes, such as nucleation, condensation, coagulation, dry deposition, grid-scale cloud condensation and ice nuclei activation, and the subsequent cloud microphysical processes (rainout) and washout processes. An ensemble Kalman filter (EnKF) data assimilation system coupled with the JMA non-hydrostatic meteorological model (NHM-LETKF) (Kunii, 2013) was used to produce the meteorological field. There were 213 × 257 grids with a 3-km horizontal grid resolution in the NHM-LETKF and RAQM2. There were 50 vertical layers to 50 hPa in the NHM-LETKF and 20 layers to 10 km in the RAQM2.

For the radioactive aerosols, we used a number equivalent to the geometric mean dry diameter $D_{g,n,dry}$ = 100 nm, geometric standard deviation σ_g = 1.3, particle density ρ_p = 2.0 g cm^{-3}, and hygroscopicity κ = 0.4 (internal mixture with sulfate and others assumed). We assumed I$_2$ for the chemical composition of gaseous iodine. When emitted, 20% and 80% of ^{131}I are assumed to exist in the gas and aerosol phases, respectively. The release rates of ^{131}I, ^{137}Cs, and ^{134}Cs were from Terada et al. (2012).

3A.8. National Institute for Environmental Studies (NIES)

A modeling group from the NIES simulated the distributions of ^{137}Cs using WRF version 3.1 (Skamarock et al., 2008) and the three-dimensional chemical transport model Models-3 Community Multiscale Air Quality (CMAQ) (Byun and Schere, 2006) for the period from March 10 to April 20 2011. The deposition schemes used in the CMAQ were detailed in Byun and Ching (1999) and Byun and Schere (2006). The dry deposition was simulated using a resistance model. The cloud module of the CMAQ includes parameterizations for sub-grid convective precipitating and non-precipitating clouds and grid-scale resolved clouds. They assumed that all of the ^{137}Cs were in the particulate phase with a diameter of 1 μm (Sportisse, 2007). The model domain covered most of the Tohoku region (711 × 711 km^2) at a 3-km grid resolution and 34-layer vertical structure with a surface layer thickness of approximately 60 m. For the WRF simulation, analysis nudging was conducted with the three-dimensional meteorological fields from the Japan Meteorological Agency Meso-Scale Model datasets that had 5 × 5 km^2 horizontal resolution for 3-h intervals. The emission data from the FDNPP were from Terada et al. (2012).

In CMAQ, the wet scavenging of particulate matter is calculated by the following equation:

$$\frac{dQ_i}{dt} = Q_i \left(\frac{\exp\left(-\tau_{cld}/\tau_{washout}\right) - 1}{\tau_{cld}} \right)$$

(S1)

where Q_i is the in-cloud concentration of pollutant i, τ_{cld} is the cloud timescale, and $\tau_{washout}$ is the washout time calculated from

$$\tau_{washout} = \frac{W_T \Delta z}{\rho_{H2O} p_0}$$

(S2)

where W_T is the mean total water content, Δz is the cloud thickness, ρ_{H2O} is the density of water, and p_0 is the precipitation rate (mm hr^{-1}).

3A.9. Seoul National University (SNU)

The Eulerian transport model (ETM) was obtained from a modification of the Asian Dust Aerosol Model 2 (ADAM2) (Park et al., 2010). The ADAM2 model used 11 particle-size bins with nearly the same logarithmic intervals for the particles with radii of 0.1-37 μm, and it was adapted to a logarithmic size distribution with an aerodynamic mean diameter of 0.4 μm and a logarithmic standard deviation of 0.3 for ^{137}Cs (Stohl et al., 2012) For ^{131}I, the ADAM2 model was adapted to handle the gas phase contaminants. The horizontal resolution of the ETM was 27 km, which was the ETM domain centered by the FDNPP. The meteorological model used in this study was the fifth-generation mesoscale model of the non-hydrostatic version (MM5; Grell et al. 1994). The wet deposition amounts of radionuclides were determined by the precipitation rate, and the average concentration in the cloud water was estimated by the sub-grid cloud scheme followed by the diagnostic cloud model in the ADAM2 and the Regional Acid Deposition Model (RADM) version 2.6 (Chang et al., 1987). The below-cloud scavenging process was also included (Park, 1998). The emission rate of ^{131}I and ^{137}Cs from the accident at the FDNPP by JAEA (Chino et al., 2011; Katata et al., 2012) was used. The details of the ETM can be found in Park et al. (2013).

Appendix 4A. Model descriptions for global atmospheric model intercomparison

4A.1. SPRINTARS

SPRINTARS (Spectral Radiation-Transport Model for Aerosol Species) (Takemura et al., 2000; Takemura et al., 2002; Takemura et al., 2005) is a global aerosol model developed by the Research Institute for Applied Mechanics, Kyushu University. The model simulates the effect of atmospheric aerosols on climate systems and atmospheric pollution over a global scale. The model is based on the atmosphere-ocean coupled climate model MIROC, which was developed by the Atmosphere and Ocean Research Institute, University of Tokyo, National Institute for Environmental Studies, and the Japan Agency for Marine-Earth Science and Technology (Watanabe et al., 2010).

SPRINTARS calculates the transport processes of aerosols (emission, advection,

diffusion, wet deposition, dry deposition, and gravitational settling). The aerosol direct effect, which is caused by the scattering and absorption of solar and terrestrial radiation by aerosols, and the indirect effect, which is an act of aerosols as cloud condensation nuclei and ice nuclei, are included in the calculation. SPRINTARS is the only aerosol model from the Asian research community that was adopted by the 4th assessment of the Intergovernmental Panel on Climate Change (IPCC). In June 2011, Takemura et al. (2011) published a simulated result of the global transport of a tracer from the FDNPP just after the accident. The horizontal resolution of the model is approximately $0.56° \times 0.56°$ in latitude and longitude (T213 spectral truncation in the dynamical core), and the model has 20 vertical layers up to 8 hPa, including 4 layers below an altitude of 1 km (approximately at the 50, 200, 500 and 1000-m levels). The horizontal wind field components and air temperature internally generated by the dynamical core are nudged by 6-hourly NCEP GFS data.

In the intercomparison study, simulations of ^{137}Cs, ^{131}I and ^{133}Xe have been submitted. The dry and wet deposition parameterizations of ^{137}Cs and ^{131}I were the same as sulfate aerosol, whereas ^{133}Xe was assumed to be only removed by the radioactive decay. The source terms of ^{137}Cs and ^{131}I were from the estimated values by the JAEA (Terada et al., 2012). For the ^{133}Xe experiment, the inversely estimated source term of Stohl et al. (2012) was used. Two sets of the experiment, namely the standard experiment, "SPRINTARS," and an experiment with stronger wet deposition parameters "SPRINTARS1," were submitted to the intercomparison.

4A.2. MASINGAR-1 and MASINGAR mk-2

MASINGAR (model of aerosol species in the global atmosphere) is a global aerosol model developed by the Meteorological Research Institute of Japan Meteorological Agency. For the intercomparison, the simulated results with two versions of the model were submitted. MASINGAR-1 was coupled with an AGCM called the MRI/JMA 98, which has been used as the operational dust forecasting model by the Japan Meteorological Agency (JMA) since January 2004 (Tanaka et al., 2003). The model resolutions were set to a T106 Gaussian horizontal grid (approximately $1.125° \times 1.125°$) and 30 vertical layers from the surface to a height of 0.4 hPa. A newer version of this aerosol model called the MASINGAR mk-2 was coupled with an AGCM called the MRI-AGCM3 as a component of the earth system model of the Meteorological Research Institute, MRI-ESM1 (Yukimoto et al., 2011; Yukimoto et al., 2012), and used as the global aerosol model for the CMIP5 climate change experiment. The

model resolutions were set to a TL319 horizontal grid (approximately 0.5625° × 0.5625°) and 40 vertical layers from the ground surface to a height of 0.4 hPa.

In this intercomparison experiment, the horizontal wind fields were assimilated with the six-hourly 1.25° ×1.25° data of the JCDAS global reanalysis (Onogi et al., 2007) with the Newtonian relaxation nudging technique. The JCDAS reanalysis was also used for the sea-surface temperature data. The released ^{137}Cs was assumed to be readily attached to the ambient aerosols, which had a uni-modal lognormal distribution with a mode radius of 0.07μm and a dispersion of 2.0 (Tanaka et al., 2013).

For the intercomparison, the simulated results of ^{137}Cs with the source terms of the JAEA (Terada et al., 2012) and Stohl et al. (2012) were submitted. For the ^{133}Xe experiment, the inversely estimated source term of Stohl et al. (2012) was used.

4A.3. EMAC

The simulations by the Cyprus Institute were conducted using the global atmospheric chemistry model EMAC (the ECHAM/MESSy Atmospheric Chemistry) version 1.9 (Christoudias and Lelieveld, 2013). The dynamical field of this model was calculated by the fifth generation European Centre Hamburg general circulation model (ECHAM5; Roeckner et al., 2003; 2006) version 5.3. The simulations were conducted with horizontal resolutions of T255 (approximately 0.5° × 0.5°) and T106 (approximately 1.125°× 1.125°). The vertical coordinate was a hybrid, and the number of vertical layers was 31 up to 10 hPa. The large-scale component of the model circulation dynamics was nudged by applying a Newtonian relaxation towards the European Centre for Medium-range Weather Forecasts (ECMWF) ERA-Interim reanalysis data (Simmons et al., 2007). The nudged variables were vorticity, divergence, temperature and surface pressure. The ERA-Interim data were used for dynamics only; therefore, the precipitation was model-generated.

For the intercomparison, the simulated results of ^{137}Cs, ^{131}I, and ^{133}Xe were submitted. The source terms of ^{137}Cs estimated by the JAEA (Chino et al., 2011) and Stohl et al. (2012) were used. For the ^{133}Xe experiment, the inversely estimated source term of Stohl et al. (2012) was used.

4A.4. KNMI TM5

The Royal Netherlands Meteorological Institute (KNMI) participated in the model

intercomparison of the transport of the radionuclides using the global chemistry Transport Model, version 5 (TM5) (Huijnen et al., 2010; Krol et al., 2005). TM5 is a global offline transport model that has been applied for many atmospheric chemistry and aerosol studies (e.g., de Meij et al., 2006; Vignati et al., 2010) and chemical weather and climate simulations, in which TM5 is driven by ERA-Interim data or the Integrated Forecasting System (IFS) (Flemming et al., 2009) meteorological model. TM5 allows a two-way nesting of regions (Krol et al., 2005), however, the nesting was not applied to the simulations submitted to the intercomparison.

The simulations were conducted with horizontal resolutions of $3° \times 2°$ and 31 vertical layers. The 3-hourly European Centre for Medium-range Weather Forecasts (ECMWF) ERA-Interim reanalysis data (Simmons et al., 2007) were used for the calculation of the atmospheric transport.

The simulated results of ^{137}Cs and ^{131}I were submitted to the intercomparison. The source terms of ^{137}Cs and ^{131}I estimated by the JAEA (Terada et al., 2012) were used. In the simulation, all of the radionuclides were assumed to be removed by wet deposition only. The parameterization of the wet deposition was assumed to be the same as that of the soluble carbon monoxide.

4A.5. Meteorological Research Institute - Passive-tracers Model for radionuclides (MRI-PM/r)

MRI-PM/r (Meteorological Research Institute (MRI) - Passive-tracers Model for radionuclides; MRI-PM/r) is a regional off-line chemistry transport model developed by the Meteorological Research Institute of the Japan Meteorological Agency. The intercomparison of the long-range transport of radionuclides used a regional domain in the Mercator map projection of 107°E-252°E and 3°N – 61°N with 234 ×120 grids, which corresponded to approximately 60 km × 60 km horizontal resolution. The vertical coordinate was a terrain-following coordinate with 13 vertical layers up to 10 hPa. The Advanced Research Weather Research and Forecasting (WRF) model was used to simulate the meteorological field. The U.S. National Center for Environmental Prediction (NCEP) 6 h, 1°×1° final operational global analysis dataset ds083.2 (http://dss.ucar.edu /datasets/ds083.2) was used for the initial and boundary conditions of the WRF and also for the analysis nudging method.

The aerosol module uses a category approach to describe the interaction between radionuclides and environmental species (Kajino and Kondo, 2011) in which the aerosol

particles are grouped into six categories: primary hot particles (PRI), Aitken mode (ATK), accumulation mode (ACM), dust particles (DU), sea-salt particles (SS), and pollen (POL). The aerosol chemical and dynamic processes, such as nucleation, condensation, coagulation and deposition, are calculated based on the modal moment dynamics approach (Kajino and Kondo, 2011; Kajino, 2011). The emission inventory of the environmental species, such as dust, sea-salt, SOx, NOx, and NHx, and the elemental and organic carbon compounds from anthropogenic, biogenic and biomass burning origins were common to Kajino and Kondo (2011). Five percent of the Cs was assumed to form radioactive primary particles (PRI), and the remaining (95%) Cs was assumed to condense onto pre-existing particles (ATK, ACM, DU, SS and POL) with the mass fluxes proportional to the surface area concentrations of each aerosol category. A revised version of the JAEA inventory (Terada et al., 2012) was used for the emissions of ^{134}Cs and ^{137}Cs.

Appendix 4B. Observational data

4B.1. Atmospheric concentrations

To verify the global simulations, measurements of the atmospheric concentrations from the Comprehensive Nuclear Test Ban Treaty Organization (CTBTO) were used in the intercomparison. At the time of the accident at the FDNPP, the CTBTO had set up 64 observation points for particulate radionuclides as well as 27 observatories for radioactive Xenon as part of a standard procedure by the International Monitoring System (IMS) to supervise the manufacture of nuclear weapons and experiments and operation of nuclear facilities (Medici, 2001; CTBTO, 2011; Yonezawa and Yamamoto, 2011). The CTBTO observatories in Japan are located in Gunma and Okinawa, from which measurement information was released after the accident (Yonezawa and Yamamoto, 2011; Center for the Promotion of Disarmament and Non-Proliferation, 2011). Radionuclides were detected in most of the observatories in the Northern Hemisphere; however, they were diluted during transport and the concentration levels have been low outside of Japan. Therefore, they were not considered to have had an impact on the human body.

4B.2. Measurements of depositions

For the comparison of the deposition of radionuclides, observations of ^{131}I, ^{134}Cs, and ^{137}Cs by the RadNet (National Air and Radiation Environmental Laboratory) of the U.S. Environmental Protection Agency (EPA) and National Atmospheric Deposition Program (NADP) (Wetherbee et al., 2012) were used. Wetherbee et al. (2012) indicated that the ^{131}I observed in the USA had the typical features of atmospheric long-range transport and decreased during transportation from the east to west. Moreover, the radioactive material fallout from the accident at the FDNPP found in the U.S. was reported to be larger than the fallout from the Chernobyl accident.

Appendix 5A. Model descriptions for cceanic dispersion model intercomparison

5A.1. CRIEPI

The CRIEPI employed the Regional Ocean Modeling System (ROMS; Shchepetkin and McWilliams, 2005) to simulate the behavior of ^{137}Cs released from the 1F NPP reactors off of Fukushima (Tsumune et al., 2012; 2013). The ROMS is a three-dimensional Boussinesq free-surface ocean circulation model formulated using terrain-following coordinates. The model domain in this study covered the oceanic area off of Fukushima (35°54′N–40°00′N, 139°54′E–147°00′E). The horizontal resolution was 1 km in both the zonal and meridional directions. The vertical resolution of the σ coordinate was 30 layers. The ocean bottom was set at a depth of 1000 m to reduce the computer resources required for the simulation. We used a third-order upwind difference for the advection scheme for both the momentum and tracers and a fourth-order centered difference scheme for the viscosity and diffusivity in the model. The horizontal viscosity and diffusion coefficient were 5.0 m^2 s^{-1}. The vertical viscosity and diffusion coefficient were obtained by a K-profile parameterization (Large et al., 1994). The background value of the vertical viscosity and diffusion coefficient was 10^{-5} m^2 s^{-1}. The model was forced at the sea surface by wind stress and by heat and freshwater fluxes, and their values were acquired by a real-time nested simulation system (Hashimoto et al.,

2010) of the Weather Research and Forecasting model version V3.2.1 (WRF; Skamarock et al., 2008), which is a global spectral model used for numerical weather prediction created by the Japan Meteorological Agency (JMA).

During the simulation, the horizontal currents, temperature, salinity, and sea-surface height along the open boundary were restored to those of the JCOPE2 reanalysis data (JCOPE2, Japan Coastal Ocean Prediction Experiment 2, Miyazawa et al., 2009). The temperature and salinity were nudged by the JCOPE2 reanalysis results to represent mesoscale eddies in the simulation period in the ROMS with a higher resolution. The nudging parameter was 1 d^{-1}. The initial conditions of temperature, salinity, horizontal current velocities, and sea-surface height were set by the JCOPE2 reanalysis output. Previous simulations considered the tidal effect (Tsumune et al., 2012). We subsequently confirmed that the tidal effects on the behavior of ^{137}Cs were small in these simulations. Therefore, we omitted the tidal effect in this study to simplify the model simulation (Tsumune et al., 2013).

We modeled ^{137}Cs as a passive tracer, with its movement into the ocean interior controlled by advection and diffusion (Tsumune et al., 2011). We assumed that the activity of ^{137}Cs in seawater would decrease as a result of radioactive decay because it has a half-life of 30 years. The direct discharge scenario is from Tsumune et al. (2012; 2013); the total amount of radionuclides was 3.5 PBq at the end of June 2011. The spatial and temporal distributions of the atmospheric deposition of ^{137}Cs were estimated by CAMx (ENVIRON, 2009) and described by Hayami et al. (2012) and Tsumune et al. (2013); the total amount of atmospheric deposition was 1.14 PBq in this region for the period from March 11 to April 1, 2011. The release rate to the atmosphere is from Terada et al. (2012); the total amount of radionuclides was 9.0 PBq. In addition, an inflow flux through the boundary was employed in the simulated results by the North Pacific model (Tsumune et al., 2013).

5A.2. GEOMAR

"GEOMAR" is the name of the model used and described in Dietze and Kriest (2012). It is a global configuration of the MOM4 P0d (GFDL Modular Ocean Model v.4, Griffies et al., 2005) z-coordinate, free surface ocean general circulation model. The horizontal configuration is an eddy resolving around Japan and coarser elsewhere. The vertical grid has a total of 59 levels. The bottom topography is interpolated from the ETOPO5 dataset with a 5-min gridded elevation data set from the National Geophysical Data Center (http://www.ngdc.noaa.gov/mgg/fliers/ 93 mgg01.html). We use partial cells, and the

atmospheric forcing consists of (6 hourly) wind stress, heat, and freshwater flux fields derived from the 40 ERA-Interim re-analyses by the European Centre for Medium-Range Weather Forecasts (ECMWF) (Uppala et al., 2005, and many more to follow). In addition to the heat fluxes from the ECMWF, a flux correction restores the sea-surface temperatures (SSTs) with a time scale of 30 days to the monthly mean SSTs derived from a blend of satellite products (C. Rathbone, personal communication, 2006). Sea-surface salinity is restored to the World Ocean Atlas 2005 (Antonov et al., 2006) annual mean climatology with a timescale of 90 days. The vertical mixing of the momentum and scalars is parameterized with the KPP approach of Large et al. (1994). The relevant parameters are (1) a critical bulk Richardson number of 0.3 and (2) a vertical background diffusivity and viscosity of 10^{-5} m^2/s. We also account for the double-diffusive and nonlocal fluxes. The integration starts from rest with initial temperatures and salinities interpolated from the World Ocean Atlas 2005 annual mean (Locarnini et al., 2006; Antonov et al., 2006) onto the model grid. After a spinup of 5 yr that covers the period from 1993 to 1998, the clock assigning the model forcing is reset to 1993, and the model is integrated for another 5 yr. A comparison of the simulated currents with those derived from the satellite altimetry suggests (as shown by Dietze and Kriest, 2012) that our nominal "1993 state" (following the spinup) is similar to the actual conditions during the accident in 2011. Note that this is a pragmatic approach. Ideally, we should have applied actual and realistic fluxes to drive the circulation model. Nonetheless, as a result of uncertainties in the initial conditions and the highly nonlinear dynamics of ocean eddies, an exact hindcast is impossible without constructing a complex data assimilation machinery.

The accidental release of ^{137}Cs is simulated by embedding (online) an artificial tracer into the MOM4 P0d circulation model. The tracer (2.3PBq) is released into a surface grid-box comprised of the 10×10 km grid closest to the location of the nuclear power plant on April 1. The tracer is conservative; therefore, it does not decay but behaves similarly to a dye and is subject to mixing and advection only. For timescales much shorter than the ≈30 yr half-life of ^{137}Cs, the behavior of our artificial tracer mimics that of ^{137}Cs. Because we released all of the ^{137}Cs within one time step into one grid box, in the first days following the release, the numerical dispersions were smoothed until the initial steep spatial gradients. Although this is clearly spurious behavior, we find that the associated fluxes are insignificant when compared to the total release.

5A.3. IRSN

The IRSN used the Model for Application at Regional Scale (MARS3D) (Lazure and Dumas, 2008) to simulate the dispersion of ^{137}Cs released from the FDNPP reactors towards the open sea. The MARS3D is a three-dimensional free-surface ocean circulation model formulated using sigma coordinates. To remain applicable in a "crisis" situation, we use the MARS3D model "as is." This model is usually applied along the European continental shelf in both tidal and thermohaline contexts (Bailly du Bois et al., 2012a; Batifoulier et al., 2012; Garreau et al., 2011). The model domain covers the oceanic area off of Fukushima: 31°N - 43.2°N, 137°E - 150°E (1000 km × 1200 km, Fig. 5.1), and the horizontal resolution is approximately 1.852 km (one nautical mile, 1/60°) in an E-W and N-S direction, with 742 grid cells in the E-W direction and 622 in the N-S direction. The vertical resolution of the sigma coordinate is 40 layers that are refined near the surface. The bathymetric data are derived from the JODC (JODC, 2011). The model accounts for the regional and local circulation, i.e., the Kuroshio Current, flux through the Tsugaru Strait, wind forcing and tides. The tide at the open boundary conditions is described using 16 tidal harmonic components from the FES2004 numerical atlas (Lyard et al., 2006) with a horizontal resolution of 1/8°. At the scale of thermohaline and geostrophic effects, the initial and boundary conditions are derived from the daily oceanic forecast and hindcast of the global model proposed by the MERCATOR-ocean model with a resolution of 1/12° (http://www.mercator-ocean.fr/eng (Ferry et al., 2007)). For the downscaling procedure, the temperature, salinity, currents and sea level are interpolated in both time and space to provide the boundary conditions. Similarly, the wind forcing, water and heat flux are downscaled from the atmospheric forecast and hindcast of the NCEP meteorological global model (http://www.ncep.noaa.gov/) with a resolution of 1/2°.

The ^{137}Cs source term from the direct release is derived from the calculated flux provided in Bailly du Bois et al. (2012b) and amounts to 27 PBq. The atmospheric deposition is calculated from the hourly deposition derived from the atmospheric dispersion calculations using the IRSN's Gaussian puff model pX (Korsakissok et al., 2013), which estimates a total deposition onto the sea of 3 PBq on March 23, 2011.

The initially applied wind drag coefficient (Cd) initially is a classically adopted value with p=0 in Cd=0.0015×Wp. W represents the wind vector module (Wx, Wy) at 10 m. We have fixed p=0.8 to fit with the measured time-evolution of the ^{137}Cs amounts based on hundreds of measurements integrated over space and time in an area of 50 × 100 km facing the FDNPP. We consider that the environmental half-time measured in this area is a robust

parameter for the model comparison. With regards to general circulation, this modification of the drag coefficients does not change the main patterns, such as the position and strength of the Kuroshio Current and generation of eddies and loops; however, it obviously increases the surface current variability.

5A.4. JAEA

An oceanic forecasting system of radionuclide dispersion was developed by the Japan Marine Science Foundation of Kyoto University and the JAEA to predict the radionuclide dispersion associated with a spent nuclear fuel reprocessing plant in Rokkasho Village, Aomori Prefecture. A three-dimensional ocean general circulation model developed at Kyoto University and the Japan Marine Science Foundation calculates the ocean current, temperature, salinity, etc., whereas the oceanic dispersion model SEA-GEARN developed at the JAEA predicts the radionuclide dispersion (Kobayashi et al., 2007). We performed a downscaled calculation from the North Pacific with a horizontal resolution of $1/8° \times 1/6°$ to a finer domain in the northwestern North Pacific with a horizontal resolution of $1/24° \times 1/18°$. Subsequently, a similar downscale calculation predicted an oceanic condition for a coastal area off of the Fukushima Prefecture with a horizontal resolution of $1/72°$ in latitude and $1/54°$ in longitude. The finest model was forced by the data from the National Centers for Environmental Prediction-Department of Energy (NCEP-DOE) Reanalysis 2 and the Mesoscale Model (MSM) wind data constructed at the Japan Meteorological Agency. In addition, a data assimilation with the four-dimensional variational method was adopted to perform a reanalysis in a northwestern region of the North Pacific (Ishikawa et al., 2009). The assimilated data consisted of the satellite altimeter data from the Archiving, Validation, and Interpretation of Satellite Oceanographic data/Collect Localisation Satellites (AVISO/CLS) and sea-surface temperature data from the Operational Sea-Surface Temperature and Sea Ice Analysis (OSTIA), etc.

We used a source term for the ^{137}Cs amount discharged into the ocean that was primarily based on the term estimated by Kawamura et al. (2011). They successfully constructed a source term using the oceanic monitoring data obtained near the northern and southern discharge channels at the FDNPP. The airborne ^{137}Cs amount deposited at the sea surface was calculated using the Worldwide Version of System for Prediction of Environmental Emergency Dose Information (WSPEEDI-II) developed at the JAEA (Terada et al., 2008).

5A.5. JCOPET

The JCOPET is a high-resolution nested coastal ocean model that is based on the Princeton Ocean Model with a generalized sigma-coordinate in the vertical direction (see Guo et al., 2010 and Miyazawa et al., 2012 for more details) and developed for coastal ocean prediction studies for Japan. It has a 1/36° horizontal grid spacing both in latitude and longitude and covers a domain at 28°N-44°N, 125°E-148°E with 46 vertical levels. The JCOPET is nested in a 1/12° resolution JCOPE2 model of the western North Pacific domain, which is also embedded in a coarser Pacific Ocean model. The JCOPE2 incorporates a sophisticated ocean data assimilation scheme that assimilates the satellite sea-surface height anomaly, satellite-observed sea-surface temperature, and in situ temperature and salinity data that are observed by vessels. The required lateral boundary conditions for the JCOPET calculations are derived from these JCOPE2 values. The JCOPET does not possess a data assimilation scheme except for a simple nudging of temperature and salinity towards the JCOPE2 fields; however, the tidal forcing of 16 constituents is imposed at the open boundaries. The freshwater inputs of 35 major rivers within Japan are also considered in the JCOPET calculations. The horizontal mixing coefficients are calculated using a Smagorinsky (1963)-type formula, and the vertical mixing coefficients are derived from a turbulent closure model of Mellor and Blumberg (2004). The surface forcing is obtained by the Japan Meteorological Agency's nonhydrostatic Mesoscale Model (JMA_MSM) with a 5 km resolution.

For the ^{137}Cs dispersion calculation, the velocity fields are obtained from the JCOPET model with the ocean reanalysis output of the JCOPE2 assimilative system (Masumoto et al., 2012). The ^{137}Cs concentrations are dispersed as passive tracers in the JCOPET with a 30.1-year half-life of radioactivity. We adopt both the direct discharge to the ocean from the FDNPP and atmospheric deposition onto the sea surface as source terms of ^{137}Cs for this particular calculation. The direct discharge scenario is similar to the one used by Tsumune et al. (2012), in which the total amount of radionuclides is 5.7 PBq. The spatial and temporal distributions of the atmospheric deposition of ^{137}Cs are estimated by a one-way nested regional air quality forecasting (AQF) system described by Honda et al. (2012), with the total amount of the atmospheric deposition of 0.3 PBq in the western North Pacific for the period from March 11 to May 6, 2011.

5A.6. KIOST/IMMSP

The KIOST/IMMSP is a high-resolution coastal ocean model for radionuclide transport that is based on the finite-element SELFE model (Zhang and Baptista, 2008; Roland et al., 2012). The model was developed by the Korea Institute of Ocean Science and Technology (S. Korea) and the Institute of Mathematical Machine and System Problems (Ukraine). The model domain is 135°-148°E, 32°-43°N with the finest grid resolution close to the FDNPP at approximately 500 m; the total number of elements is 97,989. The vertical coordinate is s-system with 36 s-levels refined near the surface. The vertical viscosity and diffusivity are calculated from the $k - \varepsilon$ model. The surface forcing is obtained from the ERA-Interim reanalysis. The lateral boundary conditions for the KIOST/IMMSP calculations are obtained from the HYCOM nowcast/forecast system. The KIOST/IMMSP temperature is nudged towards the HYCOM fields, and the tidal forcing is imposed at open boundaries using the NAO.99b tidal prediction system.

The Eulerian radionuclide transport model describes the transport of radionuclides in a solution or on suspended sediments and as they settle, resuspend and diffuse into the bottom sediments (Margvelashvily et al., 1997). The sediment (silt) concentration was prescribed, and the liquid release scenario from the FDNPP was adopted from Kawamura et al. (2011); the total amount of ^{137}Cs released was 3.8 PBq.

5A.7. Kobe University

A synoptic, oceanic downscaling based on the UCLA-ROMS (Shchepetkin and McWilliams, 2005) in a double-nested configuration with an Eulerian passive tracer module is developed for the initial oceanic dispersal of dissolved radioactive ^{137}Cs (Uchiyama et al., 2012; Uchiyama et al., 2013). The outer-most boundary condition and initial condition are provided by the assimilative daily-mean JCOPE2 reanalysis (Miyazawa et al., 2009). The 12-hourly averaged solution of the parent ROMS-L1 model at a horizontal resolution of dx = 3 km ($256 \times 256 \times 32$) is projected onto the perimeters of the child ROMS-L2 at dx = 1 km ($512 \times 512 \times 32$) in time and space with a one-way offline nesting approach (Mason et al., 2010; Buijsman et al., 2012; Romero et al., 2013). Both the L1 and L2 domains are rotated horizontally to approximate an alignment with the coastline of Fukushima Prefecture. A vertically stretched s-coordinate is introduced so that the grid refinement occurs near the surface. Neither the lateral viscosity nor diffusivity is considered other than the intrinsic hyper-diffusion caused by the third-order upwind-biased advection scheme. The KPP model

is used for the surface and bottom planetary boundary layers. The model topography is based on the JODC's J-EGG bathymetry at $dx = 0.5$ km, which is complemented by the SRTM30 dataset at 30 arc-seconds. An hourly reanalysis of the JMA's assimilative GPV-MSM atmospheric product determines the surface wind stress. The surface heat, freshwater and radiation fluxes and the SSS (with a weak restoring force at a time scale of 90 days) are from the COADS monthly climatology. The monthly climatology of freshwater discharge from all of the major rivers in the model domains is considered as the mass point sources. The online Eulerian tracer tracking is conducted in the L2 model by exploiting the leakage scenario proposed by Tsumune et al. (2012), which ignores the atmospheric fallout and half-life decay of the nuclide. A near-field dilution submodel similar to what is used in Uchiyama et al. (2014) is utilized to avoid underestimating the unresolved dilution near the release site. The relative concentration of ^{137}Cs as a result of the unit leakage flux (1 Bq/s) is computed and then compared to the observed data collected just off of the FDNPP for rescaling to the actual concentration. The L1 model is initialized on Oct. 1, 2010, whereas the L2 model begins on Jan. 1, 2011 to spinup the model ocean sufficiently. The computed circulation, SSH, and ^{137}Cs concentrations are carefully verified against the AVISO satellite altimetry and in situ concentration data of the sampled radionuclides to confirm a reasonable consistency.

5A.8. MSSG

The MSSG is an air-sea-coupled model developed at the JAMSTEC (see Takahashi et al., 2008 for more details). Only the oceanic component is used here. This model has a z-coordinate in the vertical direction and latitude-longitude coordinates in the horizontal direction. The model domain covers and area at 140.2°E-143.2°E and 34.85°N-39.14°N with a resolution of approximately 2 km. The bottom depths are based on the ETOPO1 (Amante and Eakins, 2009) with 73 levels in the vertical direction and a 3 m resolution near the surface. The lateral boundaries of the flow field, temperature, and salinity as well as the surface temperature and salinity are set by the JCOPE2 (Miyazawa et al., 2009). The surface wind stress is estimated based the 10-m wind from the Grid Point Value of Meso-Scale Model (GPV/MSM) from the Japan Meteorological Agency. For the subgrid scale parameterization, a Smagorinsky-type Laplacian viscosity and diffusion are used in the lateral and a Noh-Kim vertical mixing scheme is used in the vertical (Noh and Kim, 1999). There are no freshwater inputs or atmospheric fallout. The model is integrated from Dec. 1, 2010 to June 30, 2011.

A Lagrangian particle-tracking model is used to solve the dispersion of radionuclides (See Choi et al. (2013) for more details). The model simulates the migration of radionuclides between three phases: dissolved in sea-water, adsorbed in large-particulates, and adsorbed in bottom-sediments. Radionuclides are transferred between the sea-water and large-particulates or sea-water and bottom-sediments through adsorption and desorption. Transfers between large-particulates and bottom-sediments occur through settling and erosion, and the radionuclides adsorbed in the bottom sediment are not advected. The oceanic discharge of radionuclides from the FDNPP occurs according to a scenario proposed by Tsumune et al. (2012), which produces a total amount of radionuclide adjusted to 5.5 PBq and assumes that the radionuclides are dissolved in sea water.

5A.9. NIES

An ocean model has been developed by the National Institute for Environmental Studies (NIES) to evaluate and predict pelagic-benthic environments, especially eutrophication phenomena in coastal bays and shallow shelves. The model is composed of the following three sub-models: hydrodynamic, biogeochemical cycle, and bivalve life-cycle (Higashi et al., 2012). In the latest NIES model, the hydrodynamic sub-model consists of hydrostatic-Boussinesq primitive equations solved by the finite difference method in a collocated grid system. The free sea surface is tracked by the volume-of-fluid (VOF) method (Hirt and Nichols, 1981) in a z-level vertical grid. The vertical mixing process is parameterized using the Level 2.5 turbulence-closure model (Mellor, 2001), and the horizontal mixing is calculated according to Smagorinsky (1963). The sea-surface fluxes are the boundary conditions for the momentum and heat transport equations and evaluated using the method of Kondo (1975).

In the NIES simulation, the ^{137}Cs dispersion was obtained by solving an advection-diffusion equation with source/sink terms from the same numerical method as the heat and the salinity transports with 2.2 km horizontal resolution. The source terms included the direct discharge to the ocean from the FDNPP and atmospheric deposition onto the sea surface. The spatial and temporal distributions of the atmospheric deposition of ^{137}Cs were simulated by the WRF-CMAQ model (Morino et al., 2013) with a 3 km horizontal resolution. The time series data of the ^{137}Cs direct discharge was identical to the data estimated by Tsumune et al. (2012). The sink term only considered the radioactive decay, and the current fields were simulated by the hydrodynamic sub-model under the following conditions. For

the atmospheric conditions, we used the surface data (hourly, 5 km resolution) of the wind velocity, air temperature, specific humidity, and air pressure from the grid point value-mesoscale model (GPV-MSM) provided by the Japan Meteorological Agency (JMA). For the downward short-wave and long-wave radiations, we used the grid data (6 hourly, 110 km resolution) produced by the JMA climate data assimilation system (JCDAS). The current field data derived from the FRA-JCOPE2 (Miyazawa et al., 2009) (daily, 1/12° resolution) was applied to the lateral open-boundary conditions and T-S assimilation data (simple nudging). The simulation was completed with the supercomputer at the NIES.

5A.10. WHOI-2D

Observation-based two dimension velocity fields are from the daily near-surface geostrophic currents (on a regular Mercator 1/3°×1/3° grid) from AVISO with 6-hourly Ekman velocities (2°×2° degree) based on the NOAA NCEP/ NCAR wind stresses. The wind stress at a 10 m height, τ, was converted to the ocean velocity at a depth of 15 m, u_{Ek} and v_{Ek}, using the Ralph and Niiler (1999) formula $u_{Ek} + iv_{Ek} = \beta\, e{-}i\theta/(f\rho)\, (\tau_x + i\tau_y)/\sqrt{|\tau|}$, where $\rho = 1{,}027$ kg·m^{-3} is the assumed seawater density, f is the Coriolis parameter, $\theta = 55°$ is the rotation angle of the Ekman current, and $\beta = 0.065$ s$^{-1/2}$. This observation-based velocity is reliable and provides global coverage; however, it has sparse temporal and spatial resolution and a two-dimensional nature and lacks ageostrophic components. To account for the lateral diffusion and the influence of the unresolved scales, a small stochastic velocity (of a random sign taken from the normal distribution with a standard deviation of 5 cm s^{-1}) was added to the sum of the geostrophic and Ekman velocities. We have verified that the results of our simulations are not sensitive to the specifics of this stochastic velocity field; however, we have listed these details for thoroughness.

The spread of ^{137}Cs is modeled using a Lagrangian framework by repeatedly releasing large numbers of simulated water parcels inside the source domain over the full duration of the source time series. These water parcels are advected by the velocity fields described above, and their trajectories are estimated using a fixed-step (RK4 for runs with the stochastic velocity component) or variable-step (RK4(5) for runs without the stochastic velocity component) Runge–Kutta integration scheme with a bilinear interpolation in time and space between the grid points. The exponential decay of ^{137}Cs concentrations from the initial source value (half-life of 30.16 years) is applied to estimate the concentration of ^{137}Cs following each water parcel. This Lagrangian model provides an intuitive framework that

illuminates the physical mechanisms by which the contaminated waters are brought from the source region to their position at any given time. The disadvantage of this framework is its numerical intensity, which result from the large number of released water parcels and the simplified method by which the calculation treats the diffusion process. As the number and frequency of the released parcels increases, the resulting Lagrangian distribution of ^{137}Cs approaches the value estimated from an Eulerian calculation with the corresponding value of diffusivity. To validate the process, the results of our simulations were tested to ensure that they were not sensitive to further increases in the number of the released parcels. The lack of sensitivity to such an increase suggests that the observed distribution of ^{137}Cs is close to the limiting value (i.e., for an infinitely number of parcels).

5A.11. WHOI-3D

The ^{137}Cs dispersion calculation was the same as in the WHOI-2D model; however, three dimension velocity fields were from the Navy Coastal Ocean Model (NCOM), a high-resolution numerical model (Barron et al., 2004; 2006). A regional model with a 3 km horizontal resolution was nested with open boundaries within the HYCOM global 1/8° model. The model has a hybrid vertical coordinate system with 15 z-levels at the top and 35 density-defined levels underneath for a total of 50 vertical levels. The model was forced with wind and heat fluxes from the Coupled Ocean/Atmosphere Mesoscale Prediction System for the Western Pacific (COAMPS_WPAC). Tides at the boundaries were provided by the Oregon State Model (Egbert and Erofeeva, 2002). The SSH, SST and available T-S profile data from the Naval Oceanographic Office were assimilated into this model using optimal interpolation. The model was run each day, and the data from the previous day were assimilated to provide a 48-hour forecast. One-day segments at the beginning of each run were then stacked together to create a longer time-series covering the time interval from mid-March until the end of June 2011. There were discontinuities in the velocity field between the end of one day and beginning of the next day; however, these were small and did not create any known issues in our evaluation. Unlike our observation-based circulation, the NCOM 3-D velocities varied with depth throughout the water column and had the advantage of improved spatial and temporal resolution than what was provided by the observations. The disadvantages of the NCOM were the smaller model domain and limited ability to match specifically measured oceanic features, such as the exact position of the Kuroshio Current and mesoscale eddies present during the spring of 2011, with the model estimate of the

circulation field. Compared to the observation-based model, the NCOM generally overestimated the mean Kuroshio Current velocity; however, it slightly underestimated the mean currents throughout the rest of the domain. The general shape of the mean Kuroshio Current was captured relatively well in the NCOM; however, its exact position meandered, and the mesoscale eddies were slightly misplaced in the NCOM compared to observations. The variability in the eddy velocities was of the same order in the two models, with the highest variability in the general area of the Kuroshio extension.

Appendix 5B. Horizontal distribution maps

The 10-day averaged horizontal distributions of ^{137}Cs (surface velocities) for the end of March and April are shown in Figs. 5.4 and 5.6 (Figs. 5.5 and 5.7), respectively, and the general descriptions of the figures are written in the main text. However, to view the details of the similarities and differences among the models in terms of shorter time-scale variations, finer-scale velocity distributions, and associated dispersions of the radionuclides, it is helpful to show all of the 10-day averaged maps for all of the model results. Here, we show a sequence of 10-day averaged maps for the ^{137}Cs and surface velocity distributions from March 22-31 to June 20-29, 2011, including Figures 4 to 7 again for thoroughness.

5B.1. 10-day averaged maps of ^{137}Cs at the sea surface
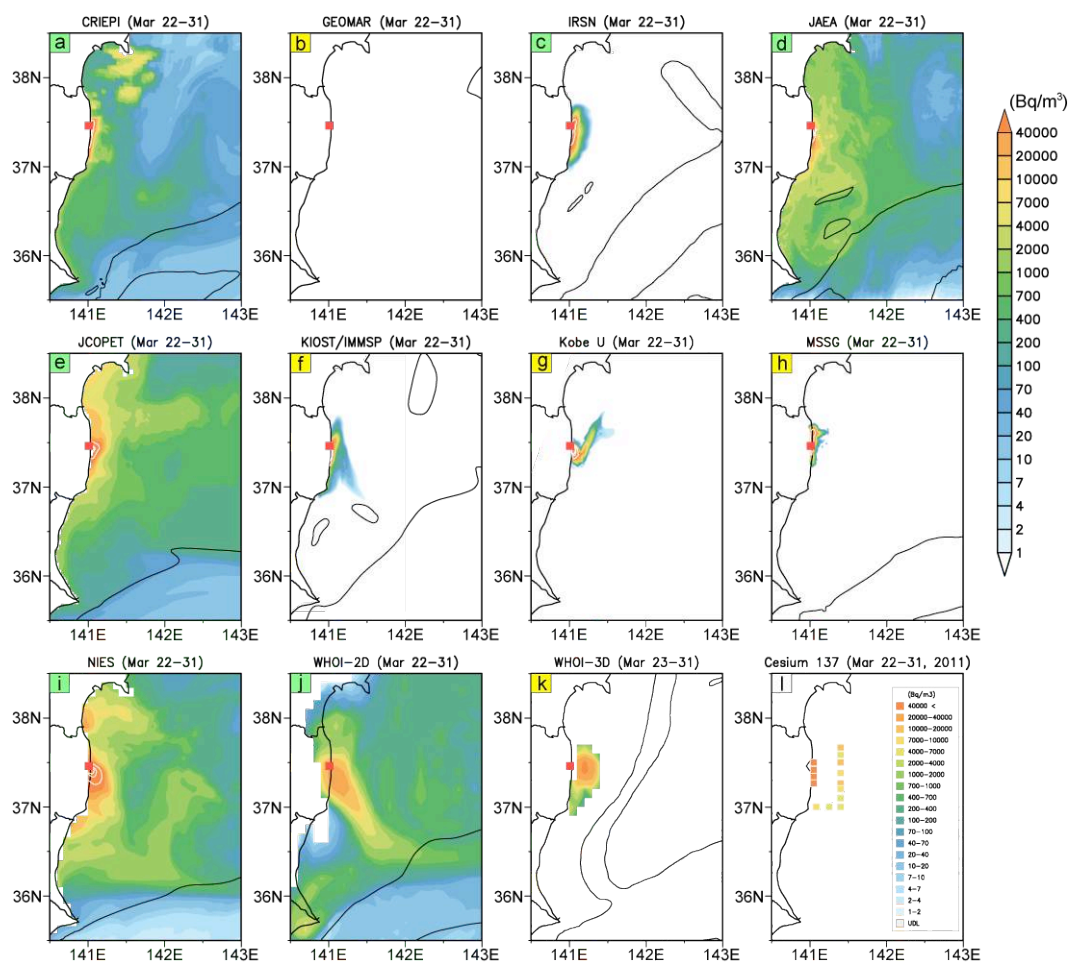
Figure 5B.1. (a)-(j) Horizontal distributions of ^{137}Cs concentration averaged over a 10-day period from March 22 to 31, 2011, with the name of the models indicated above each panel. Red squares indicate the location of the FDNPP. Black thin lines superposed on ^{137}Cs concentration indicate the contours of 0.5 m/s of the surface current magnitude, which show the general locations of the Kuroshio Current and other dominant features in this region. Panels with green (yellow) labels show results from models with (without) atmospheric deposition. Panel (l) shows the distribution of observed ^{137}Cs concentration during the same 10-day period.
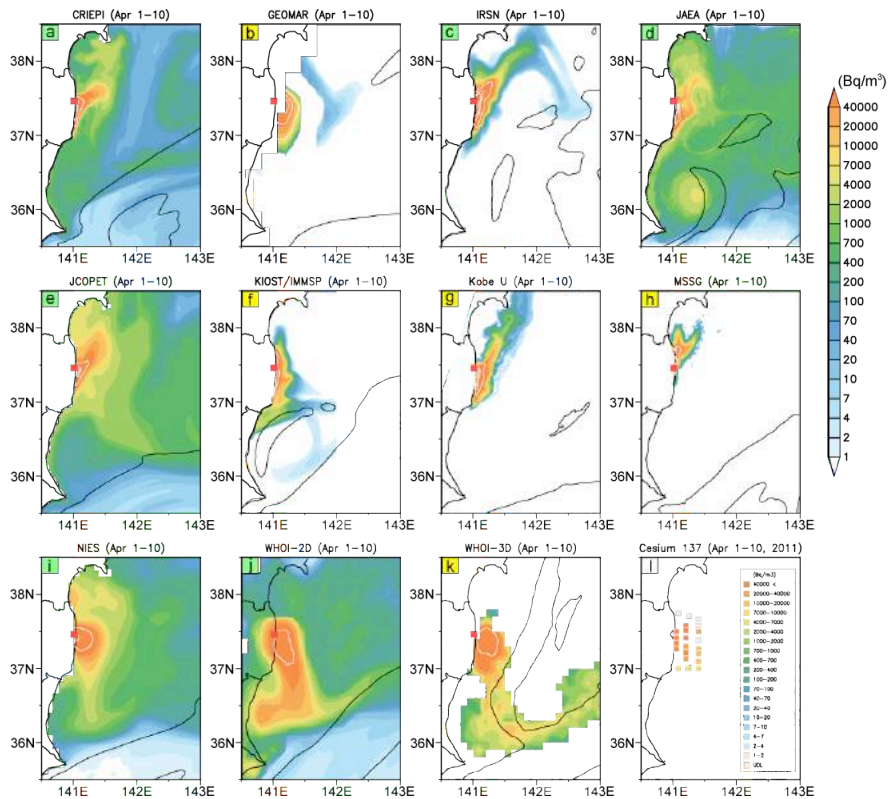
Figure 5B.2. Same as Fig. 5B.1 except for a period between April 1 and April 10.
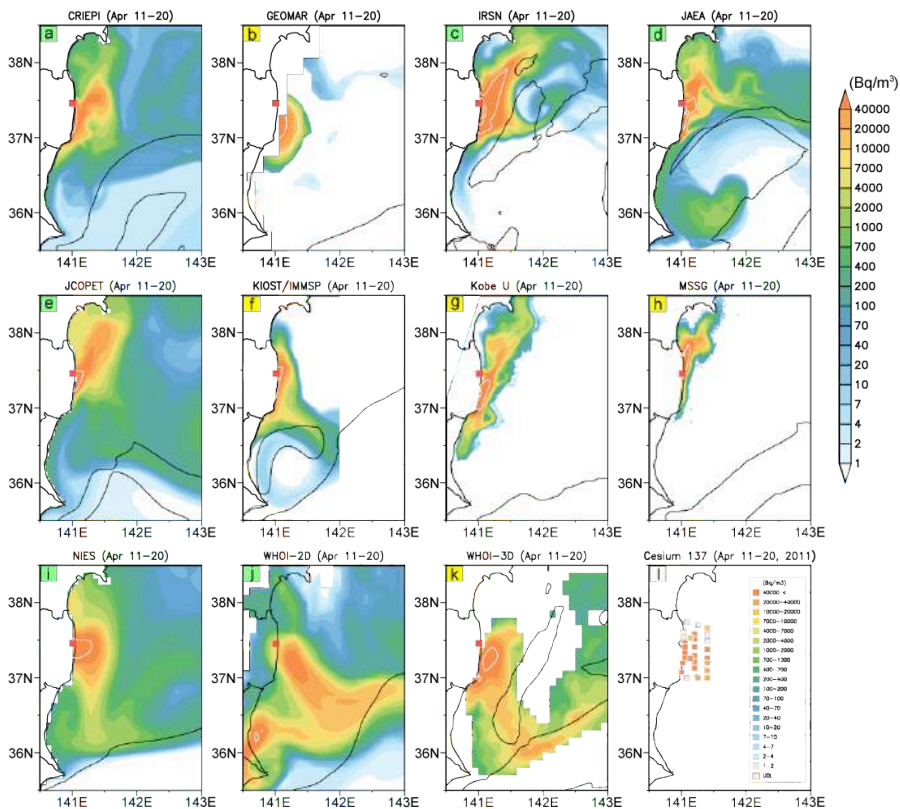
Figure 5B.3. Same as Fig. 5B.1 except for a period between April 11 and April 20.
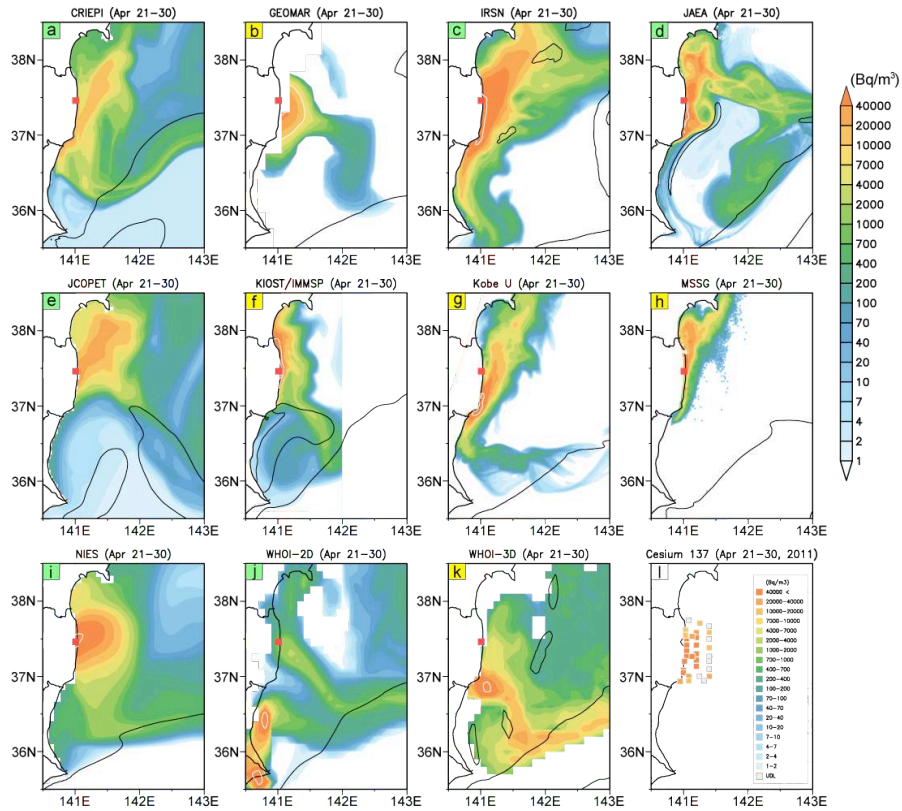
Figure 5B.4. Same as Fig. 5B.1 except for a period between April 21 and April 30.
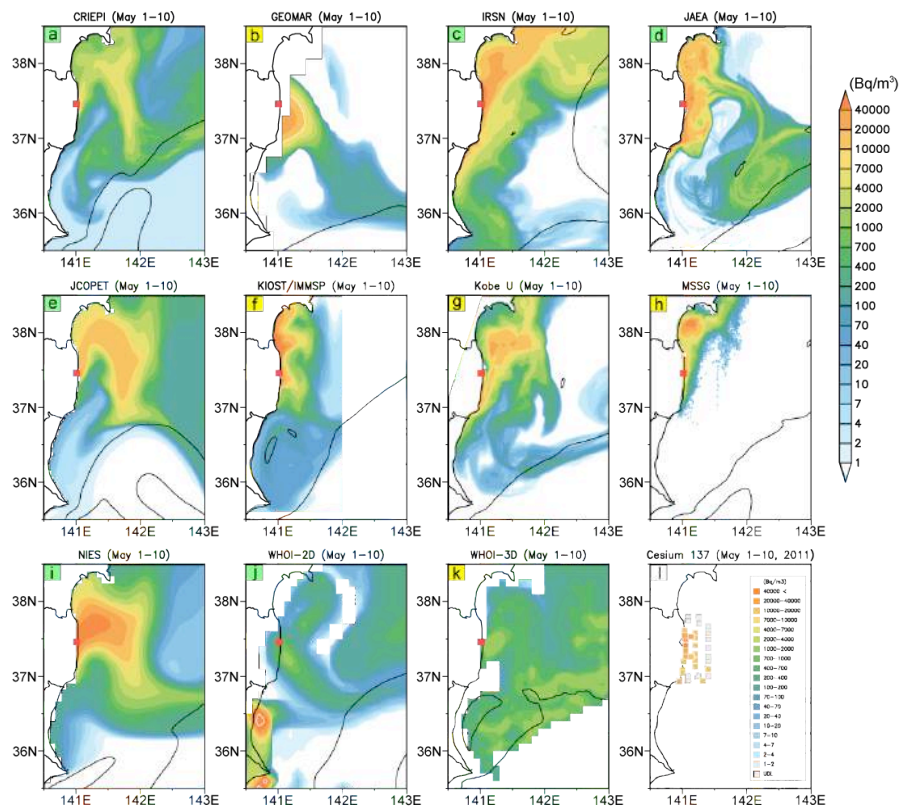
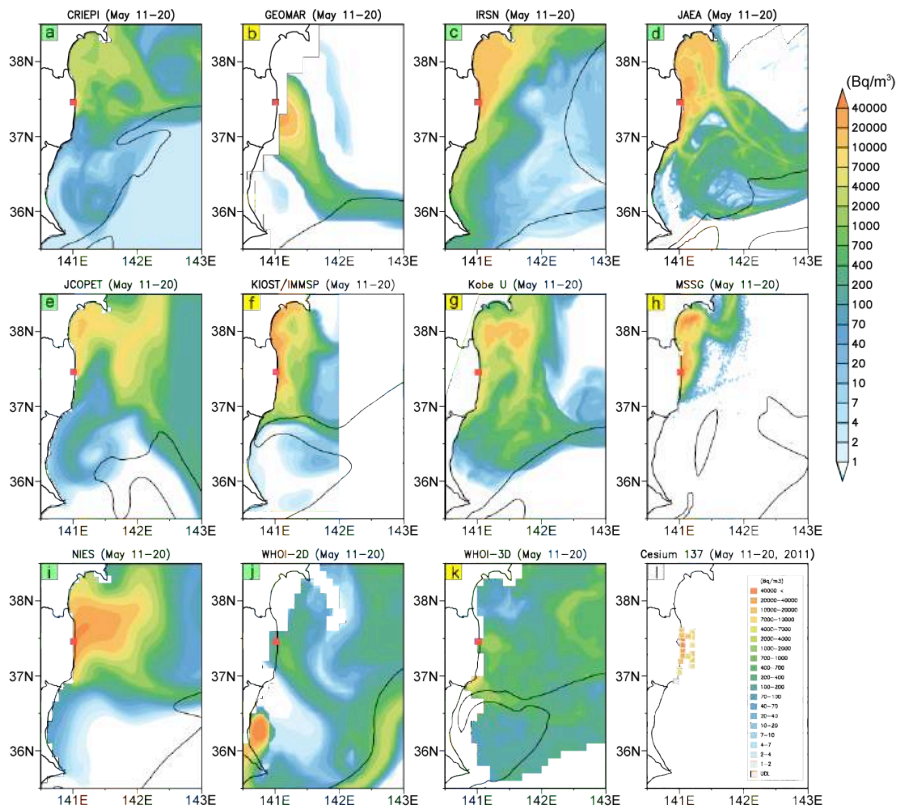Figure 5B.5. Same as Fig. 5B.1 except for a period between May 1 and May 10.

Figure 5B.6. Same as Fig. 5B.1 except for a period between May 11 and May 20.
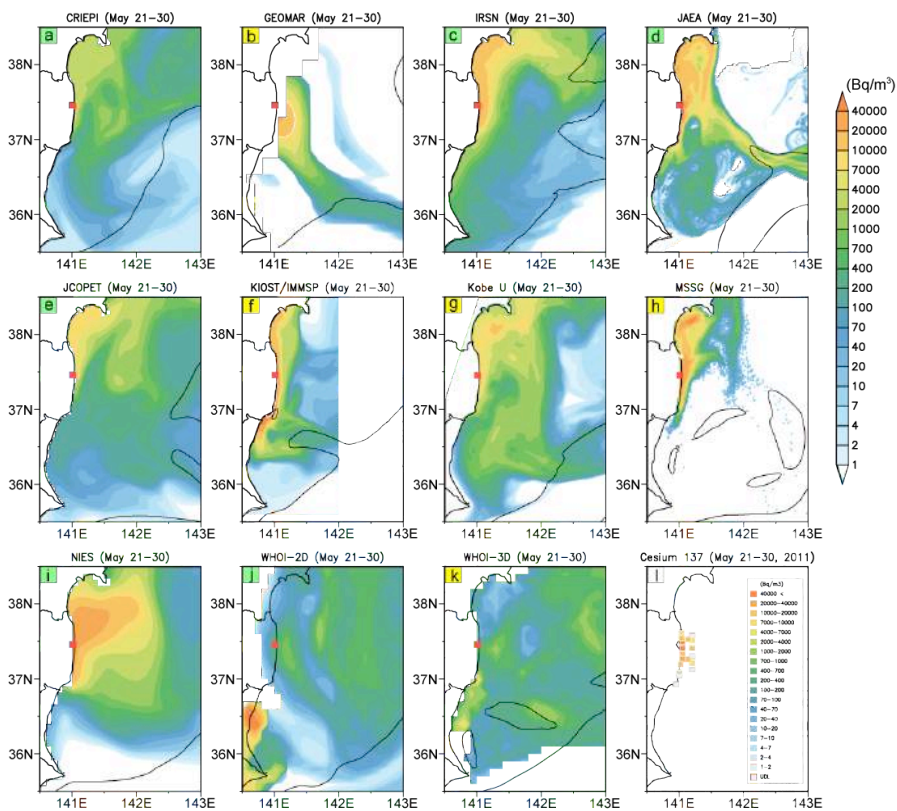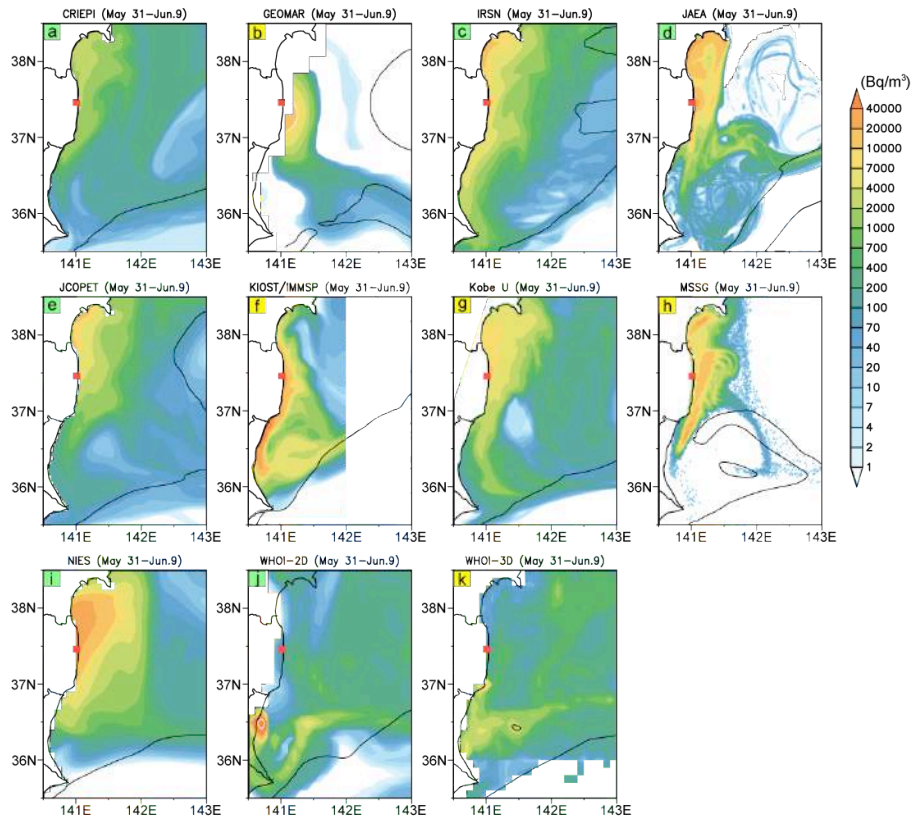

Figure 5B.7. Same as Fig. 5B.1 except for a period between May 21 and May 30.

Figure 5B.8: Same as Fig. 5B.1 except for a period between May 31 and June 9.
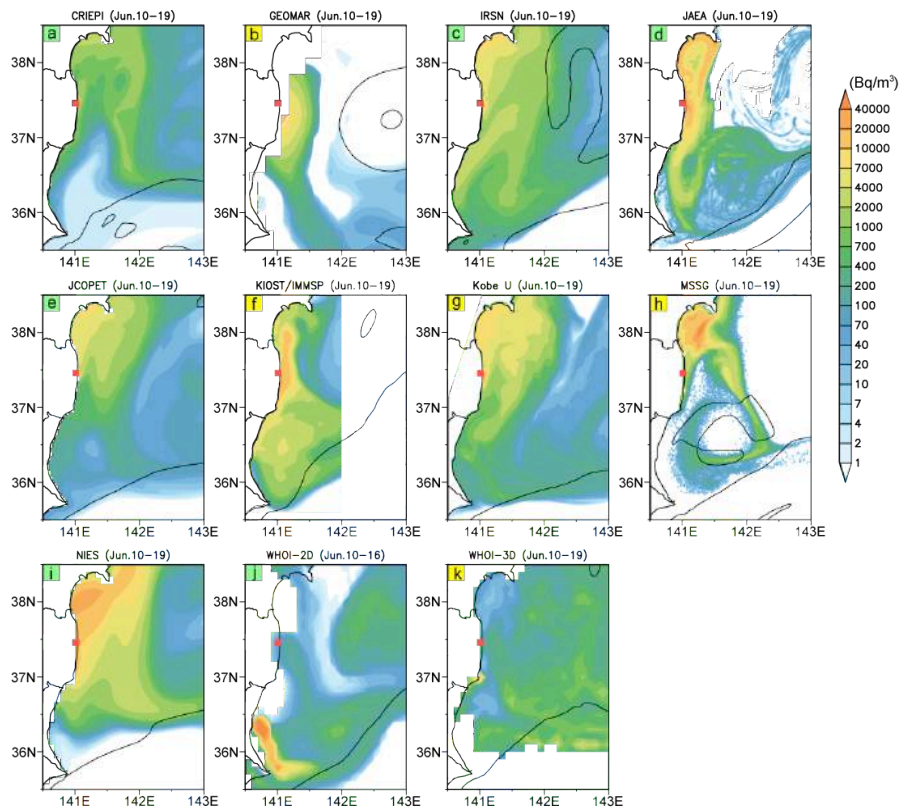

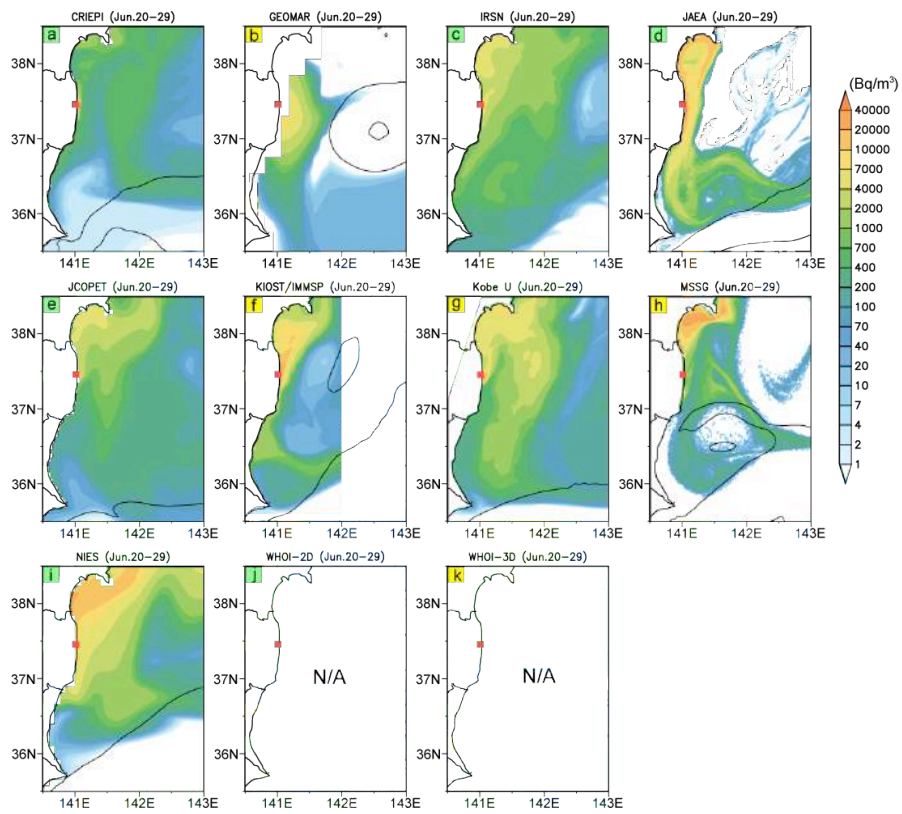Figure 5B.9. Same as Fig. 5B.1 except for a period between June 10 and June 19.

Figure 5B.10. Same as Fig. 5B.1 except for a period between June 20 and June 29.

5B.2. 10-day averaged maps of the surface velocity fields

The surface horizontal velocity fields are obtained from the velocity data at the upper most level of each model.
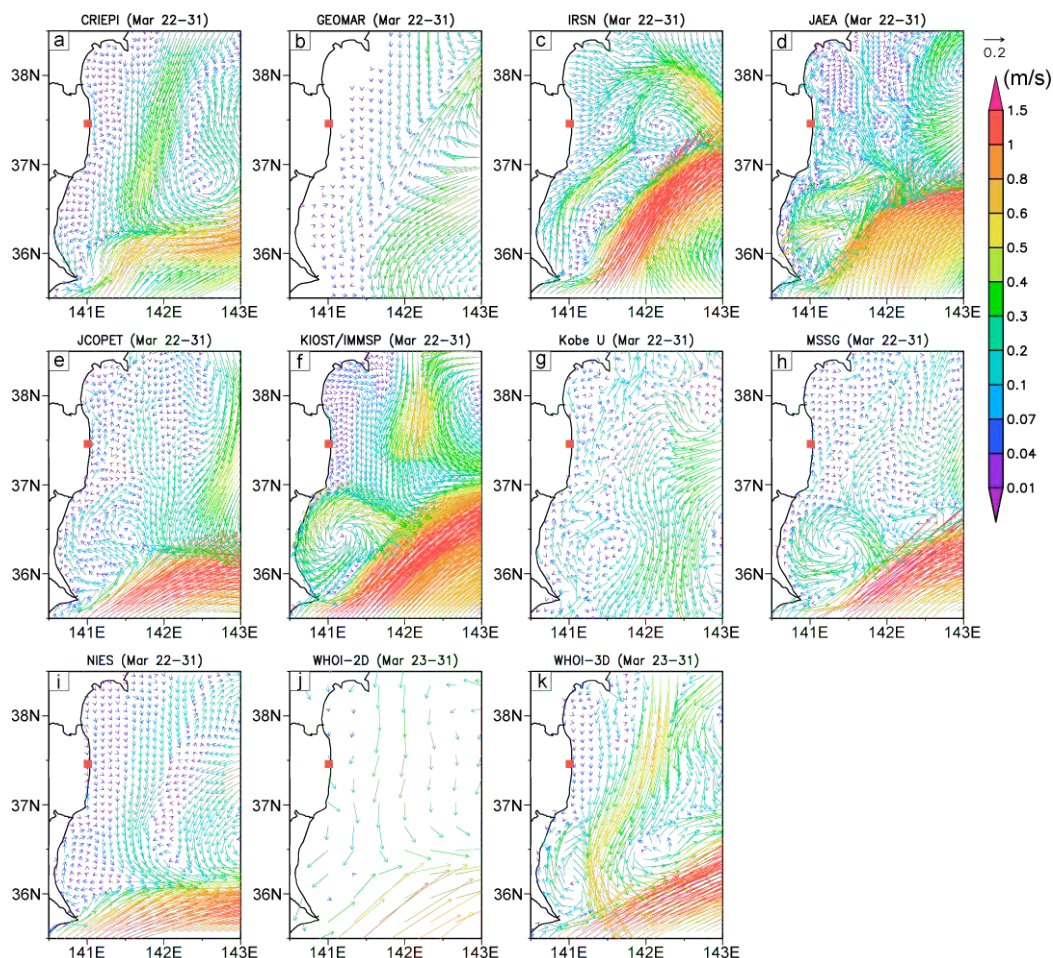

Figure 5B.11. Horizontal distribution of the surface velocity fields averaged over a 10-day period from March 22 to 31, 2011, and simulated in each model; the model name appears above each panel. No velocity data are provided from the IRSN, and the WHOI-2D has a course resolution based on the observed sea-surface height data with the geostrophic calculation. Other results are based on high-resolution ocean models. Note that the GEOMAR is forced by the ECMWF fluxes from 1993, which yields oceanic conditions similar to those that were actually encountered (Dietze and Kriest, 2012).
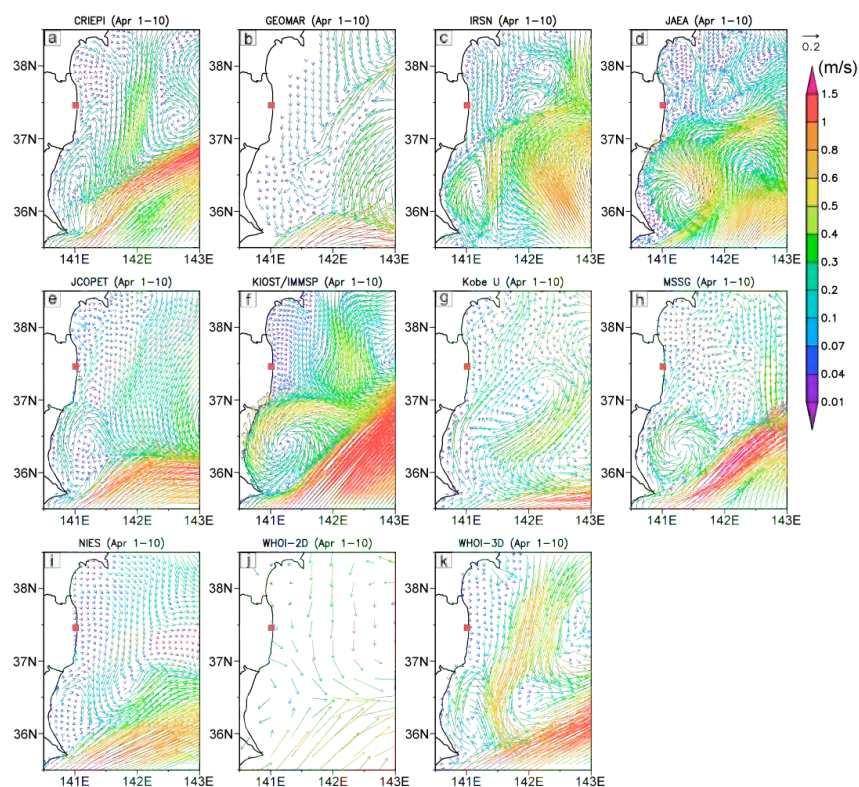
Figure 5B.12. Same as Fig. 5B.11 except for a period between April 1 and April 10.
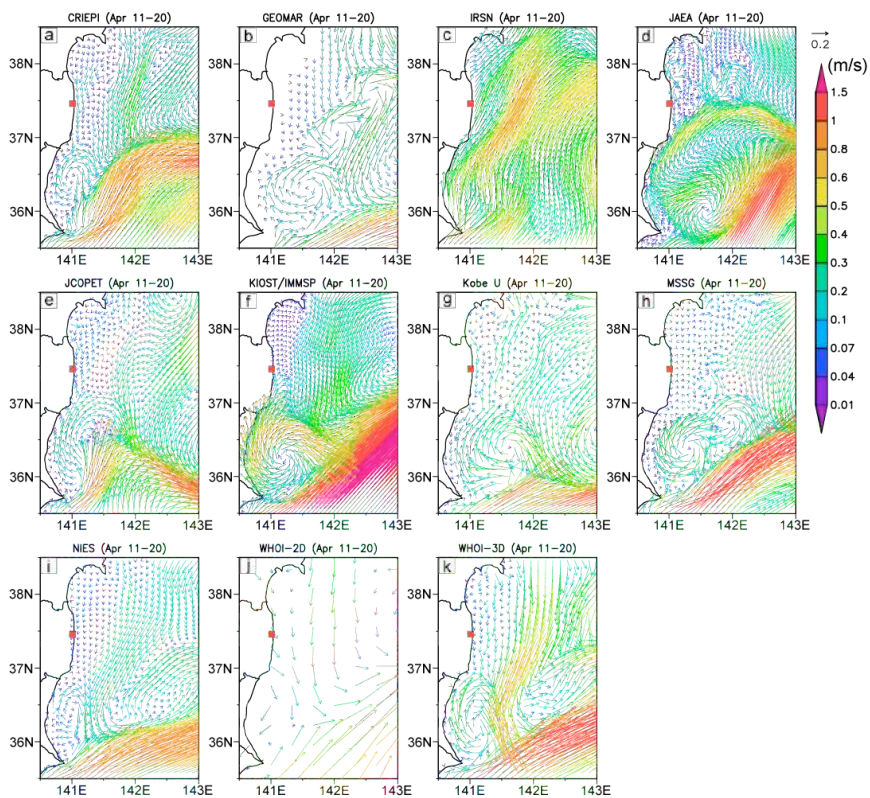

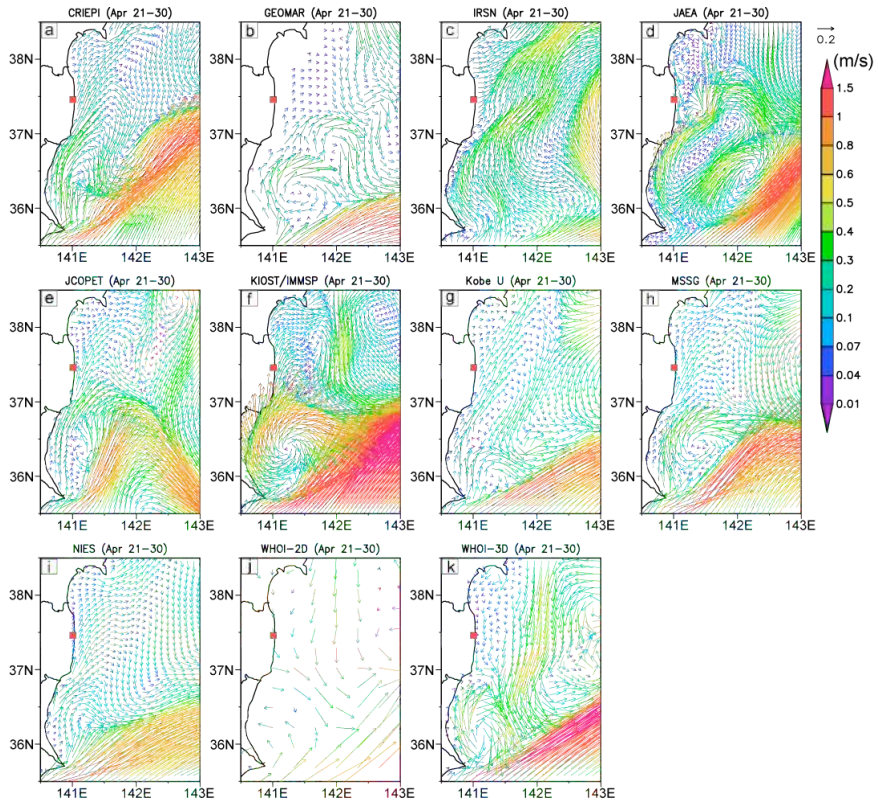Figure 5B.13. Same as Fig. 5B.11 except for a period between April 11 and April 20.

Figure 5B.14. Same as Fig. 5B.11 except for a period between April 21 and April 30.
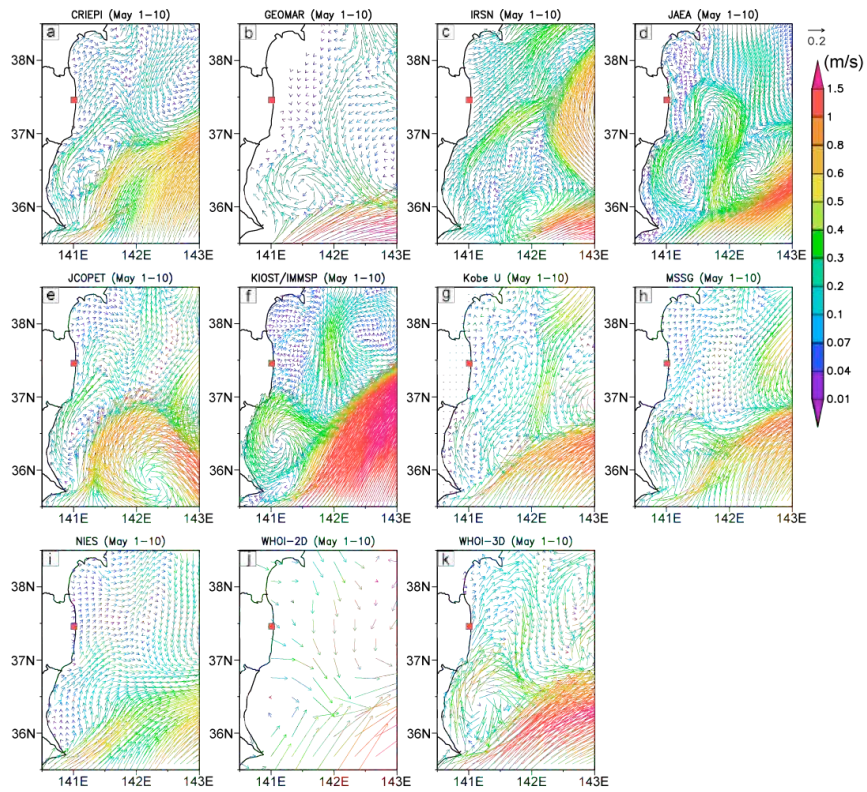

Figure 5B.15. Same as Fig. 5B.11 except for a period between May 1 and May 10.
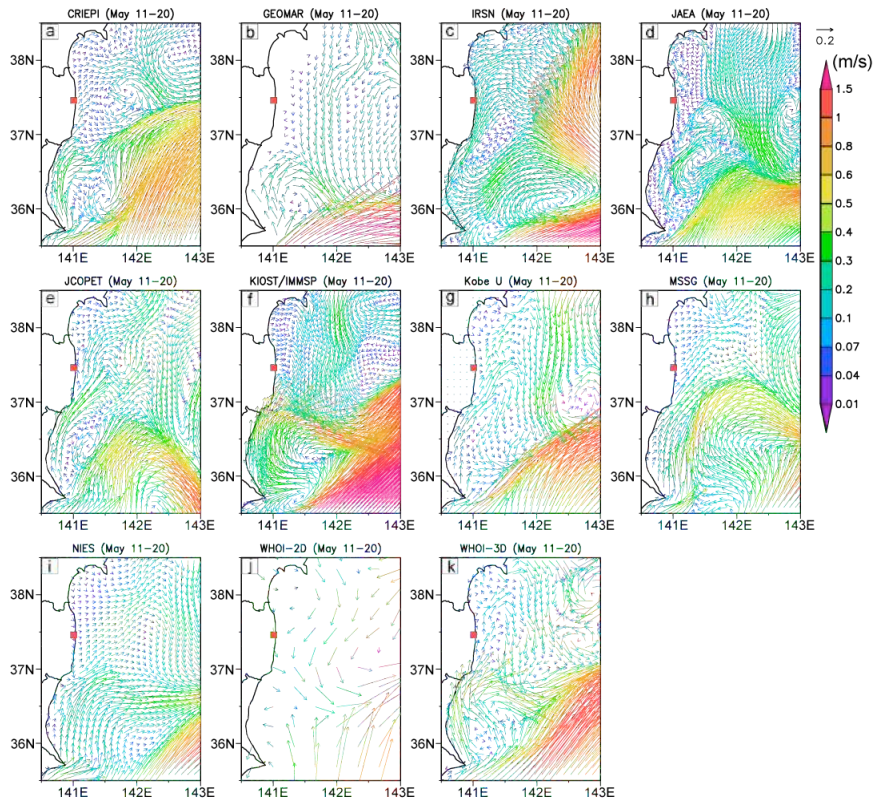
Figure 5B.16. Same as Fig. 5B.11 except for a period between May 11 and May 20.
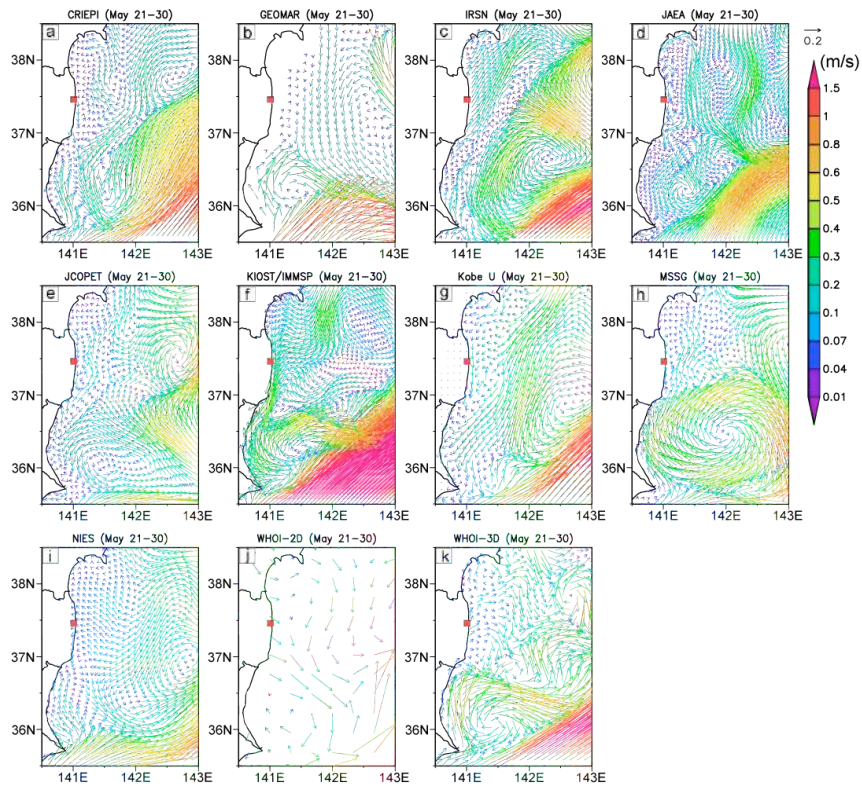

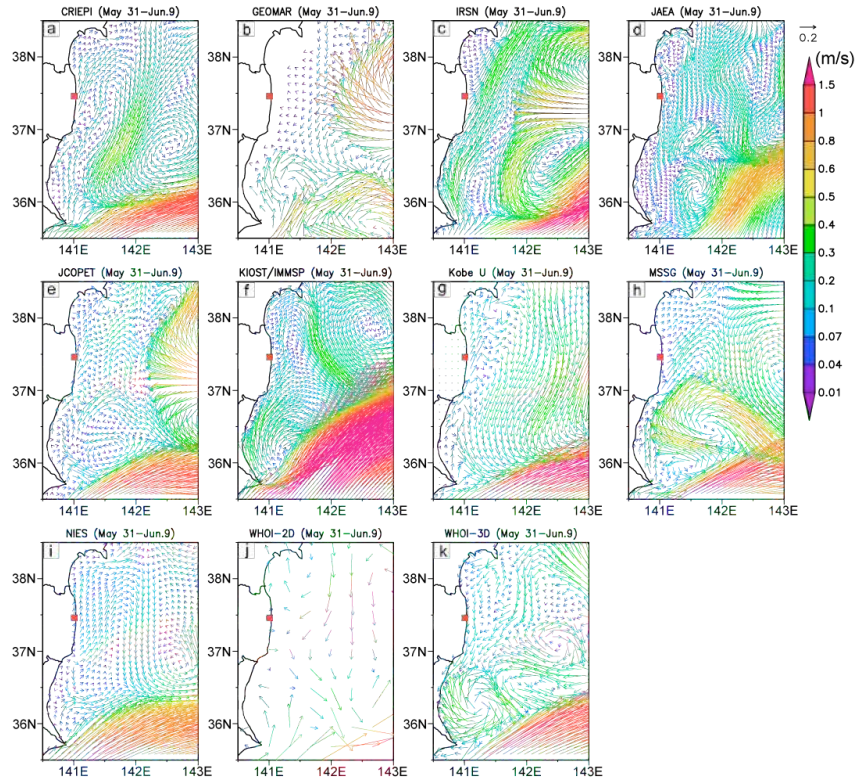Figure 5B.17. Same as Fig. 5B.11 except for a period between May 21 and May 30.

Figure 5B.18. Same as Fig. 5B.11 except for a period between May 31 and June 9.
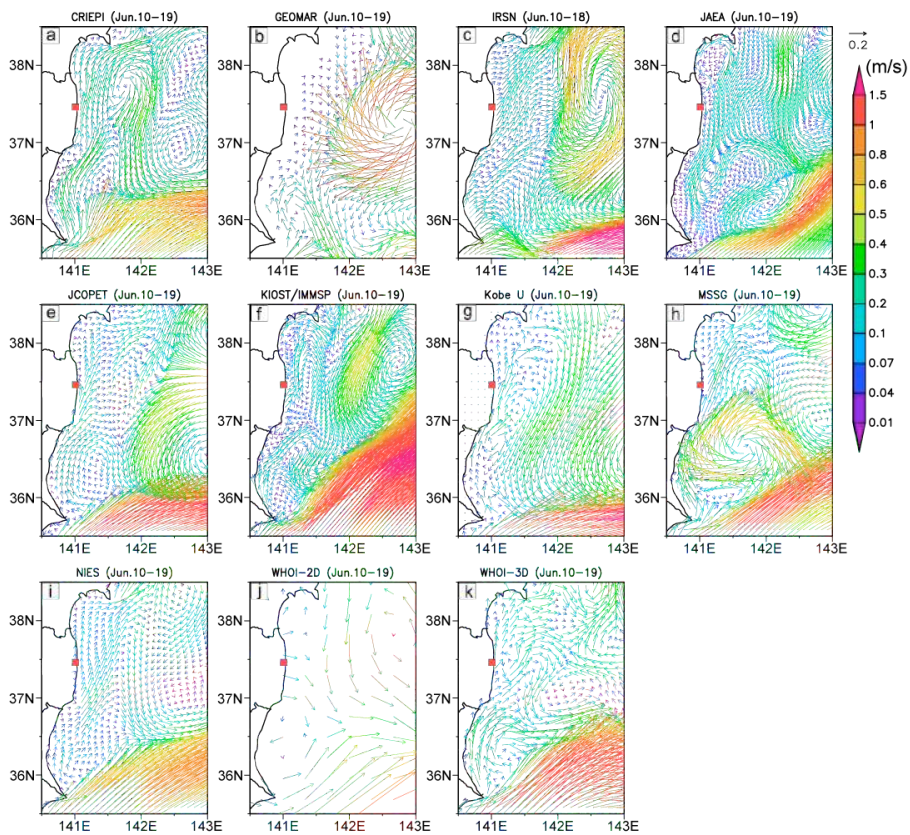
Figure 5B.19. Same as Fig. 5B.11 except for a period between June 10 and June 19.
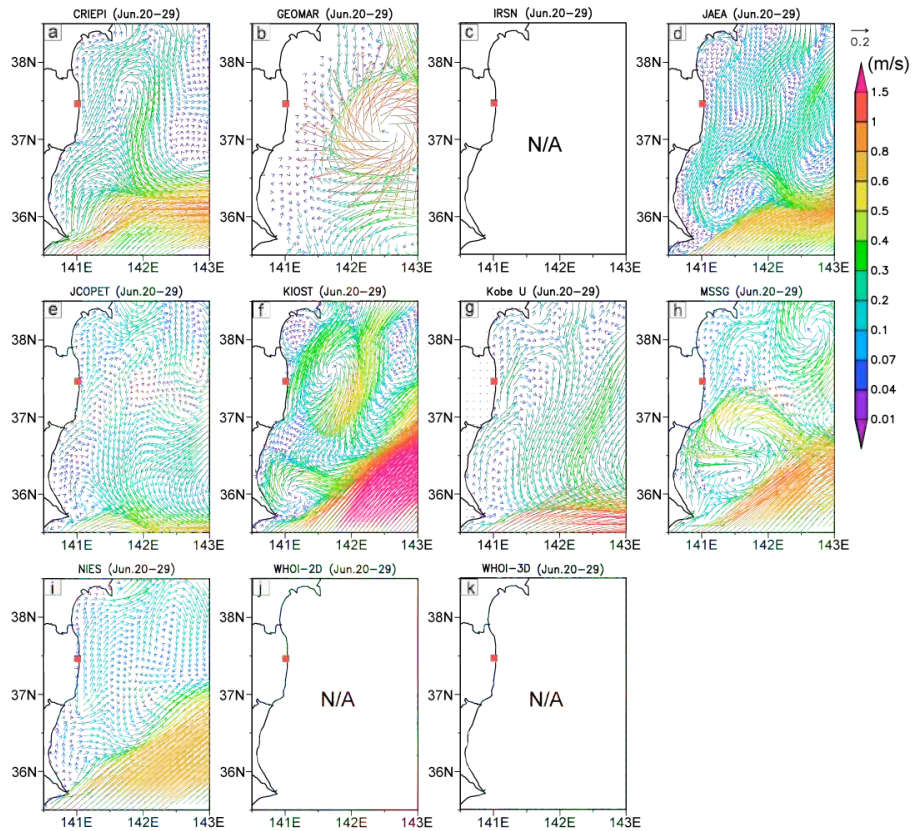
Figure 5B.20. Same as Fig. 5B.11 except for a period between June 20 and June 29.

Appendix 5C. Satellite Observations of the Anticyclonic Eddy off of the Ibaraki Coast

Evidence of the anticyclonic meso-scale eddy off of the coast of Ibaraki from late April to May can be obtained from several satellite images. Here, we show two examples of the sea-surface temperature and chlorophyll concentration observed by the Terra/MODIS satellite. A warm meso-scale eddy structure (Fig. 5C.1) with low chlorophyll-a concentration at the center of the eddy surrounded by high chlorophyll-a streamers (Fig. 5C.2) can be observed in a region off of the Ibaraki coast. Most of the models can capture this anticyclonic eddy in their simulations, although the detailed structure and location of the eddy differs among the models (see Fig.5.7).
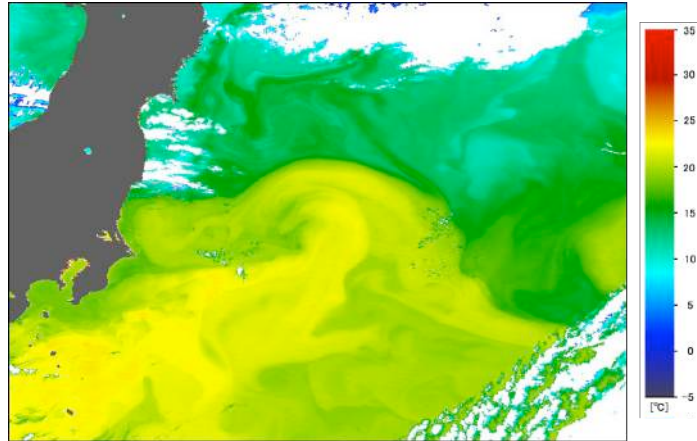
Figure 5C.1. Horizontal distribution of sea-surface temperature on May 15, 2011 observed by the Terra/MODIS satellite.
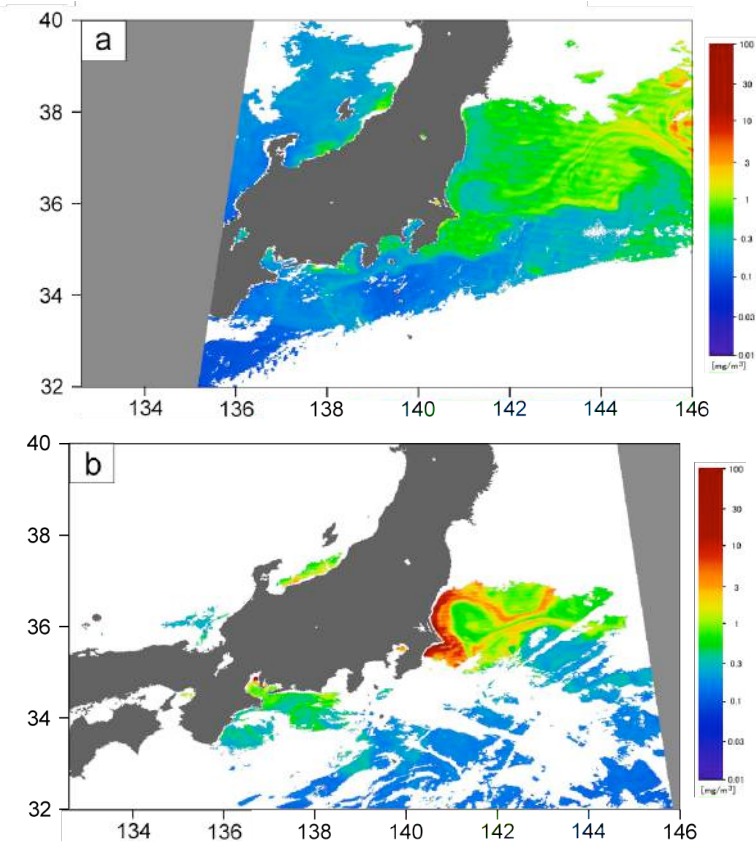
Figure 5C.2. Horizontal distribution of chlorophyll-a concentrations on (a) May 19, 2011 and (b) May 21, 2011 observed by the Terra/MODIS satellite.

Appendix 5D. Aerial measurements of radioactivity
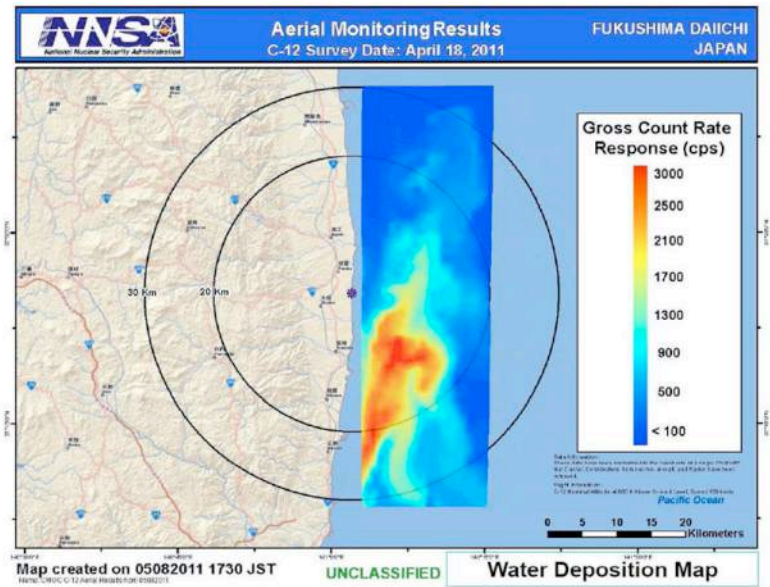
Figure 5D.1. An aerial measurement of the radioactivity (gross count rate response in cps) at the sea surface around the FDNPP on April 18, 2011. These data have been normalized to the count rate of a single $2 \times 4 \times 10$ NaI crystal, and radon has been removed (Guss, 2011). Their flight altitudes were from 150 to 700 m above the ground (MEXT, 2011).

References

Adachi, K., M. Kajino, Y. Zaizen, and Y. Igarashi, 2013: Emission of spherical cesium-bearing partilces from an early stage of the Fukushima nuclear accident. *Nature Scientific Reports*, 3 , 2554, doi:10.1038/srep02554.

Adachi, Y., S. Yukimoto, M. Deushi, A. Obata, H. Nakano, T.Y. Tanaka, M. Hosaka, T. Sakami, H. Yoshimura, M. Hirabara, E. Shindo, H. Tsujino, R. Mizuta, S. Yabu, T. Koshiro, T. Ose, and A. Kitoh, 2013: Basic performance of a new earth system model of the Meteorological Research Institute (MRI-ESM1). *Papers in Meteorology and Geophysics,* **64,** 1 -19, doi: 10.2467/mripapers.64.1

Amante, C. and B. W. Eakins, 2009: ETOPO1 1 Arc-Minute Global Relief Model: Procedures, Data Sources and Analysis. *NOAA Technical Memorandum NESDIS NGDC-24*, 19 pp.

Antonov, J. I., R. A. Locarnini, T. P. Boyer, A. V. Mishonov, H. E. Garcia, and S. Levitus, 2006: World Ocean Atlas 2005, Volume 2 : Salinity. NOAA Atlas NESDIS 62, U.S. Government Printing Office, Washington, DC, 182 pp.

Aoyama, M., D. Tsumune and Y. Hamajima, 2012: Distribution of ^{137}Cs and ^{134}Cs in the North Pacific Ocean: Impacts of the TEPCO Fukushima-daiichi NPP accident. *J. Radioanal. Nucl. Chem.*, doi: 10.1007/s10967-012-2033-2.

Appel, K.W., K.M. Foley, J.O. Bash, R.W. Pinder, R.L. Dennis, D.J. Allen, and K. Pickering, 2011: A multi-resolution assessment of the Community Multiscale Air Quality (CMAQ) model v4.7 wet deposition estimates for 2002-2006. *Geosci. Model Dev.*, 4 , 357-371, doi:10.5194/gmd-4-357-2011.

Bailly du Bois, P., F. Dumas, L. Solier, and C. Voiseux, 2012a: In-situ database toolbox for short-term dispersion model validation in macro-tidal seas, application for 2D-model. *Continental Shelf Res.*, **26**, 63-82. doi:10.1016/j.csr.2012.01.011.

Bailly du Bois, P., P. Laguionie, D. Boust, I. Korsakissok, D. Didier, and B. Fiévet, 2012b: Estimation of marine source-term following Fukushima Dai-ichi accident. *J. Environ. Radioactivity*, **114**, 2-9. doi:10.1016/j.jenvrad.2011.11.015.

Barron, C. N., A. B. Kara, H. E. Hurlburt, C. Rowley, and L. F. Smedstad, 2004: Sea surface height predictions from the Global Navy Coastal Ocean Model (NCOM) during 1998-2001. *J. Atmos. Oceanic Technol.*, **21**, 1876-1894.

Barron, C. N., A. B. Kara, P. J. Martin, R. C. Rhodes, and L. F. Smedstad, 2006: Formulation, implementation and examination of vertical coordinate choices in the global Navy Coastal

Ocean Model (NCOM). *Ocean Modeling*, **11**, 347-375.

Batifoulier, F., P. Lazure, and P. Bonneton, 2012: Poleward coastal jets induced by westerlies in the Bay of Biscay. *J. Geophys. Res.*, **117**, doi:10.1029/2011JC007658.

Brandt, J., J.H. Christensen, and L.M. Frohn, 2002: Modeling transport and deposition of cesium and iodine from the Chernobyl accident using the DREAM model. *Atmos. Chem. Phys.* **2**, 397-417.

Brenk, H.D., and Vogt, K.J., 1981: The calculation of wet deposition from radioactive plumes. *Nuclear Safety*, **22**, 362-371.

Buesseler, K. O., S. R. Jayne, N. S. Fisher, I. I. Rypina, H. Baumann, Z. Baumann, C. F. Breier, E. M. Douglass, J. George, A. M. Macdonald, H. Miyamoto, J. Nishikawa, S. M. Pike, and S. Yoshida, 2012: Fukushima-derived radionuclides in the ocean and biota off Japan. *P. Natl. Acad. Sci.*, **109**, 5984-5988.

Buijsman, M., Y. Uchiyama, J.C. McWilliams, and C.R. Hill-Lindsay, 2012: Modeling semiduirnal internal tides in the Sourthern California Bight. *J. Phys. Oceanogr.*, **42**, 62-77.

Byun, D., J.K.S. Ching, and Eds., 1999: Science algorithms of the EPA Models-3 Community Multiscale Air Quality (CMAQ) Modeling System. EPA-600/R-99/030, Office of Research and Development, U.S. Environmental Protection Agency, Washington D.C.

Byun, D., and K. Schere, 2006: Review of the governing equations, computational algorithms, and other components of the models-3 Community Multiscale Air Quality (CMAQ) modeling system. *Appl. Mech. Rev*. **59**(1-6), 51-77.

Chang, J.S., R.A. Brost, I.S.A. Isaksen, S. Madronich, P. Middleton, W.R. Stockwell, and C.J. Walcek, 1987: A three-dimensional Eulerian acid deposition model: Physical concepts and formulation. *J. Geophys. Res.*, **92**, 14,681-14,700.

Chino, M., H. Nakayama, H. Nagai, H. Terada, G. Katata, and H. Yamazawa, 2011: Preliminary estimation of release amounts of ^{131}I and ^{137}Cs accidentally discharged from the Fukushima Daiichi Nuclear Power Plant into the atmosphere. *J. Nucl. Sci. Tech.*, **48**, 1129-1134.

Choi, Y., S. Kida, and K. Takahashi, 2013: The impact of oceanic circulation and phase transfer on the dispersion of radionuclides released from the Fukushima Dai-ichi Nuclear Power Plant. *Biogeosciences*, **10**, 4911-4925, doi:10.5194/bg-10-4911-2013.

Christoudias, T., and J. Lelieveld, 2013: Modelling the global atmospheric transport and deposition of radionuclides from the Fukushima Dai-ichi nuclear accident. *Atmos. Chem. Phys.*, **13**, 1425-1438, doi:10.5194/acp-13-1425-2013.

Comprehensive Nuclear-Test-Ban Treaty Organization Preparatory Commission, 2011a: Fukushima-related measurements by the CTBTO.

http://www.ctbto.org/press-centre/highlights/2011/fukushima-related-measurements-by-the-ctbt o.

Comprehensive Nuclear-Test-Ban Treaty Organization Preparatory Commission, 2011b: The 11 March Japan Disaster. http://www.ctbto.org/verification-regime/the-11-march-japan-disaster/.

de Meij, A., Krol, M., Dentener, F., Vignati, E., Cuvelier, C., and Thunis, P., 2006: The sensitivity of aerosol in Europe to two different emission inventories and temporal distribution of emissions. *Atmos. Chem. Phys.*, **6**, 4287-4309, doi:10.5194/acp-6-4287-2006.

Dietze, H., and I. Kriest, 2012: Cs-137 off Fukushima Dai-ichi, Japan – model based estimates of dilution and fate. *Ocean Sci.*, **8** , 319-332, doi:10.5194/os-8-319-2012.

Draxler, R., D. Arnold, S. Galmarini, M. Hort, A. Jones, S. Leadbetter, A. Malo, C. Maurer, G. Rolph, K. Saito, R. Servranckx, T. Shimbori, E. Solazzo, and G. Wotawa, 2013: Evaluation of meteorological analyses for the radionuclide dispersion and deposition from the Fukushima Daiichi Nuclear Power Plant accident. *WMO Technical Publication, **1120**, 64pp,* https://www.wmo.int/e-catalog/detail_en.php?PUB_ID=669.

Egbert, G. D., and S. Y. Erofeeva, 2002: Efficient inverse modeling of barotropic ocean tides. *J. Atmos. Ocean. Tech.*, **19**, 183-204.

ENVIRON International Corporation, 2009: CAMx USER'S GUIDE. pp.280.

ENVIRON, 2011: CAMx 5.40 User's Guide. http://www.camx.com/files/camxusersguide_v5-40.aspx.

Estournel, C., E. Bosc, M. Bocquet, C. Ulses, P. Marsaleix, V. Winiarek, I. Osvath, C. Nguyen, T. Duhaut, F. Lyard, H. Michaud, and F. Auclair, 2012: Assessment of the amount of Cesium-137 released into the Pacific Ocean after the Fukushima accident and analysis of its dispersion in Japanese coastal waters. *J. Geophys. Res.*, **117**, C11014, doi:10.1029/2012JC007933.

Ferry N., E. Rémy, P. Brasseur, and C. Maes, 2007: The Mercator global ocean operational analysis system: Assessment and validation of an 11-year reanalysis. *J. Marine Systems*, **65**, 540-560.

Flemming, J., Inness, A., Flentje, H., Huijnen, V., Moinat, P., Schultz, M. G., and O. Stein, 2009: Coupling global chemistry transport models to ECMWF's integrated forecast system. *Geosci. Model Dev.*, **2** , 253-265, doi:10.5194/gmd-2-253-2009.

Furuno, A., H. Terada, M. Chino, and H. Yamazawa, 2004: Experimental verification for real-time environmental emergency response system: WSPEEDI by European tracer experiment. *Atmos. Environ*. **38**, 6989-6998.

Garreau, P., V. Garnier, and A. Schaeffer, 2011: Eddy resolving modelling of the Gulf of Lions and Catalan Sea. *Ocean Dynamics*, **61**, 991-1003, doi:10.1007/s10236-011-0399-2.

Grell, G.A., J. Dudhia, and D.R. Stauffer, 1994: A Description of the Fifth-Generation Penn

State/NCAR Mesoscale Model (MM5). *NCAR Tech*, Note NCAR/TN-3921STR, 122pp.

Grell, G.A., S.E. Peckham, R. Schmitz, S.A. McKeen, G. Frost, W.C. Skamarock, and B. Eder, 2005: Fully coupled "online" chemistry within the WRF model. *Atmospheric Environment*, **39**, 6957-6975.

Griffies, S. M., A. Gnanadesikan, K. W. Dixon, J. P. Dunne, R. Gerdes, M. J. Harrison, A. Rosati, J. L. Russell, B. L. Samuels, M. J. Spelman, M. Winton, and R. Zhang, 2005: Formulation of an ocean model for global climate simulations. *Ocean Sci.*, **1**, 45-79, doi:10.5194/os-1-45-2005.

Guo, X., S. M. Varlamov, and Y. Miyazawa, 2010: Coastal ocean modeling by nesting method. *Bull. Coast. Oceanogr.*, **47**, 113-123 (in Japanese with English abstract and figure captions).

Guss, P., 2011: DOE response to the radiological release from the Fukushima Dai-ichi Nuclear Power Plant, DOE/NV/25946-1236, *Proc. the NEI RETS/REMP Workshop*, Oak Brook, IL, 30 June 2011.

Hashimoto, A., H. Hirakuchi, Y. Toyoda, and K. Nakaya, 2010: Prediction of regional climate change over Japan due to global warming (Part 1) - Evaluation of Numerical Weather Forecasting and Analysis System (NuWFAS) applied to a long-term climate simulation. *CRIEPI report*, N10044 (in Japanese).

Hayami, H., A. Sato, M. Tsuzaki, and H. Shimadera, 2012: Atmospheric transport and deposition modeling of radioactive materials released from the Fukushima Daiichi nuclear power plant. *CRIEPI report*, V11054 (in Japanese).

Higashi, H., Y. Hanamachi, H. Koshikawa, S. Murakami, and K. Kohata, 2012: A numerical study on relationships between climate change and short-necked clam (Ruditapes philippinarum) biomass in 1990s in Ise Bay. Japan, *Proc. 9th International Symposium on Ecohydraulics 2012*, 13389.

Hirt, C.W., and B. D. Nichols, 1981: Volume of fluid method for the dynamics of free boundaries. *J. Comput. Phys.*, **39**, 201-225.

Hoffmann, W., R. Kebeasy, and P. Firbas, 2000: Introduction to the verification regime of the Comprehensive 5 Nuclear-Test-Ban Treaty. *Phys. Earth and Planetary Interiors*, **113**, 5 - 9 .

Honda, M., T. Aono, M. Aoyama, Y. Hamajima, H. Kawakami, M. Kitamura, Y. Masumoto, Y. Miyazawa, M. Takigawa, and T. Saino, 2012: Dispersion of artificial caesium-134 and -137 in the western North Pacific one month after the Fukushima accident. *Geochemical J.*, **46**, e1–e9.

Hsu, S.-C., C.-A. Huh, C.-Y. Chan, S.-H. Lin, F.-J. Lin, and S. C. Liu, 2012: Hemispheric dispersion of radioactive plume laced with fission nuclides from the Fukushima nuclear event. *Geophys. Res. Lett.*, **39**, L00G22, doi:10.1029/2011GL049986.

Huh, C.-A., Hsu, S.-C., and C.-Y. Lin, 2012: Fukushima-derived fission nuclides monitored around

Taiwan: Free tropospheric versus boundary layer transport. *Earth and Planetary Science Letters,* 319-320, 9-14. doi: 10.1016/j.epsl.2011.12.004

Huijnen, V., J. Williams, M. van Weele, T. van Noije, M. Krol, F. Dentener, A. Segers, S. Houweling, W. Peters, J. de Laat, F. Boersma, P. Bergamaschi, P. van Velthoven, P. Le Sager, H. Eskes, F. Alkemade, R. Scheele, P. Nédélec and H.-W. Pätz, 2010: The global chemistry transport model TM5: description and evaluation of the tropospheric chemistry version 3.0. *Geosci. Model Dev.*, **3**, 445-473, doi:10.5194/gmd-3-445-2010.

Igarashi, Y., Y. Inomata, M. Aoyama, K. Hirose, H. Takahashi, Y. Shinoda, N. Sugimoto, A. Shimizu, and M. Chiba, 2009: Plausible change in Asian dust source suggested by atmospheric anthropogenic radionuclides-observation of single wet deposition events during spring of 2007. *Atmospheric Environment* ,**43**, 2971-2980.

International Commission on Radiological Protection (ICRP), 1995: ICRP Publication 71: Age-Dependent Doses to Members of the Public from Intake of Radionuclides: Part 4 Inhalation Dose Coefficients. *Ann. ICRP*, vol. 25/3-4, Pergamon, Oxford, U. K.

Ishikawa, Y., T. Awaji, T. Toyoda, T. In, K. Nishina, T. Nakayama, S. Shima, and S. Masuda, 2009: High-resolution synthetic monitoring by a 4-dimensional variational data assimilation system in the northwestern North Pacific. *J. Mar. Syst.*, **78**, 237-248.

Iwasaki, T., T. Maki, and K. Katayama, 1998: Tracer transport model at Japan Meteorological Agency and its application to the ETEX data. *Atmos. Env.*, **32**, 4285-4295.

JAEA workshop, 2012: JAEA Open Workshop 'Reconstruction of the Emission and diffusion processes of materials released by the Fukushima Daiichi Atomic Power Plant accident', March 6 , 2012, Tokyo,

http://nsed.jaea.go.jp/ers/environment/envs/FukushimaWS/index.htm.

JODC, 2011: JODC-Expert Grid data for Geography (J-EGG500), 500m gridded bathymetric data set of Japan. http://www.jodc.go.jp/data_set/jodc/jegg_intro.html.

Kajino, M., 2011: MADMS: Modal Aerosol Dynamics model for multiple Modes and fractal Shapes in the free-molecular and near-continuum regimes. *J. Aerosol Sci.*, **42**, 224-248.

Kajino, M., and Y. Kondo, 2011: EMTACS: Development and regional-scale simulation of a size, chemical, mixing type, and soot shape resolved atmospheric particle model. *J. Geophys. Res.*, **116**, D02303, doi:10.1029/ 2010JD015030.

Kajino, M. Y. Inomata, K. Sato, H. Ueda, Z. Han, J. An, G. Katata, M. Deushi, T. Maki, N. Oshima, J. Kurokawa, T. Ohara, A. Takami, and S. Hatakeyama, 2012: Development of the RAQM2 aerosol chemical transport model and predictions of the Northeast Asian aerosol mass, size, chemistry, and mixing type. *Atmos. Chem. Phys.*, **12**, 11833-11856,

doi:10.5194/acp-12-11833-2012.

Katata, G., M. Ota, H. Terada, M. Chino, and H. Nagai, 2012: Atmospheric discharge and dispersion of radionuclides during the Fukushima Dai-ichi Nuclear Power Plant accident. Part I: Source term estimation and local-scale atmospheric dispersion in early phase of the accident. *J. Environ. Radioactivity*, **109**, 103-113, doi:10.1016/j.jenvrad.2012.02.006.

Kawamura, H., T. Kobayashi, A. Furuno, T. In, Y. Ishikawa, T. Nakayama, S. Shima, and T. Awaji, 2011: Preliminary numerical experiments on oceanic dispersion of 131I and 137Cs discharged into the ocean because of the Fukushima daiichi nuclear power plant disaster. *J. Nucl. Sci. Tech.*, **48**, 1349-1356.

Kinoshita, N., K. Sueki, K. Sasa, J-I. Kitagawa, S. Ikarashi, T. Nishimura, Y-S. Wong, Y. Satou, K. Handa, T. Takahashi, M. Sato, and T. Yamagata, 2011: Assessment of individual radionuclide distributions from the Fukushima nuclear accident covering central-east Japan. *Proceedings of the National Academy of Sciences of the United States of America*, 4pp, doi:10.1073/pnas.1111724108.

Kitada, T., 1994: Modelling of transport, reaction and deposition of acid rain. *Kishou Kenkyu Note*, **182**, 95–117 (in Japanese).

Klug, W., G. Graziani, G. Gripa, D. Pierce, and C. Tassone, 1992: Evaluation of long range atmospheric transport models using environmental radioactivity data from the Chernobyl accident. *the ATMES report*, Technical report, Elsevier Applied Science.

Kobayashi, T., S. Otosaka, O. Togawa, and K. Hayashi, 2007: Development of a non-conservative radionuclides dispersion model in the ocean and its application to surface cesium-137 dispersion in the Irish Sea. *J. Nucl. Sci. Technol.*, **44**, 238-247.

Kobayashi T., H. Nagai, M. Chino, and H. Kawamura, 2013: Source term estimation of atmospheric release due to the Fukushima Dai-ichi Nuclear Power Plant accident by atmospheric and oceanic dispersion simulations. *J. Nucl. Sci. Technol.*, **50**, 255-264, doi:10.1080/00223131.2013.772449.

Kondo, J., 1975: Air-sea bulk transfer coefficients in diabatic conditions. *Bound.-Layer Meteor.*, **9**, 91-112.

Korsakissok, I., D. Didier, A. Mathieu, D. Quelo, J. Groell, E. Quentric, M. Tombette, J.P. Benoit, and O. Saunier, 2011: Evaluation of the atmospheric releases of the Fukushiam accident and their consequences. *Institute de Radioprotection et de Sûreté Nucléaire (IRSN)*, PRP-CRI/SESC n 2011-00299, 38p.

Korsakissok, I., A. Mathieu, and D. Didier, 2013: Atmpsoheric dispersion and ground deposition induced by the Fukushima Nuclear power plant accident: a loca-scale simulation and sensitivity

study. *Atmos. Environ.*, **70**, 267-279.

Krol, M., S. Houweling, B. Bregman, M. van den Broek, A. Segers, P. van Velthoven, W. Peters, F. Dentener and P. Bergamaschi, 2005: The two-way nested global chemistry-transport zoom model TM5: algorithm and applications. *Atmos. Chem. Phys.*, 5 , 417-432, doi:10.5194/acp-5-417-2005.

Kunii, M., 2013: Mesoscale data assimilation for a local severe fainfall event with the NHM-LETKF system. *Weather and Forecasting*, e-View, doi: http://dx.doi.org/10.1175/WAF-D-13-00032.1.

Large, W.G., J. C. McWilliams, and S. C. Doney, 1994: Ocean vertical mixing: A review and a model with a nonlocal boundary layer parameterization. *Rev. Geophys.*, **32**, 363-403.

Lazure, P., and F. Dumas, 2008: An external-internal mode coupling for a 3D hydrodynamical model for applications at regional scale (MARS). *Adv. Water Resources*, **31**, 233-250.

Locarnini, R. A., A. V. Mishonov, J. I. Antonov, T. P. Boyer, H. E. Garcia, and S. Levitus, 2006: World Ocean Atlas 2005, Volume 1: Temperature, NOAA Atlas NESDIS 61, U.S. Government Printing Office, Washington, DC, 182 pp.

Long, N.Q., Y. Truong, P.D. Hien, N.T. Binh, L.N. Sieu, T.V. Giap, and N.T. Phan, 2012: Atmospheric radionuclides from the Fukushima Dai-ichi nuclear reactor accident observed in Vietnam. *J. of Environmental Radioactivity*, **111**, pp.53-58, doi: 10.1016/j.jenvrad.2011.11.018.

Lyard, F., F. Lefevre, T. Letellier, and O. Francis, 2006: Modelling the global ocean tides: modern insights from FES2004. *Ocean Dynamics*, **56**, 394-415. doi:10.1007/s10236-006-0086-x.

Maki, T., T. Y. Tanaka, T. T. Sekiyama, and M. Mikami, 2011: The impact of ground-based observations on the inverse technique of Aeolian dust aerosol. *SOLA*, **7A**, 21-24.

Margvelashvily, N., V. Maderich, and M. Zheleznyak, 1997: THREETOX - computer code to simulate three-dimensional dispersion of radionuclides in homogeneous and stratified water bodies. *Radiation Protection Dosimetry*, **73**, 177-180.

Maryon, R.H., F.B. Smith, B.J. Conwy, and D.M. Goddard, 1992: The UK nuclear accident response model (NAME). *Progress in Nuclear Energy*, **26**, 85-104.

Maryon, R.H., J. Saltbones, D.B. Ryall, J. Barnicki, H.A. Jakobsen, and E. Berge, 1996:An intercomparison of three long range dispersion models developed for the UK meterological office, DNMI and EMEP. *UK Met Office Turbulence and Diffusion Note*, **234**, ISBN: 82-7144-026-08, pp. 44.

Mason, E., J. Molemaker, A.F. Shchepetkin, F. Colas, J.C. McWilliams, and P. Sangra, 2010: Procedures for offline grid nesting in regional ocean models. *Ocean modelling*, **35**, 1 -15.

Masson., O., et al., 2011: Tracking of Airborne Radionuclides from the Damaged Fukushima Dai-Ichi Nuclear Reactors by European Networks. *Environ. Sci. Technol.*, **45**, 7670-7677, doi:

10.1021/es2017158.

Masumoto, Y., Y. Miyazawa, D. Tsumune, T. Kobayashi, C. Estournel, P. Marsaleix, L. Lanerolle, A. Mehra, and Z. D. Garraffo, 2012: Oceanic dispersion simulation of Cesium 137 from Fukushima Daiichi Nuclear Power Plant. *Elements*, **8**, 207-212.

Mathieu, A., I. Korsakissok, D. Quélo, J. Groëll, M. Tombette, D. Didier, E. Quentric, O. Saunier, J.-P. Benoit. and O. Isnard, 2012: Atmospheric dispersion and deposition of radionuclides from the Fukushima Daiichi nuclear power plant accident. *Elements*, **8**, 195-200.

Medici, F., 2001: The IMS radionuclide network of the CTBT. *Radiat. Phys. Chem.*, **61**, 689-690.

Mellor, G. L., 2001: One-dimensional, ocean surface layer modeling: A problem and a solution. *J. Phys. Oceanogr.*, **31**, 790-809.

Mellor, G. and A. F. Blumberg, 2004: Wave breaking and ocean surface layer thermal response. *J. Phys. Oceanogr.*, **34**, 693-698.

MEXT, 2011: Results of airborne monitoring by the Ministry of Education, Culture, Sports. Science and Technology and the U.S. Department of Energy. Available at
http://radioactivity.nsr.go.jp/ja/contents/4000/3710/24/1305820_20110506.pdf,
http://radioactivity.nsr.go.jp/ja/contents/5000/4858/24/1305819_0708.pdf,
http://radioactivity.nsr.go.jp/ja/contents/5000/4901/24/1910_1216.pdf.

Miyazawa, Y., R. Zhang, X. Guo, H. Tamura, D. Ambe, J.-S. Lee, A. Okuno, H. Yoshinari, T. Setou, and K. Komatsu, 2009: Water mass variability in the western North Pacific detected in a 15-year eddy resolving ocean reanalysis. *J. Oceanogr.*, **65**, 737-756, doi: 10.1007/s10872-009-0063-3.

Miyazawa, Y., Y. Masumoto, S.M. Varlamov, T. Miyama, M. Takigawa, M. Honda and T. Saino, 2012a: Inverse estimation of source parameters of oceanic radioactivity dispersion models associated with the Fukushima accident. *Biogeosci. Discuss.*, **9**, 13783-13816, doi:10.5194/bgd-9-13783-2012.

Miyazawa, Y., Y. Masumoto, S. M. Varlamov, and T. Miyama, 2012b: Transport simulation of the radionuclide from the shelf to open ocean around Fukushima. *Cont. Shelf Res.*, **50-51**, 16-29.

Morino, Y., T. Ohara, and M. Nishizawa, 2011: Atmospheric behavior, deposition, and budget of radioactive materials from the Fukushima Daiichi nuclear power plant in march 2011. *Geophys. Res. Lett.*, **38**, doi:10.1029/2011GL048689.

Morino, Y., T. Ohara, M. Watanabe, S. Hayashi, and M. Nishizawa, 2013: Episode analysis of deposition of radiocesium form the Fukushima Daiichi Nuclear Power Plant accident. *Environ. Sci. Technol.*, **47**, 2314-2322, dx.dox.org/10.1021/es304620x.

Noh, Y., and H.J. Kim, 1999: Simulations of temperature and turbulence structure of the oceanic

boundary layer with the improved near-surface process. *J. Geophys. Res.*, **104**, 15621-15634, doi:10.1029/1999JC900068.

Onogi, K., J. Tsutsui, H. Koide, M. Sakamoto, S. Kobayashi, H. Hatsushika, T. Matsumoto, N. Yamazaki, H. Kamahori, K. Takahashi, S. Kadokura, K. Wada, K. Kato, R. Oyama, T. Ose, N. Mannoji, and R. Taira, 2007: The JRA-25 Reanalysis. *J. Meteor. Soc. Japan*, **85**, 369-432.

Park, S.-U., 1998: Effects of dry deposition on near-surface concentrations of SO_2 during medium-range transport. *J. Applied Meteor.*, **37**, 486-496.

Park, S.-U., A. Choe, M.-S. Park, and Y. Chun, 2010: Performance tests of the Asian Dust Aerosol Model 2 (ADAM2). *J. of Sustainable Energy and Environ.* **1** , 77-83.

Park, S.-U., A. Choe, and M.-S. Park, 2013: Atmospheric dispersion and deposition of radionuclides (^{137}Cs and ^{131}I) released from the Fukushima Dai-ichi nuclear power plant. *Computational Water, Energy, and Environ. Engineering,* **2** , 61-68.

Quélo, D., M. Krysta, M. Bocquet, O. Isnard, Y. Minier, and B. Sportisse, 2007: Validation of the Polyphemus platform on the ETEX, Chernobyl and Algeciras cases. *Atmos. Environ.*, **41**, 5300-5315.

Ralph, E. A., and P. P. Niiler, 1999: Wind-driven currents in the tropical Pacific. *J. Phys. Oceanogr.*, **29**, 2121-2129.

Roeckner, E., G. Bäuml, L. Bonaventura, R. Brokopf, M. Esch, M. Giorgetta, S. Hagemann, I. Kirchner, L. Kornblueh, E. Manzini, A. Rhodin, U. Schlese, U. Schulzweida and A. Tompkins, 2003: The atmospheric general circulation model ECHAM5.PART I: Model description. *Technical report, Max Planck Institute for Meteorology*.

Roeckner, E., R. Brokopf, M. Esch, M. Giorgetta, S. Hagemann, L. Kornblueh, E. Manzini, U. Schlese., and U. Schulzweida, 2006: Sensitivity of simulated climate to horizontal and vertical resolution in the ECHAM5 atmosphere model. *J. Climate*, **19**, 3771-3791.

Roland, A., Y. J. Zhang, H. V. Wang, Y. Meng, Y.-C. Teng, V. Maderich, I. Brovchenko, M. Dutour-Sikiric, and U. Zanke, 2012: A fully coupled 3D wave-current interaction model on unstructured grids. *J. Geophys Res.*, **117**, C00J33, p. 1 -18 doi:10.1029/2012JC007952.

Romero, L., Y. Uchiyama, C. Ohlmann, J.C. McWilliams, and D.A. Siegel, 2013: Particle-pair dispersion in the Southern California coastal zone. *J. Phys. Oceanogr.*, **43**, 1862-1879.

Saito, K., T. Shimbori, and R. Draxler, 2014: JMA's regional atmospheric transport model calculations for the WMO Technical Task Team on meteorological analyses for Fukushima Daiichi Nuclear Power Plant accident. *J. Environ. Radioact.*, doi: 10.1016/j.jenvrad.2014.02.007.(in press).

Saunier, O., A. Mathieu, D. Didier, M. Tombette, D. Quélo, V. Winiarek, and M. Bocquet, 2013: An

inverse modeling method to access the source term of the Fukushima nuclear power plant accident using gamma dose rate observations. *Atmos. Chem. Phys*, **13**, 11403-11421.

Sehmel, G.A., 1980: Particle and gas dry deposition: A review. *Atmos. Environ*. **14,** 983-1011.

Seinfeld, J.H., and S.N. Pandis, 1998: Atmospheric Chemistry and Physics, From Air Pollution to Climate Change. John Wiley and Sons, Inc., NY.

Seino, N., H. Sasaki, J. Sato, and M. Chiba, 2004: High-resolution simulation of volcanic sulfur dioxide dispersion over the Miyake Island. *Atmos. Env.*, **38**, 7073-7081.

Shchepetkin, A. F., and J. C. McWilliams, 2005: The Regional Ocean Modeling System (ROMS): a split-explicit, free-surface, topography following coordinates oceanic model. *Ocean Modelling*, **9** , 347-404.

Shimbori, T., Y. Aikawa, and N. Seino, 2009: Operational implementation of the tephra fall forecast with the JMA mesoscale tracer transport model. *CAS/JSC WGNE Res. Act. Atmos. Ocea. Model.*, **39**, 5.29-5.30.

Shimbori, T. , Y. Aikawa, K. Fukui, A. Hashimoto, N. Seino, and H. Yamasato, 2010: Quantitative tephra fall prediction with the JMA mesoscale tracer transport model for volcanic ash: A case study of the eruption at Asama volcano in 2009. *Pap. Met. Geophys.*, **61**, 13-29 (in Japanese with English abstract and figure captions).

Simmons, A., S. Uppala, D. Dee, and S. Kobayashi, 2007: ERA-Interim: New ECMWF reanalysis products from 1989 onwards. *ECMWF newsletter*, **110**, 25-35.

Skamarock, W. C., J.B. Klemp, J. Dudhia, D.O. Gill, D.M. Barker, M.G. Duda, X.Y. Huang, W. Wang, and J.G. Powers, 2008: A description of the advanced research WRF version 3, NCAR Tech. Note NCAR/TN-475+STR, 113pp.

Smagorinsky, J., 1963: General circulation experiments with the primitive equations, I. The basic experiment. *Mon. Weather Rev.*, **91**, 99-164.

Smith, A. R., K. J. Thomas, E. B. Norman, D. L. Hurley, B. T. Lo, Y. D. Chan, P. V. Guillaumon, and B. G. Harvey, 2014: Measurements of Fission Products from the Fukushima Daiichi Incident in San Francisco Bay Area Air Filters, Automobile Filters, Rainwater, and Food. *Journal of Environmental Protection*, **5** , 207-221.

Sportisse, B., 2007: A review of parameterizations for modeling dry deposition and scavenging of radionuclides. *Atmospheric Environment*, **41**, 2683-2698.

Stohl, A., P. Seibert, G. Wotawa, D. Arnold, J. F. Burkhart, S. Eckhardt, C. Tapia, A. Vargas, and T. J. Yasunari, 2012: Xenon-133 and caesium-137 releases into the atmosphere from the Fukushima Dai-ichi nuclear power plant: determination of the source term, atmospheric dispersion, and deposition. *Atmos. Chem. Phys.*, **12**, 2313-2343, doi:10.5194/acp-12-2313-2012.

Sugiyama, G., J. Nasstrom, B. Pobanz, K. Foster, M. Simpson, P. Vogt, F. Aluzzi, and S. Homann, 2012: Atmospheric dispersion modeling: challenges of the Fukushima Daiichi response. *Health Physics*, **102**, 493-508, doi:10.1097/HP.0b013e31824c7bc9.

Takahashi,K., X. Peng, R. Onishi, M. Ohdaira, K. Goto, H. Fuchigami, and T. Sugimura, 2008: Impact of coupled nonhydrostatic atmosphere–ocean–land model with high resolution. *High Resolution Numerical Modelling of the Atmosphere and Ocean*, K. Hamilton and W. Ohfuchi, Eds, Springer-Verlag, 261-274.

Takano, I., Y. Aikawa, and S. Gotoh, 2007: Improvement of photochemical oxidant information by applying transport model to oxidant forecast. *CAS/JSC WGNE Res. Act. Atmos. Ocea. Model.*, **37**, 5.35-5.36.

Takemura, T., H. Okamoto, Y. Murayama, A. Numaguti, A. Higurashi, and T. Nakajima, 2000: Global three-dimensional simulation of aerosol optical thickness distribution of various origins. *J. Geophys. Res.* **105**, 17853-17873.

Takemura, T., T. Nakajima, O. Dubovik, B.N. Holben, and S. Kinne, 2002: Single-scattering albedo and radiative forcing of various aerosol species with a global three-dimensional model. *J. Climate*, **15**, 333-352.

Takemura, T., T. Nozawa, S. Emori, T.Y. Nakajima, and T. Nakajima, 2005: Simulation of climate response to aerosol direct and indirect effects with aerosol transport-radiation model. *J. Geophys. Res.*, **110**, D02202, doi:10.1029/2004JD005029.

Takemura, T., H. Nakamura, M. Takigawa, H. Kondo, T. Satomura, T. Miyasaka, and T. Nakajima, 2011: A numerical simulation of global transport of atmospheric particles emitted from the Fukushima Daiichi Nuclear Power Plant. *SOLA*, ７ , 101-104, doi:10.2151/sola.2011-026.

Tanaka, T. Y., and M. Chiba, 2005: Global simulation of dust aerosol with a chemical transport Model, MASINGAR. *J. Meteor. Soc. Japan*, **83A**, 255-278.

Tanaka, T. Y., K. Orito, T.T. Sekiyama, K. Shibata, M. Chiba, and H. Tanaka, 2003: MASINGAR, a global tropospheric aerosol chemical transport model coupled with MRI/JMA98 GCM: Model description. *Pap. Meteor. Geophys.* **53**, 119-138.

Tanaka, T. Y., T. Maki, T.T. Sekiyama, Y. Igarashi, M. Kajino, and M. Mikami, 2013: Numerical analysis of the global transport of radionuclides from Fukushima Dai-ichi nuclear power plant accident. *93rd American Meteorological Society Annual Meeting*.

TEPCO, 2011: Press release 'Submission of a report to Ministry of Economy, Trade and Industry, Nuclear and Industrial Safety Agency, on the tsunami investitgation at Fukushima Daiichi and Daini Atomic Power Plants. July 8, 2011 (in Japanese).
Available at http://www.tepco.co.jp/cc/press/11070802-j.html.

TEPCO, 2012: Estimation of the released amount of radioactive materials into the atmosphere as a result of the accident in the Fukushima Daiichi Nuclear Power Station (in Japanese). Available at http://www.tepco.co.jp/cc/press/betu12_j/images/120524j0105.pdf.

Terada, H., A. Furuno, and M. Chino, 2004: Improvement of worldwide version of system for prediction of environmental emergency dose information (WSPEEDI), (I) new combination of models, atmospheric dynamic model MM5 and particle random walk model GEARN-new. *J. Nucl. Sci. Technol.,* **41**, 632-640.

Terada, H., and M. Chino, 2005: Improvement of Worldwide Version of System for Prediction of Environmental Emergency Dose Information (WSPEEDI), (II) evaluation of numerical models by 137Cs deposition due to the Chernobyl nuclear accident. *J. Nucl. Sci. Technol.* **42**, 651-660.

Terada, H., and M. Chino, 2008: Development of an atmospheric dispersion model for accidental discharge of radionuclides with the function of simultaneous prediction for multiple domains and its evaluation by application to the Chernobyl nuclear accident. *J. Nucl. Sci. Technol.,* **45**, 920-931.

Terada, H., H. Nagai, A. Furuno, T. Kakefuda, T. Harayama, and M. Chino, 2008: Development of worldwide version of system for prediction of environmental emergency dose information: WSPEEDI 2nd version. Trans. At. *Energy Soc. Japan,* **7**, 257-267 (in Japanese with English abstract).

Terada, H., G. Katata, M. Chino, and H. Nagai, 2012: Atmospheric discharge and dispersion of radionuclides during the Fukushima Dai-ichi Nuclear Power Plant accident Part II: verification of the source term and analysis of regional-scale atmospheric dispersion. *J. Environ. Radioact.,* **112**, 141-154.

Torii, T., T. Sugita, C. E. Okada, M. S. Reed, and D. J. Blumenthal, 2013: Enhanced analysis methods to derive the spatial distirbutions of ^{131}I deposition on the ground by airborne suveys at an early stage after the Fukushima Daiichi nuclear power plant accident. *Health Physics*, **105**, 192-200.

Tsumune, D., M. Aoyama, K. Hirose, F. O. Bryan, K. Lindsay, and G. Danabasoglu, 2011a: Transport of 137Cs to the Southern Hemisphere in an ocean general circulation model. *Progress In Oceanography*, **89**, 38-48, 10.1016/j.pocean.2010.12.006.

Tsumune, D., T. Tsubono, M. Aoyama, and K. Hirose, 2011b: Distribution of oceanic 137Cs from the Fukushima Daiichi Nuclear Power Plant simulated numerically by a regional ocean mode. *CRIEPI Environmental Science Research Laboratory Rep.*, No.V11002, (in Japanese, with English abstract and figure captions).

Tsumune, D., T. Tsubono, M. Aoyama, and K. Hirose, 2012: Distribution of oceanic 137Cs from the

Fukushima Dai-ichi Nuclear Power Plant simulated numerically by a regional ocean model. *J. Environm. Radioact.*, **111**, 100-108.

Tsumune, D., T. Tsubono, M. Aoyama, M. Uematsu, K. Misumi, Y. Maeda, Y. Yoshida, and H. Hayami, 2013: One-year, regional-scale simulation of 137Cs radioactivity in the ocean following the Fukushima Dai-ichi Nuclear Power Plant accident. *Biogeosciences*, **10**, 5601-5617, doi:10.5194/bg-10-5601-2013.

Uchiyama, Y., T. Ishii, D. Tsumune, and Y. Miyazawa, 2012: Oceanic dispersion of radioactive cesium-137 from Fukushima Daiichi Nuclear Power Plant. *J. JSCE*, **68**, 931-935 (in Japanese with English abstract).

Uchiyama, Y., T. Yamanishi, D. Tsumune, Y. Miyazawa, and T. Ishii, 2013: Influences of coastal jet and mesoscale eddies on initial dispersion of the radionuclides released from Fukushima Daiichi Nuclear Power Plant. *J. JSCE*, **69**, 1051-1055 (in Japanese with English abstract).

Uchiyama, Y., E. Idica, J.C. McWilliams, and K.D. Stolzenbach, 2014: Wastewater effluent dispersal in Southern California bays. *Cont. Shelf Res.*, **76**, 36-52. doi: http://dx.doi.org/10.1016/j.csr.2014.01.002.

Uppala, S. M., et al., 2005: The ERA-40 re-analysis. *Q. J. Roy. Meteorol. Soc.*, **131**, 2961-3012, doi:10.1256/qj.04.176.

Vignati, E., M. Karl, M. Krol, J. Wilson, P. Stier, and F. Cavalli, 2010: Sources of uncertainties in modelling black carbon at the global scale. *Atmos. Chem. Phys.*, **10**, 2595-2611, doi:10.5194/acp-10-2595-2010

Watanabe, M., T. Suzuki, R. O'ishi, Y. Komuro, S. Watanabe, S. Emori, T. Takemura, M. Chikira, T. Ogura, M. Sekiguchi, K. Takata, D. Yamazaki, T. Yokohata, T. Nozawa, H. Hasumi, H. Tatebe, and M. Kimoto, 2010: Improved climate simulation by MIROC5: Mean states, variability, and climate sensitivity. *J. Climate*, **23**, 6312-6335.

Wetherbee, G. A., D.A. Gay, T.M. Debey, C.M.B. Lehmann, and M.A. Nilles, 2012: Wet deposition of fission-product isotopes to north America from the Fukushima Dai-ichi incident. *Environ. Sci. Technol.*, **46**, 2574-2582, doi:10.1021/es203217u.

Winiarek, V., M. Bocquet, O. Saunier, and A. Mathieu, 2012: Estimation of errors in the inverse modeling of accidental release of atmospheric pollutant: Application to the reconstruction of the cesium-137 and iodine-131 source terms from the Fukushima Daiichi power plant. *J. Geophys. Res.*, **117**, D05122.

Winiarek, V., M. Bocquet, N. Duhanyan, Y. Roustan, O. Saunier, and A. Mathieu, 2014: Estimation of the caesium-137 source term from the Fukushima Daiichi nuclear power plant using a consistent joint assimilation of air concentration and deposition observations. *Atmos. Env.*, **82**,

268-279.

WMO, 2011: Final report of the Meeting of the WMO Task Team on Meteorological Analyses for Fukushima Daiichi Nuclear Power Plant Accident. Geneva, Switzerland, 30 November- 2 December 2011, Available at http://www.wmo.int/pages/prog/www/CBS-Reports/documents/FinalRep_TT_FDnpp_v6.pdf.

WMO, 2013: The World Meterological Organization's evaluation of meteorological analyses for the radionuclide dispersion and deposition from the Fukushima Daiichi Nuclear Power Plant accident. Annex III, ERA/TT-MA-NPP-accident 3rd Meeting 2012. http://www.wmo.int/pages/prog/www/CBS-Reports/documents/WMO_fnpp_final_AnnexIII_4 Feb2013_REVISED_17June2013.pdf

Yonezawa, C., and Y. Yamamoto, 2011: Meaturements of the anthropogenic atmospheric radionuclides by the observational network of radionuclides for nuclear weapons test watch. *Bunseki*, **440**, 451-458 (in Japanese).

Yukimoto, S., H. Yoshimura, M. Hosaka, T. Sakami, H. Tsujino, M. Hirabara, T.Y. Tanaka, M. Deushi, A. Obata, H. Nakano, Y. Adachi, E. Shindo, S. Yabu, T. Ose, and A. Kitoh, 2011: Meteorological Research Institute-Earth System Model Version 1 (MRI-ESM1) - Model Description. *Technical Reports of the Meteorological Research Institute*, **64**, ISSN 0386-4049, Meteorological Research Institute, Japan, 88pp.

Yukimoto, S., Y. Adachi, M. Hosaka, T. Sakami, H. Yoshimura, M. Hirabara, T.Y. Tanaka, E. Shindo, H. Tsujino, M. Deushi, R. Mizuta, S. Yabu, A. Obata, H. Nakano, T. Koshiro, T. Ose, and A. Kitoh, 2012: A new global climate model of the Meteorological Research Institute: MRI-CGCM3 -Model description and basic performance. *J. Meteor. Soc. Japan*, **90**, pp.23-64.

Zhang, L., S. Gong, J. Padro, and L. Barrie, 2001: A size-segregated particle dry deposition scheme for an atmospheric aerosol module. *Atmos. Environ.*, **35**, 549-560.

Zhang, L., J. R. Brook, and R. Vet, 2003: A revised parameterization for gaseous dry deposition in air-quality models. *Atmos. Chem. Phys.,* **3**, 2067-2082.

Zhang, Y., and A. M. Baptista, 2008: SELFE: A semi-implicit Eulerian–Lagrangian finite-element model for cross-scale ocean circulation. *Ocean Modelling*, **21**, 71-96.